New Hydrate Risk Evaluation for Processing and Transport of Natural Gas Containing Water and Impurities

Master of Science Thesis in Process Technology

By Anuli A Kulkarni

Department of Physics and Technology

University of Bergen, Norway

October 2014

Abstract

The growth of natural gas transport by pipeline has led to the establishment of a large network of pipelines throughout the world. [1]. Transport of natural gas through a network of pipelines is a challenging issue, mainly due to the hydrate risk associated with it. Hydrates are crystalline compounds in which hydrogen bonded water enclatherate one or more type of `guest' molecules inside cavities.

Natural gas hydrates can be formed both in pipelines and process equipment's, as a result of abnormalities in the flow operation [2], i.e. when pressure drop occurs across a restriction or turbine causing the water to expand and eventually drop out as liquid and during emergency shut downs due to failure of a component in the system for e.g. compressor failure. Natural gas hydrates can form in pipelines as a result of vapor deposition and or splashing of water with subsequent conversions [2].

In view of the above, the maximum allowable content of water that can be permitted in a gas stream, [in this project methane (CH_4) with impurities carbon dioxide (CO_2) and hydrogen sulphide (H_2S)] under transportation without risking the hydrate formation is a very complex issue [3]. Very complex because generally the system cannot reach equilibrium and many different competing phase transitions occur which leads to hydrate formation and phase transitions that can lead to re-dissociation. The dynamic situation further complicates the picture, which due to 1^{st} and 2^{nd} laws of thermodynamics may lead to a range of different hydrates depending on which phase the hydrate former is coming from. This is because chemical potentials for guest molecules in different phases are not the same in non-equilibrium situations. Yet another reason is that the most stable hydrates will form first even with liquid water and hydrate former from fluid phase mixture.

In this MSc project three different routes to hydrate formation have been studied and analyzed. This also includes impact of solid surfaces that can induce phase transitions. For transport in pipelines this is essentially rusty surfaces of the pipe-wall. The main aim of the study is to bring more clarity to the most important and possible events that can lead to hydrate formation and as such will dominate the hydrate risk evaluation.

The first of these routes to hydrate formation involves water condensing out as liquid and then subsequently forming hydrate together with hydrate formers from the gas. This sequence of events is the most used basis for hydrate risk analysis in industry today, i.e. hydrate risk evaluation based on dew-point calculations.

A second possibility is that hydrate forms directly from water dissolved in the gas.

A third route involves the possibility that water can adsorb on the rusty walls and then hydrate can be formed from water which is slightly (1 nm) outside the wall, by extracting hydrate formers from the gas.

Since the systems [water, gas, adsorbed phase and hydrate] generally cannot reach equilibrium (Gibbs phase rule) and the combination of 1st and 2nd law of thermodynamics will always direct the system to have lowest free energy possible [3]. Hence a primary tool for comparison will be free energy analysis.

The natural choice of method in free energy analysis is classical thermodynamics using residual thermodynamics (ideal gas as a reference state). The software developed for this purpose is developed by Professor Bjørn Kvamme. In addition, external software from DTU (Danish Technical University) has also been utilized to determine thermodynamic properties of the gas mixture. These codes are in FORTRAN language and Microsoft developer has been used as compiler.

Water available for hydrate formation can exist in three different states. The first being able to form CH_4 hydrate directly from water dissolved in CH_4 (mass transport is a limitation though), the second being hydrate formed with water either condensing out, to create a liquid water phase and the third being hydrate formation from water adsorbed on solid surfaces (hematite in our case) [4]. In routes involving liquid water drop-out the impurities like CO_2 and H_2S may follow water from the first condensation.

Sensitivity analysis was made and the maximum allowable concentration of water, before the water drop out was analyzed for different systems.
The findings were that with the presence of H_2S in a system with CH_4 and CO_2 the hydrate formation process could be faster i.e. the maximum allowable water concentration which can

be permitted in a gas stream (CH_4) during transportation of gas decreased with increasing pressures as well as for the concentration of H_2S as compared to a system with only CH_4 and CO_2. Hence it can be observed from the results how even a small amount of H_2S is able to affect the limit of water concentration in the gas stream.

Acknowledgements

Firstly, I would sincerely like to thank my supervisor, Professor Bjørn Kvamme, for his invaluable support and guidance throughout the whole period of this thesis work. I consider myself very lucky to have worked under his able guidance and would like to thank him for all his efforts, encouragement and his invaluable feedback on this thesis in spite of his very busy schedule.
I am really short of words to express my feelings as to how much I appreciate his effort. He truly is an inspiration.

I am deeply thankful to Khuram Baig, Lance and Muktikanta Sahoo for their timely assistance and help.
I would also like to express my gratitude to all my fellow classmates Jan, Aruna, Neda, and Jaime, for providing a very friendly and pleasant environment during my study period.

Finally a heartfelt thank you to my family specially my husband Alok and my son Aryan for their unconditional support, understanding and love.

Anuli A Kulkarni

Bergen, October 2014

Contents

Abstract 1
Acknowledgements 4
Contents 5
List of Figures 7
List of Tables 10
1. Introduction and history of hydrates 12
1.1 Definition of project and choice of scientific methods 16
1.2 Hydrate Structures and basic properties. 18
1.3 Hydrates in industry 22
1.4 Hydrates in nature 25
1.5 Kinetics of hydrate formation 26
1.6 Gibbs phase rule 29
2. Thermodynamics 31
2.1 Free energy 31
2.2 Equilibrium thermodynamics 32
2.3 Fluid thermodynamics 33
2.4 Aqueous thermodynamics 34
2.5 Hydrate thermodynamics 35
3. Phase envelope 38
4. Routes to hydrate formation 40
4.1 Route 5: Formation of hydrate from dissolved water and impurities in methane 44
4.2 Route 6 and route 10: Formation of hydrate from condensed water and hydrate formers from methane stream. 45
4.3 Route 9: Adsorbed water on rust forms hydrate with adsorbed hydrate formers 47
5. Results and discussion 49
5.1 Verification of the model systems for hydrate equilibrium 53
6. Sensitivity analysis 59
6.1 End-point sensitivity analysis 59
6.2 Equations used for calculation of sensitivity factors A,B,C 61
6.3 Sensitivity analysis with the inclusion of impurities H_2S and CO_2 71
6.4 Estimates for sensitivity analysis 71
6.4.1 Estimates for mole fraction of 0.001 H_2S 71
6.4.2 Estimates for mole fraction of 0.01 H_2S 78

6.4.3 Estimates for mole fraction of 0.1 H_2S 84
6.4.4 Density and compressibility table for model systems 93
6.5 Analysis of results 105
6.5.1 Case 1 (System 2.1.1: 0.01 Y_{CO2}, 0.001 Y_{H2S} remaining Y_{CH4} and System 2.3.4:...105
6.5.2 Case 2 (System 2.1.1: 0.01 Y_{CO2}, 0.001 Y_{H2S} remaining Y_{CH4} and System 2.1.4:.107
6.5.3 Case 3 (System 2.1.1: 0.01 Y_{CO2}, 0.001 Y_{H2S} remaining Y_{CH4} and System 2.3.1:...109
7. Discussion 113
8. Conclusions 116
9. Proposals for future work. 117
9.1 Kinetic modelling 117
9.2 Application of theory to other solid surfaces 117
9.3 Addition of more impurities 118
9.4 Transport of liquids 118
9.5 Account for dissolved sour gases 118
References 119
Nomenclature 121

List of Figures

FIGURE 1: SCHEMATIC ILLUSTRATION OF THE FACTORS THAT ARE NEEDED FOR FORMATION OF GAS HYDRATE [8], MODIFIED BY [ANULI KULKARNI] 15

FIGURE 1.1: SCHEMATIC ILLUSTRATION OF THE STRUCTURE OF GAS HYDRATES [14] 21
FIGURE 1.2: ILLUSTRATION OF THE UNIT CELL AND CAVITIES OF HYDRATE STRUCTURE I [2] 21
FIGURE1.3: SCHEMATIC ILLUSTRATION OF HYDRATE BLOCKAGE FORMATION IN A GAS DOMINATED PIPELINE [2]. 24
FIGURE 1. 4: SCHEMATIC ILLUSTRATION OF TYPICAL GAS-PIPELINE TRANSPORT SYSTEM [1]. 24
FIGURE 1.5 : A QUALITATIVE ILLUSTRATION OF INDUCTION TIME AND MASSIVE GROWTH. [2]..... 28

FIGURE 3.1: QUALITATIVE ILLUSTRATION OF A TYPICAL PHASE ENVELOPE [1]. 39

FIGURE 4. 1 : ILLUSTRATION OF VARIOUS ROUTES LEADING TO HYDRATE FORMATION [8],MODIFIED BY [ANULI KULKARNI] 43

FIGURE 5.1 : PHASE ENVELOPE FOR A TERNARY SYSTEM, MOLE FRACTION FOR CH_4: 0.8765 , CO_2 : 0.074 49
FIGURE 5.2 : PHASE ENVELOPE FOR A TERNARY SYSTEM, MOLE FRACTION FOR CH_4: 0.8245 , CO_2 : 0.1077 50
FIGURE 5. 3 : PHASE ENVELOPE FOR A TERNARY SYSTEM, MOLE FRACTION FOR CH_4: 0.8291 ,CO_2 : 0.0716 AND. 50
FIGURE 5.4 : PHASE ENVELOPE FOR A TERNARY SYSTEM, MOLE FRACTION FOR CH_4: 0.7771 , CO_2 : 0.0731 51
FIGURE 5.5 : PHASE ENVELOPE FOR A TERNARY SYSTEM, MOLE FRACTION FOR CH_4: 0.7548 ,CO_2 : 0.0681 51
FIGURE 5.6 : PHASE ENVELOPE FOR A BINARY SYSTEM, MOLE FRACTION FOR CH_4: 0.90 AND CO_2 : 0.10..... 52
FIGURE 5.7 : PHASE ENVELOPE FOR A BINARY SYSTEM, MOLE FRACTION CH_4 : 0.95 AND CO_2 : 0.05 52
FIGURE 5.8 : PHASE ENVELOPE FOR A BINARY SYSTEM, MOLE FRACTION $CH_{4:}$ 0.99 AND CO_2 0.01 53
FIGURE 5. 9 : ESTIMATED AND EXPERIMENTAL HYDRATE EQUILIBRIUM CURVE, FOR A SYSTEM OF 87.65% CH_4, 7.40% CO_2, 4.95% H_2S. (-) IS FOR ESTIMATED DATA AND (*) IS FOR EXPERIMENTAL DATA FROM [22]. 54
FIGURE 5.10 : ESTIMATED AND EXPERIMENTAL HYDRATE EQUILIBRIUM CURVE, FOR A SYSTEM OF 82.45% CH_4, 10.77% CO_2, 6.78% H_2S. (-) IS FOR ESTIMATED DATA AND (*) IS FOR EXPERIMENTAL DATA FROM [22]. 55
FIGURE 5.11 : ESTIMATED AND EXPERIMENTAL HYDRATE EQUILIBRIUM CURVE, FOR A SYSTEM OF 82.91% CH_4, 7.16% CO_2, 9.93% H_2S. (-) IS FOR ESTIMATED DATA AND (*) IS FOR EXPERIMENTAL DATA FROM [22]. 56
FIGURE 5.12 : ESTIMATED AND EXPERIMENTAL HYDRATE EQUILIBRIUM CURVE, FOR A SYSTEM OF 77.71% CH_4, 7.31%CO_2, 14.98% H_2S. (-) IS FOR ESTIMATED DATA AND (*) IS FOR EXPERIMENTAL DATA FROM [22]. 57
FIGURE 5. 13 : ESTIMATED AND EXPERIMENTAL HYDRATE EQUILIBRIUM CURVE, FOR A SYSTEM OF 75.48% CH_4, 6.81% CO_2, 17.71% H_2S. (-) IS FOR ESTIMATED DATA AND (*) IS FOR EXPERIMENTAL DATA FROM [22]. 58

FIGURE 6.1 : SCHEMATIC ILLUSTRATION OF END-POINT SENSITIVITY ANALYSIS. 60
FIGURE 6.2 : MAXIMUM WATER CONTENT BEFORE LIQUID WATER DROP OUT, FOR MOLE FRACTION OF 0.01 CO_2, 0.001 H_2S AND REMAINING GAS BEING $CH_{4.}$ CURVES ARE FROM TOP TO BOTTOM, FOR PRESSURES 50 BARS, 90 BARS, 130 BARS, 170 BARS, 210 BARS, 250 BARS. 72
FIGURE 6.3 : MAXIMUM WATER CONTENT BEFORE ADSORPTION ON HEMATITE, FOR MOLE FRACTION OF 0.01 CO_2, 0.001 H_2S AND REMAINING GAS BEING $CH_{4.}$ CURVES ARE FROM TOP TO BOTTOM, FOR PRESSURES 50 BARS, 90 BARS, 130 BARS, 170 BARS, 210 BARS, 250 BARS. 73

FIGURE 6.4 : MAXIMUM WATER CONTENT BEFORE LIQUID WATER DROP OUT, FOR MOLE FRACTION OF 0.025 CO_2, 0.001 H_2S AND REMAINING GAS BEING CH_4. CURVES ARE FROM TOP TO BOTTOM, FOR PRESSURES 50 BARS, 90 BARS, 130 BARS, 170 BARS, 210 BARS, 250 BARS. 74
FIGURE 6.5 : MAXIMUM WATER CONTENT BEFORE ADSORPTION ON HEMATITE, FOR MOLE FRACTION OF 0.025 CO_2, 0.001 H_2S AND REMAINING GAS BEING CH_4. CURVES ARE FROM TOP TO BOTTOM, FOR PRESSURES 50 BARS, 90 BARS, 130 BARS, 170 BARS, 210 BARS, 250 BARS. 75
FIGURE 6.6 : MAXIMUM WATER CONTENT BEFORE LIQUID WATER DROP OUT, FOR MOLE FRACTION OF 0.05 CO_2, 0.001 H_2S AND REMAINING GAS BEING CH_4. CURVES ARE FROM TOP TO BOTTOM, FOR PRESSURES 50 BARS, 90 BARS, 130 BARS, 170 BARS, 210 BARS, 250 BARS. 76
FIGURE 6.7 : MAXIMUM WATER CONTENT BEFORE ADSORPTION ON HEMATITE, FOR MOLE FRACTION OF 0.05 CO_2, 0.001 H_2S AND REMAINING GAS BEING CH_4. CURVES ARE FROM TOP TO BOTTOM, FOR PRESSURES 50 BARS, 90 BARS, 130 BARS, 170 BARS, 210 BARS, 250 BARS. 76
FIGURE 6.8 : MAXIMUM WATER CONTENT BEFORE LIQUID WATER DROP OUT, FOR MOLE FRACTION OF 0.1 CO_2, 0.001 H_2S AND REMAINING GAS BEING CH_4. CURVES ARE FROM TOP TO BOTTOM, FOR PRESSURES 50 BARS, 90 BARS, 130 BARS, 170 BARS, 210 BARS, 250 BARS. 77
FIGURE 6.9 : MAXIMUM WATER CONTENT BEFORE HYDRATE DROPS OUT, FOR MOLE FRACTION OF 0.1 CO_2, 0.001 H_2S AND REMAINING GAS BEING CH_4. CURVES ARE FROM TOP TO BOTTOM, FOR PRESSURES 50 BARS, 90 BARS, 130 BARS, 170 BARS, 210 BARS, 250 BARS. 78
FIGURE 6.10 : MAXIMUM WATER CONTENT BEFORE ADSORPTION ON HEMATITE, FOR MOLE FRACTION OF 0.1 CO_2, 0.001 H_2S AND REMAINING GAS BEING CH_4. CURVES ARE FROM TOP TO BOTTOM, FOR PRESSURES 50 BARS, 90 BARS, 130 BARS, 170 BARS, 210 BARS, 250 BARS. 78
FIGURE 6.11 : MAXIMUM WATER CONTENT BEFORE LIQUID WATER DROP OUT, FOR MOLE FRACTION OF 0.01 CO_2, 0.01 H_2S AND REMAINING GAS BEING CH_4. CURVES ARE FROM TOP TO BOTTOM, FOR PRESSURES 50 BARS, 90 BARS, 130 BARS, 170 BARS, 210 BARS, 250 BARS. 79
FIGURE 6.12 : MAXIMUM WATER CONTENT BEFORE ADSORPTION ON HEMATITE, FOR MOLE FRACTION OF 0.01 CO_2, 0.01 H_2S AND REMAINING GAS BEING CH_4. CURVES ARE FROM TOP TO BOTTOM, FOR PRESSURES 50 BARS, 90 BARS, 130 BARS, 170 BARS, 210 BARS, 250 BARS. 79
FIGURE 6.13 : MAXIMUM WATER CONTENT BEFORE LIQUID WATER DROP OUT, FOR MOLE FRACTION OF 0.025 CO_2, 0.01 H_2S AND REMAINING GAS BEING CH_4. CURVES ARE FROM TOP TO BOTTOM, FOR PRESSURES 50 BARS, 90 BARS, 130 BARS, 170 BARS, 210 BARS, 250 BARS. 80
FIGURE 6.14 : MAXIMUM WATER CONTENT BEFORE ADSORPTION ON HEMATITE, FOR MOLE FRACTION OF 0.025 CO_2, 0.01 H_2S AND REMAINING GAS BEING CH_4. CURVES ARE FROM TOP TO BOTTOM, FOR PRESSURES 50 BARS, 90 BARS, 130 BARS, 170 BARS, 210 BARS, 250 BARS. 81
FIGURE 6.15 : MAXIMUM WATER CONTENT BEFORE LIQUID WATER DROP OUT, FOR MOLE FRACTION OF 0.05 CO_2, 0.01 H_2S AND REMAINING GAS BEING CH_4. CURVES ARE FROM TOP TO BOTTOM, FOR PRESSURES 50 BARS, 90 BARS, 130 BARS, 170 BARS, 210 BARS, 250 BARS. 82
FIGURE 6.16 : MAXIMUM WATER CONTENT BEFORE ADSORPTION ON HEMATITE, FOR MOLE FRACTION OF 0.05 CO_2, 0.01 H_2S AND REMAINING GAS BEING CH_4. CURVES ARE FROM TOP TO BOTTOM, FOR PRESSURES 50 BARS, 90 BARS, 130 BARS, 170 BARS, 210 BARS, 250 BARS. 82
FIGURE 6.17 : MAXIMUM WATER CONTENT BEFORE LIQUID WATER DROP OUT, FOR MOLE FRACTION OF 0.1 CO_2, 0.01 H_2S AND REMAINING GAS BEING CH_4. CURVES ARE FROM TOP TO BOTTOM, FOR PRESSURES 50 BARS, 90 BARS, 130 BARS, 170 BARS, 210 BARS, 250 BARS. 83
FIGURE 6.18 : MAXIMUM WATER CONTENT BEFORE HYDRATE DROPS OUT, FOR MOLE FRACTION OF 0.1 CO_2, 0.01 H_2S AND REMAINING GAS BEING CH_4. CURVES ARE FROM TOP TO BOTTOM, FOR PRESSURES 50 BARS, 90 BARS, 130 BARS, 170 BARS, 210 BARS, 250 BARS. 83
FIGURE 6.19 : MAXIMUM WATER CONTENT BEFORE ADSORPTION ON HEMATITE, FOR MOLE FRACTION OF 0.1 CO_2, 0.01 H_2S AND REMAINING GAS BEING CH_4. CURVES ARE FROM TOP TO BOTTOM, FOR PRESSURES 50 BARS, 90 BARS, 130 BARS, 170 BARS, 210 BARS, 250 BARS. 84

FIGURE 6.20 : MAXIMUM WATER CONTENT BEFORE LIQUID WATER DROP OUT, FOR MOLE FRACTION OF 0.01 CO_2, 0.1 H_2S AND REMAINING GAS BEING CH_4. CURVES ARE FROM TOP TO BOTTOM, FOR PRESSURES 50 BARS, 90 BARS, 130 BARS, 170 BARS, 210 BARS, 250 BARS. 85
FIGURE 6.21 : MAXIMUM WATER CONTENT BEFORE HYDRATE DROPS OUT, FOR MOLE FRACTION OF 0.01 CO_2, 0.1 H_2S AND REMAINING GAS BEING CH_4. CURVES ARE FROM TOP TO BOTTOM, FOR PRESSURES 50 BARS, 90 BARS, 130 BARS, 170 BARS, 210 BARS, 250 BARS. 86
FIGURE 6.22 : MAXIMUM WATER CONTENT BEFORE ADSORPTION ON HEMATITE, FOR MOLE FRACTION OF 0.01 CO_2, 0.1 H_2S AND REMAINING GAS BEING CH_4. CURVES ARE FROM TOP TO BOTTOM, FOR PRESSURES 50 BARS, 90 BARS, 130 BARS, 170 BARS, 210 BARS, 250 BARS. 86
FIGURE 6.23 : MAXIMUM WATER CONTENT BEFORE LIQUID WATER DROP OUT, FOR MOLE FRACTION OF 0.025 CO_2, 0.1 H_2S AND REMAINING GAS BEING CH_4. CURVES ARE FROM TOP TO BOTTOM, FOR PRESSURES 50 BARS, 90 BARS, 130 BARS, 170 BARS, 210 BARS, 250 BARS. 87
FIGURE 6.24 : MAXIMUM WATER CONTENT BEFORE HYDRATE DROPS OUT, FOR MOLE FRACTION OF 0.025 CO_2, 0.1 H_2S AND REMAINING GAS BEING CH_4. CURVES ARE FROM TOP TO BOTTOM, FOR PRESSURES 50 BARS, 90 BARS, 130 BARS, 170 BARS, 210 BARS, 250 BARS. 88
FIGURE 6.25 : MAXIMUM WATER CONTENT BEFORE ADSORPTION ON HEMATITE, FOR MOLE FRACTION OF 0.025 CO_2, 0.1 H_2S AND REMAINING GAS BEING CH_4. CURVES ARE FROM TOP TO BOTTOM, FOR PRESSURES 50 BARS, 90 BARS, 130 BARS, 170 BARS, 210 BARS, 250 BARS. 89
FIGURE 6.26 : MAXIMUM WATER CONTENT BEFORE LIQUID WATER DROP OUT, FOR MOLE FRACTION OF 0.05 CO_2, 0.1 H_2S AND REMAINING GAS BEING CH_4. CURVES ARE FROM TOP TO BOTTOM, FOR PRESSURES 50 BARS, 90 BARS, 130 BARS, 170 BARS, 210 BARS, 250 BARS. 89
FIGURE 6.27 : MAXIMUM WATER CONTENT BEFORE HYDRATE DROP OUT, FOR MOLE FRACTION OF 0.05 CO_2, 0.1 H_2S AND REMAINING GAS BEING CH_4. CURVES ARE FROM TOP TO BOTTOM, FOR PRESSURES 50 BARS, 90 BARS, 130 BARS, 170 BARS, 210 BARS, 250 BARS. 90
FIGURE 6.28 : MAXIMUM WATER CONTENT BEFORE ADSORPTION ON HEMATITE, FOR MOLE FRACTION OF 0.05 CO_2, 0.1 H_2S AND REMAINING GAS BEING CH_4. CURVES ARE FROM TOP TO BOTTOM, FOR PRESSURES 50 BARS, 90 BARS, 130 BARS, 170 BARS, 210 BARS, 250 BARS. 90
FIGURE 6.29 : MAXIMUM WATER CONTENT BEFORE LIQUID WATER DROP OUT, FOR MOLE FRACTION OF 0.1 CO_2, 0.1 H_2S AND REMAINING GAS BEING CH_4. CURVES ARE FROM TOP TO BOTTOM, FOR PRESSURES 50 BARS, 90 BARS, 130 BARS, 170 BARS, 210 BARS, 250 BARS. 91
FIGURE 6.30 : MAXIMUM WATER CONTENT BEFORE HYDRATE DROPS OUT, FOR MOLE FRACTION OF 0.1 CO_2, 0.1 H_2S AND REMAINING GAS BEING CH_4. CURVES ARE FROM TOP TO BOTTOM, FOR PRESSURES 50 BARS, 90 BARS, 130 BARS, 170 BARS, 210 BARS, 250 BARS. 91
FIGURE 6.31 : MAXIMUM WATER CONTENT BEFORE ADSORPTION ON HEMATITE, FOR MOLE FRACTION OF 0.1 CO_2, 0.1 H_2S AND REMAINING GAS BEING CH_4. CURVES ARE FROM TOP TO BOTTOM, FOR PRESSURES 50 BARS, 90 BARS, 130 BARS, 170 BARS, 210 BARS, 250 BARS. 92

List of Tables

TABLE 2. 1: COEFFICIENT OF $\Delta G^{INCLUSION}$ IN CASE OF CARBON DIOXIDE INCLUSION. CRITICAL TEMPERATURE FOR CO_2 IS 304.13 K. AT PRESENT STAGE IT IS ASSUMED THAT NO CO_2 ENTERS THE SMALL CAVITY AND CORRESPONDINGLY IT IS 0(ZERO) FOR SMALL CAVITY. 36
TABLE 2. 2: COEFFICIENTS OF $\Delta G^{INCLUSION}$ IN CASE OF METHANE INCLUSION IN BOTH LARGE AND SMALL CAVITIES. CRITICAL TEMPERATURE FOR CH_4 USED AS REDUCING TEMPERATURE IS 190.56 K. 37
TABLE 2. 3: COEFFICIENT OF $\Delta G^{INCLUSION}$ FOR INCLUSION OF HYDROGEN SULFIDE. CRITICAL TEMPERATURE FOR H_2S IS 373.00 K. 37

TABLE 4. 1: ILLUSTRATION OF POTENTIAL HYDRATE PHASE TRANSITION SCENARIOS FOR A SYSTEM OF METHANE WITH IMPURITIES RELEVANT FOR TRANSPORTATION PIPELINE [11]. 42
TABLE 4. 2 : TABLE ILLUSTRATING WHICH COMPONENTS WILL HELP OR CONTRIBUTE IN THE PROCESS OF HYDRATE FORMATION FOR VARIOUS ROUTES. 44

TABLE 6.1: ESTIMATES FOR SENSITIVITY FACTOR A AT VARYING MOLE FRACTION OF CO_2.. TABLE SHOWS THE RELATIVE CHANGE (COMPARED TO BASE POINT) IN THE FACTOR A AT VARYING MOLEFRACTION OF CO_2 FOR THREE DIFFERENT ROUTES TO HYDRATE FORMATION. ALSO RELATIVE CHANGE IN SENSITIVITY FACTOR A FOR EACH HYDRATE ROUTE IS ESTIMATED. 62
TABLE 6.2 : ESTIMATES FOR SENSITIVITY FACTOR B AT VARYING PRESSURES. TABLE SHOWS THE RELATIVE CHANGE (COMPARED TO THE BASE POINT) IN FACTOR B, AT VARYING PRESSURES FOR THREE DIFFERENT ROUTES TO HYDRATE FORMATION. ALSO RELATIVE CHANGE IN SENSITIVITY FACTOR B FOR EACH HYDRATE ROUTE IS ESTIMATED. 63
TABLE 6.3 : ESTIMATES FOR SENSITIVITY FACTOR C AT VARYING TEMPERATURES. TABLE SHOWS THE RELATIVE CHANGE (COMPARED TO THE BASE POINT) IN FACTOR C, AT VARYING TEMPERATURES FOR THREE DIFFERENT ROUTES TO HYDRATE FORMATION. ALSO THE RELATIVE CHANGE IN SENSITIVITY FACTOR C FOR EACH HYDRATE ROUTE IS ESTIMATED. 64
TABLE 6. 4 : TABLE SHOWING WHEN WILL THE DEW POINT OCCUR AND AT WHAT POINT WILL THE HYDRATE FROM GAS BE FORMED, AT A PARTICULAR TEMPERATURE, PRESSURE AND MOLE FRACTION OF CO_2..... 65
TABLE 6. 5 : TABLE SHOWING WHEN THE HYDRATE POINT WILL OCCUR AND AT WHICH POINT WILL A DIRECT HYDRATE FORM AT A PARTICULAR TEMPERATURE, PRESSURE AND MOLE FRACTION OF CO_2 65
TABLE 6.6 : TABLE SHOWING WHEN WILL ADSORBED POINT OCCUR AND AT WHAT POINT WILL THE HYDRATE BE FORMED FROM ADSORBED SURFACE, AT A PARTICULAR TEMPERATURE, PRESSURE AND MOLE FRACTION OF CO_2 66
TABLE 6.7 : TABLE SHOWING THE SYSTEMS THAT WERE CONSIDERED FOR SENSITIVITY ANALYSIS..... 71
TABLE 6.8 : ESTIMATES FOR DENSITY (KG/M³) FOR A SYSTEM 2.1.1: CO_2 0.01. H_2S 0.001 AND REMAINING CH_4 .. 93
TABLE 6. 9 : ESTIMATES FOR COMPRESSIBILITY FACTOR Z FOR A SYSTEM 2. 1.1: CO_2 0.01. H_2S 0.001 AND REMAINING CH_4..... 93
TABLE 6. 10 : ESTIMATES FOR DENSITY (KG/M3) FOR A SYSTEM 2. 1.2 CO_2 0.025. H_2S 0.001 AND REMAINING CH_4 94
TABLE 6.11: ESTIMATES FOR COMPRESSIBILITY FACTOR Z FOR A SYSTEM2.1.2: CO_2 0.025. H_2S 0.001 AND REMAINING CH_4..... 94
TABLE 6.12 : ESTIMATES FOR DENSITY (KG/M³) FOR A SYSTEM 2. 1.3 CO_2 0.05. H_2S 0.001 AND REMAINING CH_4. 95
TABLE 6.13 : ESTIMATES FOR COMPRESSIBILITY FACTOR Z FOR A SYSTEM 2.1.3: CO_2 0.05. H_2S 0.001 AND REMAINING CH_4..... 95
TABLE 6. 14 : ESTIMATES FOR DENSITY (KG/M³) FOR A SYSTEM 2. 1.4 CO_2 0.1 H_2S 0.001 AND REMAINING CH_4... 96

TABLE 6.15 : ESTIMATES FOR COMPRESSIBILITY FACTOR Z FOR A SYSTEM 2.1.4: CO_2 0.1. H_2S 0.001 AND REMAINING CH_4 96
TABLE 6.16 : ESTIMATES FOR DENSITY (KG/M³) FOR A SYSTEM 2.2.1 CO_2 0.01. H_2S 0.01 AND REMAINING CH_4 97
TABLE 6.17 : ESTIMATES FOR COMPRESSIBILITY FACTOR Z FOR A SYSTEM 2.2.1 CO_2 0.01. H_2S 0.01 AND REMAINING CH4 97
TABLE 6.18 : ESTIMATES FOR DENSITY (KG/M³) FOR A SYSTEM 2.2.2: CO_2 0.025, H_2S 0.01 AND REMAINING CH_4 . 98
TABLE 6.19 : ESTIMATES FOR COMPRESSIBILITY FACTOR Z FOR A SYSTEM 2.2.2: CO_2 0.025. H_2S 0.01 AND REMAINING CH_4 98
TABLE 6.20 : ESTIMATES FOR DENSITY (KG/M³) FOR A SYSTEM 2.2.3: CO_2 0.05. H_2S 0.01 AND REMAINING CH_4 .. 99
TABLE 6.21 : ESTIMATES FOR COMPRESSIBILITY FACTOR Z FOR A SYSTEM 2.2.3: CO_2 0.05, H_2S 0.01 AND REMAINING CH_4 99
TABLE 6.22 : ESTIMATES FOR DENSITY (KG/M³) FOR A SYSTEM 2.2.4: CO_2 0.1. H_2S 0.01 AND REMAINING CH_4 .. 100
TABLE 6.23 : ESTIMATES FOR COMPRESSIBILITY FACTOR Z FOR A SYSTEM 2.2.4: CO_2 0.1, H_2S 0.01 AND REMAINING CH_4 100
TABLE 6.24 : ESTIMATES FOR DENSITY (KG/M³) FOR A SYSTEM 2.3.1: CO_2 0.01, H_2S 0.1 AND REMAINING CH_4 ... 101
TABLE 6.25 : ESTIMATES FOR COMPRESSIBILITY FACTOR Z FOR A SYSTEM 2.3.1: CO_2 0.01, H_2S 0.1 AND REMAINING CH_4 101
TABLE 6.26 : ESTIMATES FOR DENSITY (KG/M³) FOR A SYSTEM 2.3.2: CO_2 0.025, H_2S 0.1 AND REMAINING CH_4 . 102
TABLE 6.27 : ESTIMATES FOR COMPRESSIBILITY FACTOR Z FOR A SYSTEM 2.3.2: CO_2 0.025, H2S 0.1 AND REMAINING CH_4 102
TABLE 6. 28 : ESTIMATES FOR DENSITY (KG/M³) FOR A SYSTEM 2.3.3: CO_2 0.05, H_2S 0.1 AND REMAINING CH_4 . 103
TABLE 6.29 : ESTIMATES FOR COMPRESSIBILITY FACTOR Z FOR A SYSTEM 2.3.3: CO_2 0.05, H_2S 0.1 AND REMAINING CH_4 103
TABLE 6.30 : ESTIMATES FOR DENSITY (KG/M³) FOR A SYSTEM 2.3.4: CO_2 0.1, H2S 0.1 AND REMAINING CH_4 104
TABLE 6.31 : ESTIMATES FOR COMPRESSIBILITY FACTOR Z FOR A SYSTEM 2.3.4: CO_2 0.1, H_2S 0.1 AND REMAINING CH_4 104

1. Introduction and history of hydrates

Hydrates are crystalline compounds in which hydrogen bonded water enclatherate one or more type of `guest' molecules inside cavities [2]. Small gas molecules such as CO_2, N_2, H_2S and CH_4 get trapped inside cages formed by hydrogen bonded water molecules. Natural gas hydrates are highly flammable and hence they are known as "the ice that burns". Massive hydrates that outcrop the sea floor have been reported in the Gulf of Mexico [5] and several other places around the world. The energy contained in hydrates is very large.

Hydrates can be formed only under the presence of the following as depicted in figure 1 below.

- Water
- High pressure
- Low temperature
- A phase containing hydrate formers

Hydrate formers are limited size molecules that enter the cavities created by hydrogen bonded water molecules. The size is limited by available volume inside the cavities and the molecules that enter the cavities are called as guests molecules. The guest molecules can come from separate gas or liquid from solution in the water phase or from adsorbed state on solid surfaces. Under the absence of even one of the above properties, a hydrate cannot be formed.

In this project the guest molecules considered are methane (CH_4), carbon dioxide (CO_2) and hydrogen sulphide (H_2S).

The global demand and utilization of natural gas and its major component (methane) is in the increase due to its abundant availability. Methane is a simple chemical molecule, having the formula CH_4 and it is the principal component of natural gas. Complete combustion of methane in presence of oxygen produces carbon dioxide and water. Natural gas is used domestically and industrially. Natural gas is a gaseous fossil fuel found in oil fields, natural gas fields, and coal beds. As one of the cleanest, safest, and most useful of all energy sources, it is a vital component of the world's supply of energy. Natural gas is the result of the decay of animal remains and plant remains ***(organic debris)*** that has occurred over millions of years [6].

Two types of natural gas occurrences are present:-

- Natural gas from biogenic origin
- Natural gas from thermogenic origin

Biogenic hydrocarbon gases (which are >99% methane) are those produced due to the action of bacteria on the organic debris, accumulating in the sediments [1] and are usually generated a few tens of meters below the seabed.

In contrast, occurrence of thermo genic hydrocarbon gases usually occurs at the sea sub bottom depths exceeding 1000 m [7]. The overall mass is insoluble and constitutes kerogens (which are derived from organic matter) [1].

Natural gas hydrates were first discovered by Sir Humphrey Davy in 1810. He commented briefly on chlorine (oxymuriatic gas) in the Bakerian lecture to the Royal Society that the solution of oxymuriatic gas in water freezes more readily than pure water [2]

Joseph Priestly in 1778 performed an experiment in his laboratory, leaving the window open on that winter night before departing, and when he returned next morning, he found out that SO_2 could soak water and could cause it to freeze. In this experiment, SO_2 made hydrate with water below freezing point [8].

But these experiments did not attract much attention and gas hydrates remained only as a laboratory curiosity.

A major revolution came in 1934 when E.G Hammer Schmidt discovered plugging in the gas pipelines caused by gas hydrates. Since then a lot of study and efforts have been put in prediction and prevention of gas hydrates in pipelines during transport and in process equipment's.

From the mid-1960`s till present the discovery of hydrate formation both in deep oceans and permafrost regions has gained much fame and lots of publications have been done [2].

Hydrates have been a source of problem in the energy industry because the conditions at which oil and gas are produced, transported and processed are frequently suitable for hydrate formation. [9]. Like the Troll plant in the north sea often involves separation at low temperature (-22^0 C) and pressure (69.9 bars), the primary factors for hydrate risk in troll plant would be, separators operating at pressures (89 bars) and temperature (8^0C to -22^0C), turbines operating at pressure (69 bars) and temperatures (9^0C to -22^0C) and compressors operating at pressures (69 bars to 250 bars) and temperatures (9^0C to 15^0C). Low temperature plants like for instance Snøhvit gas processing can have conditions of low temperature (-69 C) and pressure at around 70 bars [10].

Gas processing also involves transportation of gas at even high pressure up to 250 bars and temperature is often close to seafloor temperature (1 C to 6 C typically). This is posing a high

hydrate risk factor and it is necessary to evaluate the maximum content of water that can be accepted during transportation. As mentioned, rapid cooling of gas can promote rapid hydrate formation and this can happen in the event of an emergency shutdown, compressor or dehydrator failure [2]. Therefore study of hydrates is very important for assurance of smooth flow through the pipes and also for safety purposes [8] .

Today the oil and gas industry is more interested in hydrate risk management than complete hydrate prevention as hydrate risk analysis is more economical. Companies like Gassco which are responsible for safe and efficient transport of gas from the Norwegian continental shelf to Europe, are interested in new solutions for assurance of smooth flow of gas transport. As formation of hydrate plugs in the pipeline can cause the flow to be restricted in the pipeline and if not treated on time the hydrate plugs can further cause the pipeline to be blocked causing a serious issue.

For hydrate prevention in pipelines and in process equipment's several strategies are used like addition of thermodynamic inhibitors, kinetic inhibitors and anti aggloromerents, since this is outside the focus of this thesis this will not be discussed in detail, readers can refer to [2].

The main aim of this project is to bring more clarity to the most important possible events that can lead to hydrate formation and as such will dominate the hydrate risk evaluation and also to calculate the maximum allowable content of water that can be permitted in a gas stream under transportation. Detailed discussion on definition of the project with the choice of scientific methods used, is given in section 1.1

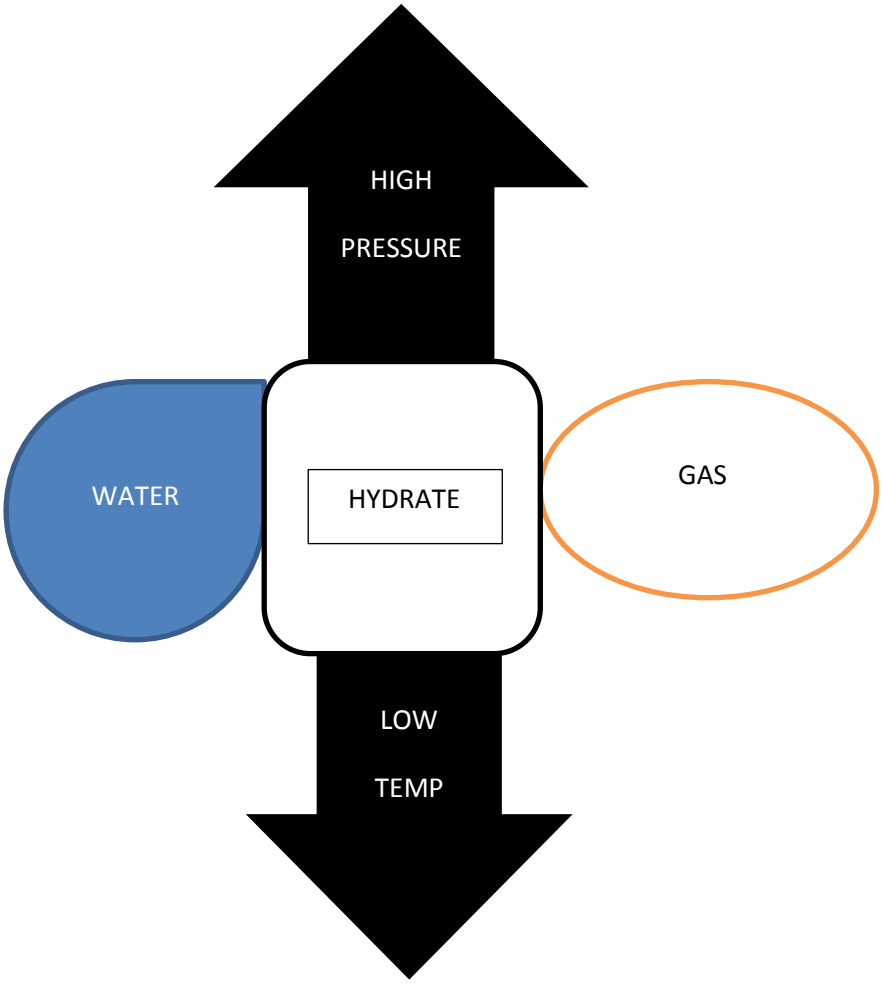

Figure 1: Schematic illustration of the factors that are needed for formation of gas hydrate **[8]**, modified by [Anuli Kulkarni]

1.1 Definition of project and choice of scientific methods

This section gives a detailed outline of the MSc project and the choice of scientific methods used for all the calculations.

Classical best practice for hydrate risk evaluation is based on 'dew-point calculations'. It does not cover all the relevant routes to hydrate formation and is over simplified, meaning only one route is considered, which is that water condenses out (dew point) and the condensed water forms hydrate with the hydrate formers from the gas phase. Recent work by [3] [11] suggests that water prefers to adsorb on rusty surfaces (pipelines) and hence makes an excellent site for hydrate formation. Ignoring this route and all other possible routes to hydrate formation can cost a lot of money to the oil and gas industry.

In this MSc project different possible routes to hydrate formation will be analyzed. This also includes impact of solid surfaces that can induce phase transitions. For transport in pipelines this is essentially rusty surfaces of the pipe-wall. The main aim of the study is to bring more clarity to the most important possible events that can lead to hydrate formation and as such will dominate the hydrate risk evaluation.

In this MSc project three different routes have been studied. The first of these routes involves water condensing out as liquid and then subsequently forming hydrate together with hydrate formers from the gas. As mentioned before this sequence of events is the most used basis for hydrate risk analysis in industry today.

A second possibility is that hydrate forms directly from water dissolved in the gas.

A third route involves the possibility that water can adsorb on the rusty walls and then hydrate can be formed from water which is slightly (1 nm) outside the wall, by extracting hydrate formers from the gas.

For more extensive overview of different possible routes, please refer to chapter 4 of this thesis.

Since the systems (water, gas, adsorbed phase and hydrate) generally cannot reach equilibrium, a primary tool for comparison will be free energy analysis. This type of analysis will also need to be based on same reference level for all components. This can be accomplished using chemical potentials for liquid water and empty hydrate structures based on molecular simulations as reported by Kvamme and Tanaka (1995) [12]. Gas or fluid phase will be based

on residual thermodynamics through the use of an equation of state Soave-Redlich-Kwong (SRK) in our case.

In summary the natural choice of method in free energy analysis is classical thermodynamics using residual thermodynamics (ideal gas as a reference state).

The software for this purpose is developed by Professor Bjørn Kvamme. In addition, external software from DTU (Danish Technical University) has also been utilized to determine thermodynamic properties of the gas mixture. These codes are in FORTRAN language and Microsoft developer has been used as compiler.

The primary focus in this thesis is

- Define the various routes to hydrate formation.
- Calculate the maximum allowable content of water for transport of natural gas through pipelines and process equipment.
- Sensitivity analysis.

.

1.2 Hydrate Structures and basic properties.

This section gives detailed information about the type of hydrate structures and its properties.

There are two most commonly found hydrate structures in the oil industry, these are Structure I (sI) and Structure II (sII) as proposed by E.D.Sloan and C.A.Koh. [2]. A third and a very rarely found hydrate structure is Structure H (rare hexagonal structure) as proposed by [13],

Structure I: -

The type I structure is cubic crystalline in shape, it forms two types of cages, one small and one large cage.

The unit cell of structure I consists of 46 water molecules. In a unit there will be two large cages versus six small cages. The small cages form the shape of a pentagonal dodecahedron as it has the shape of a 12 sided cavity with 12 pentagonal faces in each side and the larger cage has the shape of a tetra decahedron, as it has the shape of a 14 sided cavity with 12 pentagonal faces and 2 hexagonal faces.

Type I/Hydrates of structure I are formed with guests molecules having diameter between 4.2 and 6 Å. Typically guests molecules such as carbon di oxide (CO_2), Methane(CH_4), Hydrogen sulphide(H_2S) [2].

Structure II:-

The type II structure also forms two types of cages small cage and large cage.

In a unit there will be 16 small cages and 8 large cages. The small cages form the shape of a pentagonal dodecahedron (5^{12}) and the large cage forms the shape of hexagonal decahedron. It has a 16 sided cavity, with 12 pentagonal faces and 4 hexagonal faces. (5^{12}, 6^4).

Type II/Hydrates of structure II are formed by small guest molecules of O_2 and N_2 having diameter less than 4.2Å and by large guest molecules like propane or isobutene having diameter between 6Å to 7Å [2].

Structure H:-

The structure H forms three types of cages, two small cages and one huge cage. Structure H is not very common. It is formed with larger guest molecules such as iso-pentane or neo-hexane, when accompanied by smaller molecules such as methane, hydrogen sulphide or nitrogen [2].

The main focus of this thesis is on hydrates forming mainly with methane (CH_4) containing impurities like carbon dioxide (CO_2) and hydrogen sulphide (H_2S).

The above guest molecules form hydrate structure (I). Therefore for this project structure I (sI) will only be considered with focus only on CH_4, CO_2 and H_2S as guest molecules.
CH_4 and H_2S enter both the small cavities and large cavities of structure I. CO_2 enters the large cavities and is not favored to enter the small cavities, due to its size and shape as compared to the available volume in the small cavity. CO_2 has a positive charge on C and negative charge on O. The oxygen in the cavity walls create an average negative field inwards and the rotation of CO_2 gives negative field outwards i.e. negative CO_2 field and negative cavity field results in repulsion and destabilization [8] .

In a dynamic situation or dynamic flow conditions, whether CO_2 will fill the small cavities is still unverified. Hence within the scope of work for this thesis, CO_2 in small cavities is neglected. H_2S on the other hand enters both the small cavity and large cavities of structure I and has a large stabilization impact on these cavities. This is because it has an average positive charge outwards from the center of mass.
H_2S has a positive charge on H and negative charge on S. On an average, oxygen in the cavity walls creates an average negative filed inwards i.e. negative wall field rotation of H_2S inside the cavity gives a positive field outwards to the cavity walls. Hence negative wall field and positive H_2S field results in attraction and stabilization of the cavity [8] [2].

Since the structure (I) is the hydrate structure of our interest, some more details on this structure is given below for a better understanding.
As shown in figure 1.2, two small cages are located at the center of the unit cell, having one water molecule at each of its 20 vertices. Each large cavity adds up-to 24 water molecules and together there are 46 water molecules in a unit cell.

The small cavities are almost spherical in shape and the distance from oxygen molecules in water to the center of the cavity is 3.95Å. The larger cavities are slightly oblate and the distance from oxygen to the center of cavity varies between 4.04Å and 4.65Å. It is the small dimensional difference between the average cavity radius in different structures (s (I) and s (II)) that determines the size of the occupant. [2]

Hence volume and shape of guest molecule plays an important role as it prevents the cavity from collapse [8].

Hydrates have distinct properties from that of ice and liquid water, for example electrical conductivity of hydrates is lower than corresponding conductivity for both ice and liquid. This isolation property is used in the technology for detecting hydrates.

Thermal conductivity of hydrates is lower than both liquid and ice.

Also, elasticity is increasing from ice to hydrate to liquid water and the most striking property of hydrates is that it can form at temperatures higher than 0^0C if the pressure is high enough, and thus the reason for concern and problem in the oil and gas industry, that water following the hydrocarbons can cause hydrates [8].

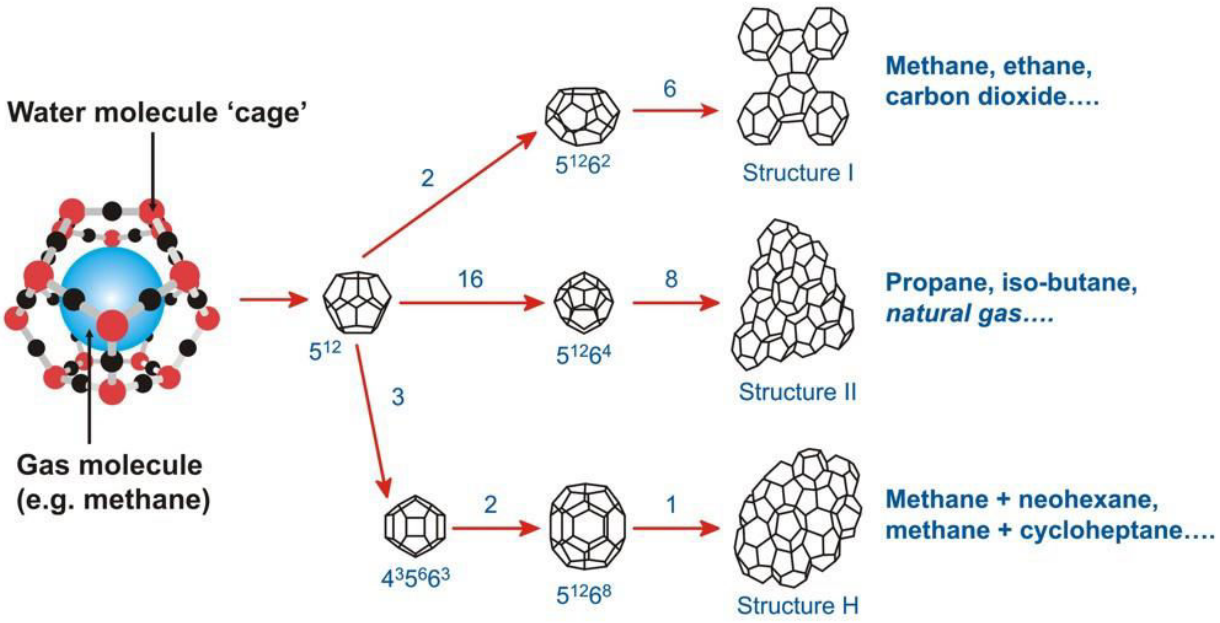

Figure 1.1: Schematic illustration of the structure of gas hydrates **[14]** .

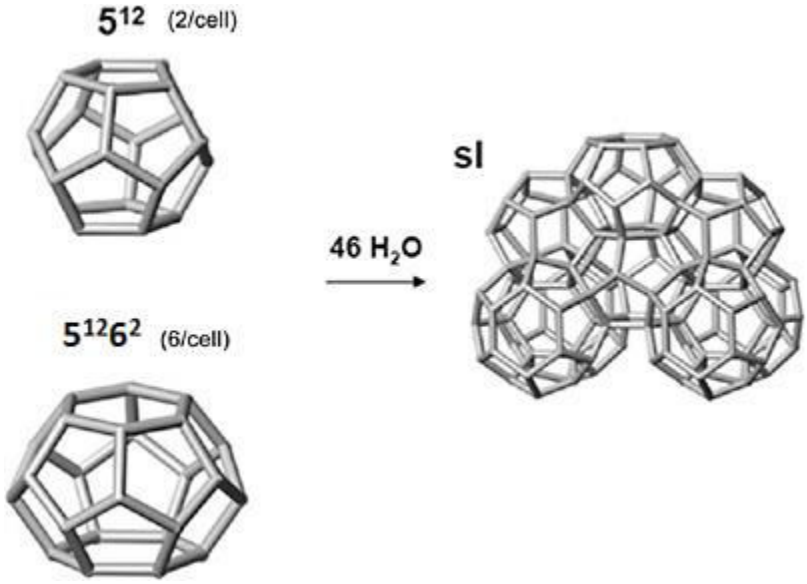

Figure 1.2: Illustration of the unit cell and cavities of hydrate structure I **[2]** .

1.3 Hydrates in industry

This section gives information about hydrates in the industry and since the focus of this thesis is on hydrates forming in industrial processing and transport, with specific focus on transport of natural gas, hence only hydrate formation during transportation will be discussed in detail.

With the growth of natural gas transport by pipeline, it has led to the establishment of a large network of pipelines throughout the world [1]. A typical gas-pipeline transport system is shown in figure (1.4)

The main steps in a gas-pipeline transport system are.

1. Collection of streams from the wells.
2. Processing of the gas produced to meet the transport specifications such as separation of heavier hydrocarbons and dehydration to prevent condensation, hydrate formation and corrosion.
3. Compression of the gas if the wellhead pressure becomes lower than the pressure required for transporting the gas.
4. Pipeline transport.
5. Recompression during transport, if the distance is long, to counteract the effect of pressure drop.
6. Further treatment, if necessary to adjust the gas to the distribution specifications.
7. Storage and transfer to the distribution network.
8. Gas distribution [1].

The processing of natural gas is necessary so as to ensure that the intended separation of gas is achieved and also to ensure that the natural gas intended for use is clean and environmentally acceptable. Gas processing consists of separation of some of the components such as heavy hydrocarbons, non-hydrocarbons/ impurities (such as CO_2 and H_2S), and fluids (H_2O), to adjust the gas to transport or commercial specifications. [1]. Some natural gas components must be extracted either for reasons imposed by transport steps or to comply with commercial or regulatory specifications [1]. For specific purpose of this thesis removal of water which can lead to hydrate formation and corrosion in pipelines and process equipment's have been studied. The water is removed at the plant, but the gas will always contain some amount of water inherently and it is this water that can condense out from the gas and form hydrates.

Hydrates or hydrate plugs (solid masses of hydrates) are the result of abnormal flow line operations like a dehydrator failure or when an inhibitor injection is lost. Also when cooling occurs with flow across a restriction i.e. when water–wet gas expands rapidly through a valve or orifice or other restriction, hydrates form due to rapid cooling of gas caused by expansion.

When natural gas is transported through the pipelines raw natural gas components combined with unwanted components of gas such as CO_2, (H_2S) and H_2O from gas hydrates, which eventually plug the pipelines. As shown in fig.1.3.

Water in the pipeline is the water that follows with the gas as a result of production. Hydrate forms at the walls of the pipeline via vapor deposition. This is because of the heat transfer with the outside environment which is at a lower temperature than the gas. As the hydrate deposition grows, narrowing of the flow channel occurs.

A point comes where the hydrate wall deposit can no longer bear the stress of the combination of the flowing fluid together with the hydrate deposited weight and sheds from the wall. As the particles travel downstream, they bridge across the flow channel to from a plug with corresponding spikes and thereby obstructing the flow completely [2].

When allowed to grow unchecked, the hydrate can severely obstruct the flow, resulting in blockage of pipeline and potential damage to equipment [11] .

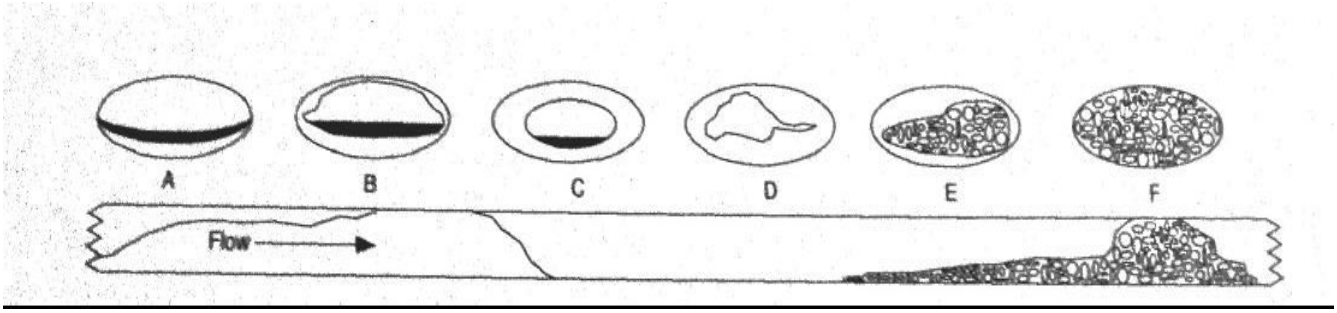

Figure1.3: Schematic illustration of hydrate blockage formation in a gas dominated pipeline **[2]**.

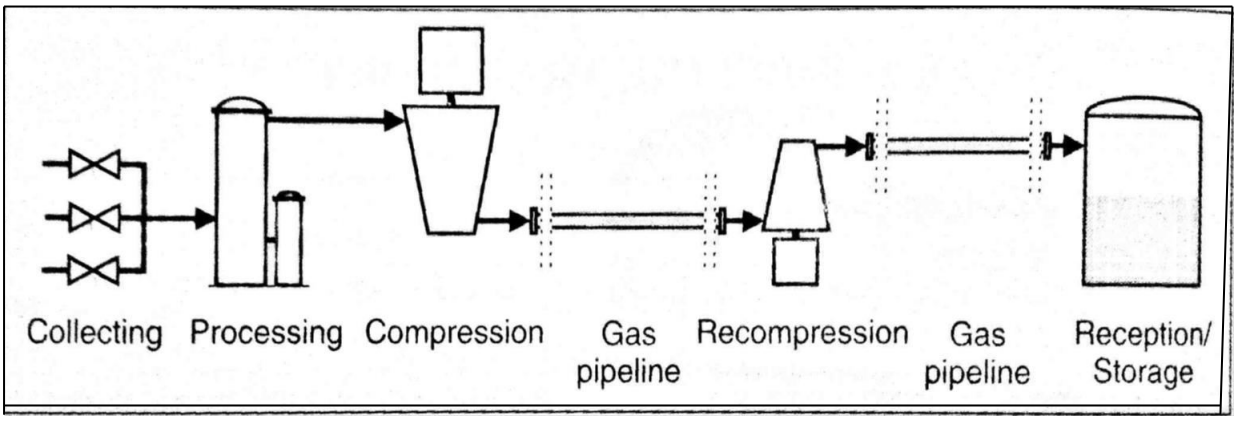

Figure 1. 4: Schematic illustration of typical gas-pipeline transport system **[1]**.

1.4 Hydrates in nature

This section is written to provide a basic understanding about hydrates in nature. Since the main focus of this thesis is on hydrates forming in industrial processing and transport, this section will not be discussed in detail.

It appears that hydrates in nature are ubiquitous, with some probability of occurrence wherever methane and water are in close proximity at low temperature and high pressure [2].

The energy in natural gas hydrate deposits is likely to be very significant as compared to all other fossil fuel deposits. Hence with the ever increasing need for energy it was very natural to turn the attention to exploit the energy stored in these gas hydrates.

The first gas hydrate deposits were found in the Messoyakha field in the Transarctic, on the western border of West Siberia [15].

The stability of gas hydrates is very much dependent on the local temperature and pressure but also on the concentrations of all the components in the surrounding phases. Hydrates in sediments are not stable, and this can be verified by the Gibbs phase rule and 1^{st} and 2^{nd} law of thermodynamics.

The vast quantities of hydrates in sediments pose a risk as geo hazard (collapse of geological structure due to hydrate dynamics).Any process that can lead to hydrate formation and dissociation will make the formations geo-mechanically unstable.

For example, an increase in the ocean temperature it leads to the reduction of the hydrate zone and hydrate dissociation which further leads to compaction of geological material.

In facture systems, supply of new hydrocarbons from below leads to hydrate formation.

Nature and industry generated processes lead to increase in the ocean temperature and fracture systems [8].

The most dynamic reservoirs are offshore so in global terms, most of the methane fluxes from hydrates are from offshore resources. But theses fluxes are buffered by the ocean and so it is still very questionable how large fluxes enter the earth's atmosphere in contrast to the leakages from tundra and permafrost region.

Methane is 20-25 times more aggressive than CO_2 in terms of greenhouse gas but the life time in atmosphere is lower for CH_4 (7-8 years) as compared to CO_2 (50-100 years) due to the density difference.

1.5 Kinetics of hydrate formation

Hydrates formation is divided into two stages which are well defined in terms of physics. The nucleation process (which is based one of the oldest theory still in use, the classical theory) and the growth stage. Hydrate nucleation is a process in which small clusters of water and gas (guest molecules) grow and detach/disperse to gain critical size for continuous growth. The critical size is the point at which the benefit (the total gain of hydrate growth dominates the penalty of pushing on the surroundings to get space) dominates and will increasingly do so. Since this process involves hundreds of molecules attaching and detaching to gain critical size, it is very difficult to observe. Critical size can be in the order of 1-5 nm and hardly measureable.
Once the critical size is reached the 'growth' starts i.e. the particles will continue to go uninhibited. The lower the change in the free energy the more rapid is the hydrate formation although it is dominated by the kinetics of mass transport.

A third stage which is not well defined is the Induction stage or the onset of massive growth. The induction is the time when the growth turns visibly fast i.e. it is the time until the solid formation is observed. It is important to understand that induction time does not mean that the hydrate is not starting to form. Nucleation is divided in to two types' homogeneous nucleation and heterogeneous nucleation.

Homogeneous nucleation occurs when all crystal formers enter the solid phase from the same original phase. Heterogeneous nucleation occurs on the interface between hydrate former phases. After the nucleation stage and the critical size has reached, crystals will grow uninhibited if there is a limited supply of mass, the growth stage will imply that the larger crystals will consume the smaller crystals [8].

In order to understand the mechanisms between the two stages it will be very useful to have a look at one of the most old and classical nucleation theory.
In this theory we consider that the nucleus is considered as a complete sphere, then the changes involved in the phase transition ΔG, can be given as

ΔGtotal = ΔG phase transition + ϒ * A Interface (1)

Free energy change. Benefit of the phase transition this is the penalty of pushing away surroundings

$$= \frac{4\pi r^3}{3} * \rho_n + \text{ɤ}.\ 4\pi r^2 \quad (2)$$

The above equation (2) is for spherical particles, where ρ_n is the molar density and n is number of molecules in the formed hydrate, r is the radius of the core. The above equation implies that ΔG reaches through a maximum at some radius r, this is the point of critical size at the turning point R^* (which is the minimum size for stable growth), the benefit dominates and continues to do so. This implies that at the turning point, the free energy gain of the phase transition turns over to dominate the total free energy change, over to the penalty of pushing away the surroundings i.e. pushing away the 'old phase' in order to give space for the new hydrate phase. As for the kinetic rates of hydrate growth in the classical theory, it is given by mass transport flux multiplied by Boltzmann constant. As for the associated heat transport, ΔH the heat added or removed during crystallization is kinetically related to the rate of conduction, convection and radiation [8].

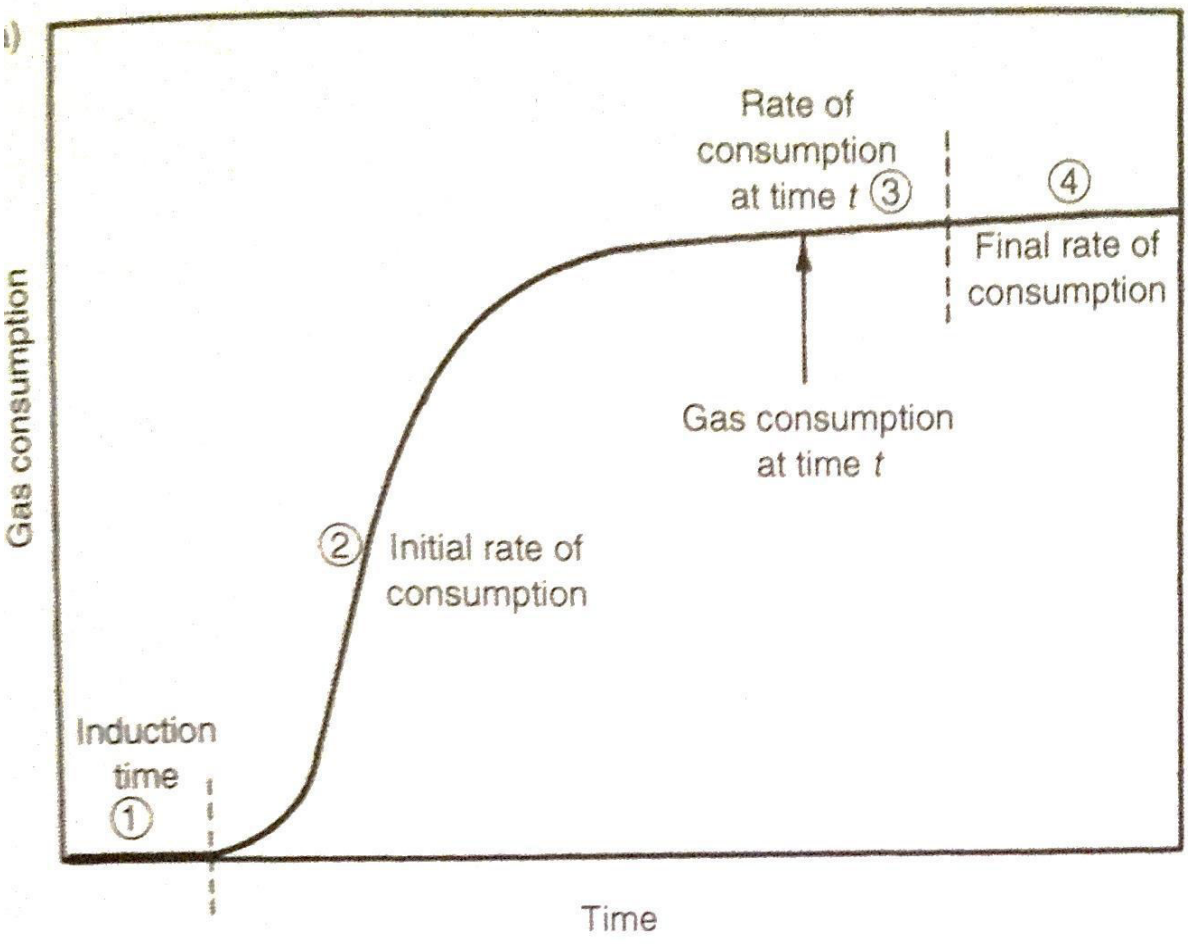

Figure 1.5 : A qualitative illustration of induction time and massive growth. **[2]**

1.6 Gibbs phase rule

A phase is a physically separable material in the system. It is possible to have more phases in the same state of matter (e.g., solid, liquid and gaseous).
Gibbs phase rule is a basic foundation used in thermodynamics for the determination of equilibrium. Basically Gibbs phase rule is just a balance of mass conservation under the constraints of equilibrium. What it tells is how many independent thermodynamic properties are needed to be defined, if the system has to reach equilibrium.

If the number of variables given by a natural situation is equal to this number of degrees of freedom (see below) then the system can reach equilibrium and corresponding equilibrium distribution of mass over the different phases can be calculated. The combined 1^{st} and 2^{nd} law of thermodynamics will always direct the system to have lowest free energy possible and if the Gibbs Phase rule cannot be fulfilled then this will be a dynamic situation, unless any of the phases are totally consumed and new Gibbs Phase rule indicates that equilibrium can now be reached.

It is necessary to know if a given system of hydrate in nature or industry can reach equilibrium or not. For this purpose the Gibbs phase rule, is used.

$$F = n - \boldsymbol{\pi} + 2 \qquad (3)$$

Where:-

F = number of variables that must be defined for equilibrium to be reached.

n = number of components.

π = number of phases.

If then F is greater than what is thermodynamically given, the system is underdetermined.

If F is less than what is given, the system is over determined [11].

Gibbs phase rule is just conservation of mass under the constraints of equilibrium.

In this case, number of components are 4, (methane (CH_4), carbon dioxide (CO_2), Hydrogen sulphide (H_2S), water (H_2O)), number of phases 4 (Fluid, adsorbed, liquid water and hydrate), F=2 (temperature and pressure defined).

This means:

2=4- 4 + 2,

2=2 since the defined parameters are 2 and F = 2. Hence we can see that system is at equilibrium, but this is not true in a dynamic situation as it is unlikely that a system can reach equilibrium due to the continues flow of gas in the pipeline.

2. Thermodynamics

This chapter gives a detailed overview of the thermodynamic functions required for the methods used for the analysis of various routes to hydrate formation. Much of the data in Section (2.1) can be found in [8] .

Hydrates are thermodynamically unstable (Gibbs phase rule). For any given phase transition (formation or dissociation), the minimum criteria for a hydrate to form is that the energy should be negative enough to overcome penalty, i.e. it overcomes the nucleation barsrier for creating space for a new phase. In the non-equilibrium situation the hydrate formed from different phases will have different free energies as the chemical potential of all the guest molecules will be different [11].

2.1 Free energy

Free energy is the 'available energy' that can be converted to do work. The conservation of energy gives rise to the 1st law of thermodynamics. The 2nd law of thermodynamics is the law of entropy, i.e. the system will always go towards maximum entropy. For an isolated system, combining the 1st and 2nd law gives the changes in the internal energy for the phase I,

$$dU^i \leq T^i\, dS^i - pdV^i + \sum_{i=1}^{n} \mu_i\, dN_l^i \qquad (4)$$

The summation runs for all the phases present i.e. i=1,2,3…...n. S is the entropy and $\mu_i\, dN_l^i$ is known as the chemical work i.e. it is the work required to put a molecule from one phase into the other, where N is the number of particles of a component. For all real and irreversible changes we have less than (<) sign. Using Legendre transforms by subtracting d (T^i S^i), for transformation of natural variables, we get Helmholtz free energy:

$$dA^i \leq -\, S^i\, dT^i - p^i\, dV^i + \sum_{i=1}^{n} \mu_i\, dN_l^i \qquad (5)$$

The above equation tells us that a system will always strike towards a minimum when subject to changes in T, V or N. Here, $p^i\, dV^i$ is the shaft work and it is not accessible because it is simply used internally to push fluids. The last term in the equation is the chemical work as explained above. Free energy can be termed as the available energy considering friction losses. For changes at constant pressure and temperature equation (4) and (5) gives:

$$dA^{i} \leq \sum_{i=1}^{n} \mu_i \, dN_i^i \quad (6)$$

For this system, reversible and irreversible processes are considered in this project. The process happens until a minimum total free energy is achieved and this can be written as

$$dA^{total} = 0 \quad (7)$$

$$dA^{total} = dA_{min}^{total} \quad (8)$$

This means that the difference in the free energy between two systems is the driving force, and the system will always strive towards minimum free energy. [10] [8] .

2.2 Equilibrium thermodynamics

Thermodynamic equilibrium is given when temperature, pressures and chemical potentials of all coexisting phases are uniform across all phase boundaries

$T^1 = T^2$ --- = T--------No net heat transport (9)

$P^1 = P^2$ --- = P--------Newton's law (10)

$\mu^1 = \mu^2$ ---- = μ-------No net chemical work (11)

To ensure the same reference values are used for free energy in all the phases, the calculations of chemical potential of all components in the different phases, ideal gas as a reference state has been used. Equation (12) and (13) and much of the data in section 2.2 can be found in [11]

$$\mu_i(T,P,\vec{y}) - \mu_i \text{ ideal gas } (T,P,\vec{y}) = RT \ln \phi_i (T,P,\vec{y}) \quad (12)$$

where ϕ_i is the fugacity coefficient for component I in given phase.

Here another reference state for the chemical potential of component i in liquid state, is also considered:

$$\mu_i(T,P,\vec{x}) - \mu_i \text{ ideal liquid } (T,P,\vec{x}) = RT \ln \gamma_i (T,P,\vec{x}) \quad (13)$$

$\lim \gamma_i = 1.0$ when $x_i \rightarrow 1.0$

where γ_i is the activity coefficient for component i in the liquid mixture.Note that equation (13) is used for water. The chemical potential of pure water has been calculated from models using molecular dynamics the data from Kvamme and Tanaka will be used [12].

2.3 Fluid thermodynamics

The chemical potential μ_i^{fluid} is given by

$$\mu_i(T,P,\vec{y})-\mu_i^{ideal\ gas}(T,P,\vec{y})=RT\ln \phi_i(T,P,\vec{y}) \quad (14)$$

Where $\mu_i^{ideal\ gas}(T,P,y)$ is the chemical potential of water in ideal gas, y is the mole fraction for component i (water in this case) in the fluid phase and can be calculated as:

$$\frac{x_w \gamma_w (T,P,\vec{x})\ \phi_w^{Pure\ gas}(T, P_w^{sat})\ P_w^{sat}(T)\ e^{\int_{P_i^{sat}}^{P}\frac{V_i}{RT}dP}}{\phi_w^{gas}(T, P, \vec{y})\ P} = y_w \quad (15)$$

In the above eqaution, the fugacity of pure water vapor at saturation pressure is approximated to unity and activity coefficient for liquid water is approximated to unity due to limited content of gas dissolved in water.Some caution on this latter approximation might be taken for substantial content of sour gases like CO_2 and H_2S. The poynting correction is aslo approximated to uniy. Hence equation (8) can be written as:

$$y_w - \frac{P_w^{sat}(T)}{\phi_w^{gas}(T, P, \vec{y})\ P} = 0 \quad (16)$$

$$y_w = \frac{P_w^{sat}(T)}{\phi_w^{gas}(T, P, \vec{y})\ P} \quad (17)$$

Equations (15), (16) and (17) and much of the data in section 2.3 can be found in [4], [16].

2.4 Aqueous thermodynamics

The chemical potential of component i in liquid state can be written as:

$\mu_i(T,P,\vec{x})-\mu_i$ ideal liquid $(T,P,\vec{x})=RT\ln \gamma_i (T,P,\vec{x})$ (18)

$\lim \gamma_i = 1.0$ when $x_i \rightarrow 1.0$

where γ_i is the activity coefficient for component i in the liquid mixture. Note that equation (above one) when used for water, the chemical potential of pure water has been calculated from models using molecular dynamics, the data from Kvamme and Tanaka will be used [12].

The chemical potential $\mu_i^{aqueous}$ of aqueous phase uses asymmetric excess thermodynamics or non symetric convention as reference state. This reference state is used in cases of gases with low solubilty in water and written as:

$$\boldsymbol{\mu}_i (T,P,\vec{x}) - \boldsymbol{\mu}_i^{\infty}(\mathbf{T},\mathbf{P},\vec{\mathbf{x}}) = RT \ln [\boldsymbol{x_i}\ \boldsymbol{\Upsilon}_i^{\infty}(\mathbf{T},\mathbf{P},\vec{\mathbf{x}})] \quad (19)$$

$\lim \gamma_i = 1.0$ when $x_i \rightarrow 0$

where $\mu_i^{\infty}(T)$ is the chemical potential of component i in water at infinite dilution. R is the universal gas constant. Υ_i^{∞} is the activity coefficient of component i in the aqueous solution in asymmetric convention, since the activity coefficient for the component i wil reach unity as its mole fraction becomes less.

The activity coefficient of water can be obtained from the Gibbs-Duhem relation [17]. (20)

The bulk of the actual pressure and temperature range corresponds to a liquid state for all the phases except the hydrate.In view of this thesis, the situations considered have very little solubilty or limited concentrations. The solubilty of H_2O in CH_4 is very low, the following approximation is used.

$$\boldsymbol{\mu}_{i,j} (T,P,\vec{x}) \equiv \mu_{i,j}^{\infty}(\mathbf{T},\mathbf{P}) + RT \ln [\boldsymbol{x}_{i,j}\ \boldsymbol{\Upsilon}_{i,j}^{\infty}(\mathbf{T},\mathbf{P},\vec{\mathbf{x}})] \quad (21)$$

where subscript j refers to components, subscript i denotes the phase.

Equations (18), (19) and (21) and much of the data in section 2.4 can be found in [4], [10].

2.5 Hydrate thermodynamics

The theory for hydrate thermodynamics used in this project is an extention of the theory based on Van der waals and platteuw's approach, as proposed by Kvamme and Tanaka. [12]

Applying the statistical mechanical model for water in hydrate, corresponding to an empty lattice of the structure, we get the following equation for chemical potential of water in hydrate as [12]:

$$\mu_w^H = \mu_w^{H,0} - \sum_{k=1,2} RT\, vi\, \ln(1 + \sum_i h_{ik}) \quad (22)$$

Where H denotes hydrate phase, $\mu_w^{H,0}$ denotes the chemical potential for water in an empty hydrate structure and h_{ik} is the cavity partition function of component k in the cavity type i.

The first sum is over cavity types and the 2nd sum runs over components i in cavity type k. vi is the fraction of cavity of type i per water molecules. Since the scope of this work only deals with hydrate structure I, it has 6 large cavities and 2 small cavities and 46 water molecules.Hence, 1/23 for small cavities and 3/23 for large cavities.

$$h_{ik} = e^{ß(\mu_i^H - \Delta g_{ik}^{inc})} \quad (23)$$

where ß is the inverse of the gas constant times temperature and Δg_{ik}^{inc} is the impact on hydrate water from inclusion of the guest molecules i in the cavity k .i.e. it is the free energy change of putting the molecule inside the cavity k. Since molecules like CH_4,CO_2,H_2S are large enough to have impact an impact on the libarsational movements, hence the cavity partition functions are intergrated on the basis that the water molecules are not fixed.Therefore the approach by Kvamme and Tanaka is used [12], [4].

The relation between mole fractions, filling fraction and the cavity partition function is given by

$$\theta_{ik} = \frac{x_{ik}^H}{v_k(1 - Xt)} = \frac{h_{ik}}{1 + \sum_i hik} \quad (24)$$

Where θ_{ik} is the filling fraction of component i in cavity type k, x_{ik}^H is the mole fraction of component i in cavity type k, x_t is the total mole fraction of all guests in the hydrate and v_k is the fraction of cavity per water of type k. At equilibrium, the chemical potential μ_i^H has to be identical to chemical potential of molecule i in the phase it has been extracted from [4].

For the purpose of this project guest molecules considered were CH_4, CO_2, and H_2S. Small cavities are occupied by CH_4 and H_2S and large cavities are occupied by CH_4, CO_2, and H_2S.

Free energies for guest inclusion i.e values for Δg_{ik}^{inc} for structure I (sI) are given below and are calculated as:

$$\Delta g^{inclusion} = \sum_{i=0}^{5} k_0 \frac{T_c}{T}$$

Where T_c is the critical temperature of the guest molecule [4].

Table 2. 1: Coefficient of $\Delta g^{inclusion}$ in case of carbon dioxide inclusion. Critical temperature for CO_2 is 304.13 K. At present stage it is assumed that no CO_2 enters the small cavity and correspondingly it is 0(zero) for small cavity.

k_i	Large cavity	Small cavity
k_0	14.852336735945610	0
k_1	2.707578918964229	0
k_2	-92.743171583430770	0
k_3	-5.077678397461901E-001	0
k_4	9.402639104940899	0
k_5	21.652443372670030	0

Although some different experimental evidence show that CO_2 enters the small cavity, during MD studies it has been found that there is no net stabilizing effect and for most CO_2 models that were tested the hydrate structure collapsed [4]. Therefore the inclusion of CO_2 in small cavities will not be considered in this project.

It does not mean that CO_2 will not be able to be "forced" into the small cavities but it still remains unverified if this would happen in dynamic flow situations to any significant extent.
So as far as practical hydrate predictions related to flow problems and corresponding dynamic situations are considered, it is not obvious that possible inclusion in small cavities needs to be included since the cavity partition function (equation (23)) might be close to zero anyway.

The free energy of inclusion in equation (23) can be estimated according to Kvamme and Tanaka [12] and Kvamme *et al* [11] for H_2S. Thermodynamic consistency has been a high priority throughout this work, and it was not our intention to adjust any parameters to fit experimental data.

Updated parameters for free energy of inclusion are given in tables 2.1 to 2.2.

Table 2. 2: Coefficients of $\Delta g^{inclusion}$ in case of methane inclusion in both large and small cavities. Critical temperature for CH_4 used as reducing temperature is 190.56 K.

k_i	Large cavity	Small cavity
k_0	17.971499327861170	-42.476832934435530
k_1	-23.440125959452020	119.241243535365700
k_2	-161.815346774489700	-183.195646307320200
k_3	45.205610253462990	128.392520963906600
k_4	36.672606092509880	-54.987841897868170
k_5	138.002169135313400	-78.556708653191480

Table 2. 3: Coefficient of $\Delta g^{inclusion}$ for inclusion of hydrogen sulfide. Critical temperature for H_2S is 373.00 K.

k_i	Large cavity	Small cavity
k_0	-9.867851530796533E-001	-35.841596491485960
k_1	-5.091001628046955E-001	75.644235713727100
k_2	-41.197126767481830	-49.924309029873280
k_3	-13.013675083152700	-31.868805469546190
k_4	5.462790477011296	-1.638643733127986
k_5	8.535406376549272	12.738557911032440

3. Phase envelope

This section deals with phase envelopes. A region in which two phases coexist in equlibrium is commonly referred to as the phase envelope or simply the two phase region.
The various important features of the phase envelope include the bubble point, dew point, bubble point curve, dew point curve,critical point [18].

First satge of a hydrate analysis would be to characterize the system in terms of number of co-existing phases for use in the Gibbs phase rule to establish whether equilibrium can be reached or not. In this picture, one also has to distinguish the hydrates which will be different because the composition of the hydrate former from a liquid and gas co-existing in the two-phase region is different.
So a hydrate forming liquid composition gives at least one unique hydrate phase while the gas gives at least one hydrate phase. It means that the most stable hydrates will form first so a hydrocarbon mixture will form first (as a consequence of 1^{st} and 2^{nd} law of thermodynamics) from those hydrocarbons that gives lowest free energy for the hydrate and then gradually towards methane hydrate.
Estimating the phase envlope for the hydrate fromer phase will enbale us to evaluate if the actual operating window of temperatures and pressures will enter the two phase region and if so what the compositions of the gas and liquid phases will be.

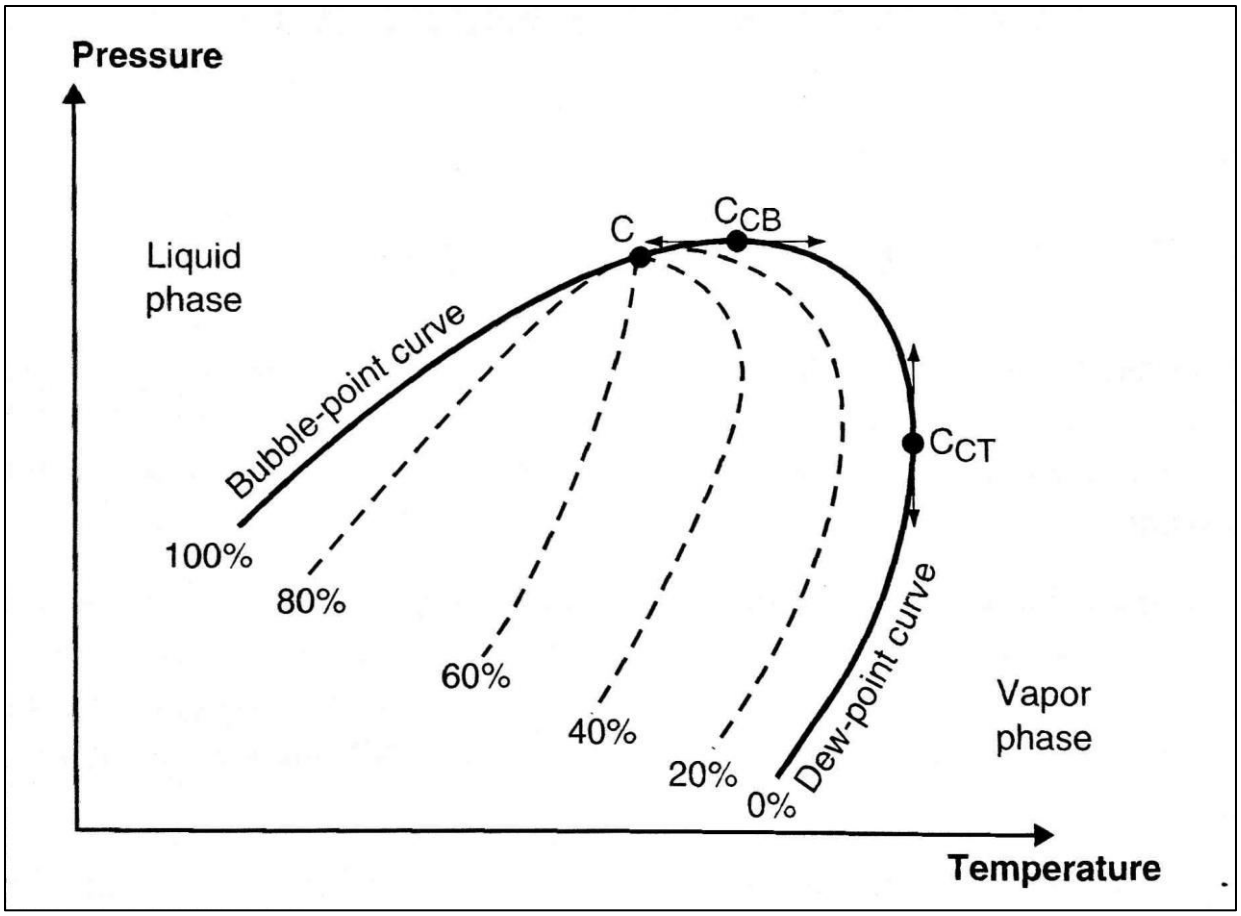

Figure 3.1: Qualitative illustration of a typical phase envelope **[1]**.

4. Routes to hydrate formation

For this thesis a system with CH_4 as the main fluid phase with impurities CO_2 and H_2S is considered. Originally no free water available is considered and only the water dissolved in CH_4 is considered. Systems of CH_4 with dissolved water can have several routes to hydrate formation as shown in table 2.1 and since the system is unable to reach equilibrium (Gibbs phase rule), the chemical potentials of each component in the different phases are different and different hydrates will have different free energies.

Due to the combined 1st and 2nd laws of thermodynamics the most stable hydrate will form first and as a consequence of this the composition of the forming hydrate will vary over time with the gradual change in the hydrate free energy [4].
A more stable hydrate will be unable to reform into a less stable hydrate and on the other hand a less stable hydrate will not be able to reform into a more stable hydrate without the access of new hydrate formers that will increase its stability. In a dynamic situation the latter option is more likely due to the continuous flow of fresh components from the gas stream. Hence it is unlikely that hydrate equilibrium can be reached during the transport of CH_4 with impurities [8].

Table 4.1 shows the potential hydrate phase transition scenarios for a system of methane with impurities relevant for transportation pipeline, based on free energy changes associated with the phase transitions.

$$\Delta G_{i=} \delta \left[x_w^{H,i}(\mu_w^{H,i} - \mu_w^{p}) + x_{gas}^{H,i}(\mu_{gas}^{H,i} - \mu_{gas}^{p})\right] \qquad (25)$$

In the above equation (3), 'H' denotes the hydrate phase, i denotes any of the phase transition, P indicates liquid, gas and adsorbed phases. X denotes the composition and μ is the chemical potential. Δ will be +1 for hydrate formation and -1 for hydrate dissociation.One should keep in mind that the hydrates created along the pathways in table 4.1 will have different filling fractions and corresponding different free energies, thus resulting in a unique phase [11].

There are various routes to hydrate formation as seen in Fig. 4.1, which gives a Schematic representation (a route map) to all the possible routes to hydrate formation. Depending on the

composition of the system considered, there can be many possibilities to hydrate formation. For example if route 5 is considered (shown in table 4.1 and corresponding figure 4.1). The formation of hydrate is due to dissolved water and impurities in methane. For this particular route water is a dominating factor so if $\mu_{Water}^{Hydrate} < \mu_{Water}^{CH4}$ then the hydrate will form. The impurities also play an important role in hydrate formation as seen in table 4.2. Table 4.2 represents the impurities that help in formation of hydrate, making the hydrate more stable.

The formation of hydrate via this route is strongly limited by mass transport. For more detailed analysis of each route, its formation criteria, mass transport limitations etc., please refer to sections 4.1, 4.2, 4.3 and table 4.1, table 4.1.

These sections describe various routes to hydrate formation [11]. Since the focus in this thesis is routes to hydrate formation, routes to dissociation will not be discussed. Hence the analysis will be limited to three of the possible routes to hydrate formation route [5, (6, 10), 9].

Table 4. 1: Illustration of potential hydrate phase transition scenarios for a system of methane with impurities relevant for transportation pipeline **[11]**.

i	δ	Initial phase(s)	Driving force	Final phase(s)
1	-1	Hydrate	Outside stability in terms of local P and/or T	Gas, Liquid water
2	-1	Hydrate	Sublimation (gas under saturated with water)	Gas
3	-1	Hydrate	Outside liquid water under saturated with respect to carbon dioxide and/or other enclathrated impurities originating from the carbon dioxide phase	Liquid water, (Gas)
4	-1	Hydrate	Hydrate gets in contact with solid walls at which adsorbed water have lower chemical potential than hydrate water	Liquid water, Gas
5	+1	Gas/fluid	Hydrate more stable than water and hydrate formers in the fluid phase	Hydrate
6	+1	Gas + Liquid water	Hydrate more stable than condensed water and hydrate formers from gas/fluid	Hydrate
7	+1	Surface reformation	Non-uniform hydrate rearranges due to mass limitations (lower free energy hydrate particles consumes mass from hydrates of higher free energy)	Hydrate
8	+1	Aqueous Phase	Liquid water super saturated with carbon dioxide and/or other hydrate formers, with reference to hydrate free energy	Hydrate
9	+1	Adsorbed	Adsorbed water on rust forms hydrate with adsorbed hydrate formers.	Hydrate
10	+1	Adsorbed +fluid	Water and hydrate formers from gas/fluid forms hydrate	Hydrate

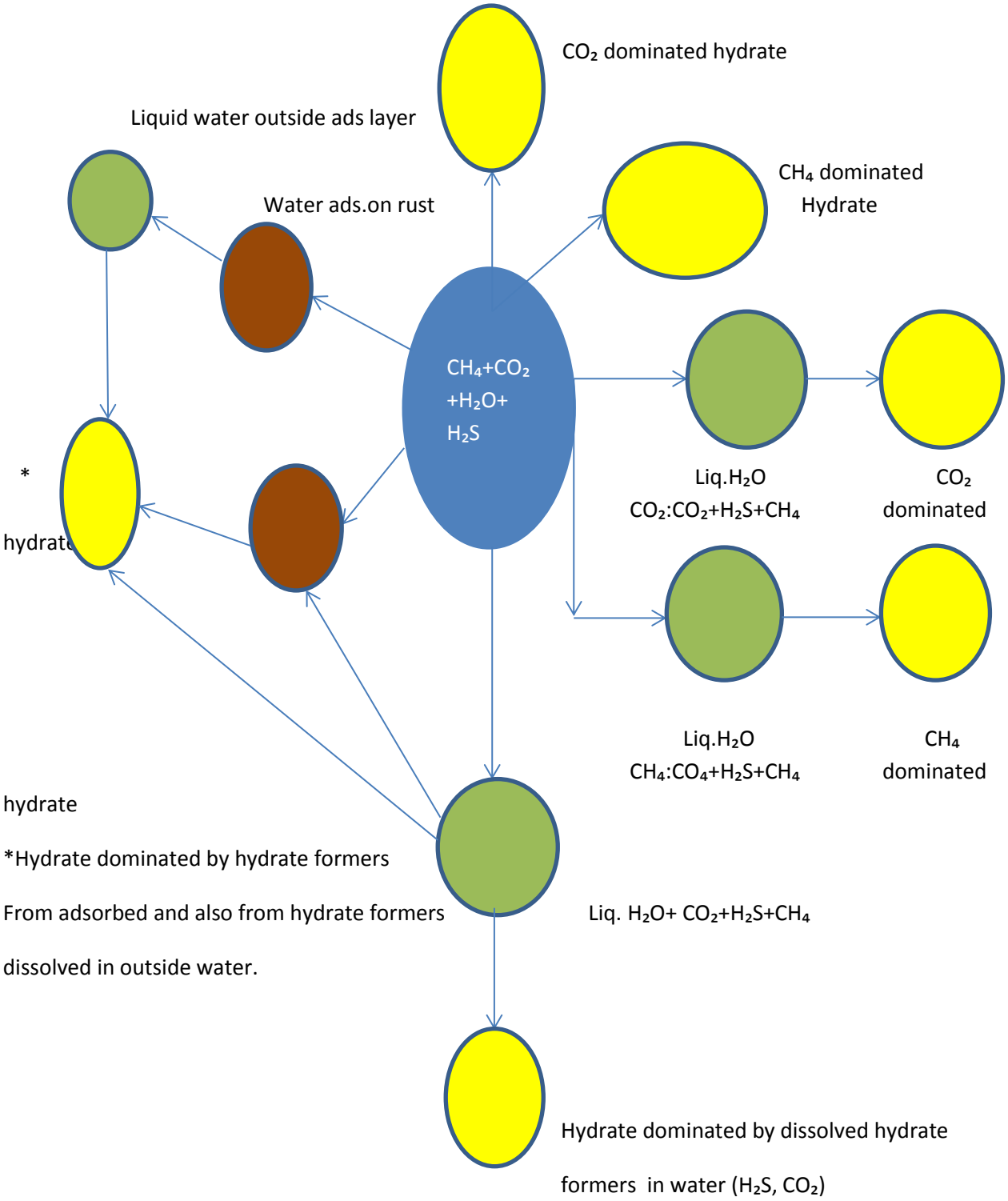

Figure 4. 1 : Illustration of various routes leading to hydrate formation [8],modified by [Anuli Kulkarni]

Below is a table which shows which components contribute in forming hydrate.

Table 4. 2 : Table illustrating which components will help or contribute in the process of hydrate formation for various routes.

	COMPONENTS		
ROUTE	**H2S**	**CO2**	**CH4**
5	X	X	X
6	X	X	X
8	X	X	X
9	X	X	X
10	X	X	X

4.1 Route 5: Formation of hydrate from dissolved water and impurities in methane

Let us consider a system of CH_4 with dissolved H_2O and impurities CO_2, H_2S. When hydrate is formed via this route (refer figure 4.1 and table 4.1) due to low temperature and high pressure, the system will already be in the hydrate formation and stability zone.

If $\mu_W^{Hydrate} < \mu_W^{CH4}$ then the hydrate will form.

Where superscript denotes the phase and subscript denotes the component and μ is chemical potential.

For direct hydrate forming from CH_4 fluid phase we have $\mu_W^{Hydrate} = \mu_W^{CH4}$ using equation (22) for chemical potential of water in hydrate and equation (12) for calculation of chemical potential of water in gas.

Hydrate formation has been found thermodynamically feasible but due to the mass transport limitations by water, it is still very questionable that if the hydrate can form as compared to other routes for hydrate formation under the same conditions [4].

The heat transport is limited for the hydrate formed via this route. This is due to the low heat conductivity and low heat convection.

4.2 Route 6 and route 10: Formation of hydrate from condensed water and hydrate formers from methane stream.

Route 6:- The criteria for hydrate formed via this route is (refer figure 4.1and table 4.1) the dew point. The dew point is defined as the point at which first microscopic droplets of water are condensed out. Therefore the hydrate formed via this route will be formed when water condenses out from the gas and the hydrate is formed then, together with the hydrate formers from the gas (CH_4 in this case). i.e. $\mu_{CH4}^{Hydrate} < \mu_{CH4}^{CH4}$

where superscript denotes the phase, subscript denotes the component and **μ** is chemical potential.

In the view of above, the limit at which water drops out as a separate phase in equilibrium with water dissolved in CH_4 is given by

$$\mu_{W}^{liquid} = \mu_{W}^{CH4}$$

where superscript denotes the phase and subscript denotes the component and **μ** is chemical potential. Liquid denotes water phase

To calculate $\mu_{W}^{CH_4}$, a reference state is required, the reference state used here is residual thermodynamics.

To calculate μ_{W}^{liquid} , a reference state is required. The reference state used is symmetric excess thermodynamics. But pure liquid water chemical potential is estimated using molecular simulations as reported by Kvamme and Tanaka(1995) [12].

Using equation (12) for water dissolved in CH_4 and equation (13) for liquid water. The equation for water that drops out is:

$$\frac{x_w \gamma_w (T,P,\vec{x}) \, \phi_{w}^{Pure\ CH4} (T, P_{w}^{sat}) \, P_{w}^{sat} (T) \, e^{\int_{P_w^{sat}}^{P} \frac{V_i}{RT} dP}}{\phi_{w}^{CH_4} (T, P, \vec{y}) \, P} = y_w \qquad (26)$$

$e^{\int_{P_i^{sat}}^{P} \frac{V_i}{RT} dP}$ = poynting correction it is normally 1.0 for large regions of pressure due to low molar volume of water. For approximate evaluation the activity coefficient of water is assumed to be unity. Also $\boldsymbol{P}_{\boldsymbol{w}}^{\boldsymbol{sat}}(T)$ is low enough such that the fugacity of pure gas in water is very close to unity, and activity coefficient are approximated to unity, due to the low content of water in the fluid phase. The expression for liquid drop out is given by

$$y_w - \frac{\mathbf{P}_{\mathbf{w}}^{\mathbf{sat}}(\mathbf{T})}{\emptyset_{\mathbf{w}}^{\mathbf{CH4}}(T, P, \vec{y})\, P} = 0 \qquad (27)$$

Using the symmetric excess thermodynamic formulation for liquid side and residual thermodynamics on the gas side equation 27 is given by

$$y_w = \frac{\emptyset_{\mathbf{w}}^{\mathbf{Pure\ liquid}}(\mathbf{T}, \mathbf{P})}{\emptyset_{\mathbf{w}}^{\mathbf{CH4}}(T, P, \vec{y})} \qquad (28)$$

For hydrate formed via this route there is little limit to mass transport.

Route 10:- The hydrate is formed from liquid water outside the adsorbed layer of water. The primary difference from route 6 is therefore the limit of water in the gas before adsorbing out and eventually creating a water layer thick enough to result in almost bulk water (3-4 water layers outside the rusty surface). Practically this only implies a water film in order of 1.2 nm of water.

$$\text{If } \mu_w^{Hydrate} < \mu_w^{liquid}$$

where superscript denotes the phase, subscript denotes the component and μ is chemical potential.

Route 6 and route 10 together represent the route to hydrate forming at the interface, i.e. hydrate forming form the gas side and hydrate forming from the liquid side. Mass transport across the interface gives instantly good access to water and CH_4 with some limitations.

Combining equation (13) for water in condensed liquid phase using symmetric access as a reference state with pure water chemical potential in ideal liquid water taken from Kvamme and Tanaka [12].

Using residual thermodynamics equation (12) for water dissolved in CH_4 gives an approximate water dew point concentration of water in CH_4 at given T and P. For the liquid water drop out combined mass balances and equilibrium for $\mu_{CH4}^{Hydrate} = \mu_{CH4}^{CH4}$ and $\mu_{w}^{Hydrate} = \mu_{w}^{liquid}$ can be solved.

It means inserting the chemical potential of H_2S, CH_4 and CO_2 in equation (12) and then into the below equation [4].

$$\mu_{\mathbf{W}}^{\mathbf{H,0}} - \sum_{\cdot} \mathbf{RT\ vk\ ln}(\ \mathbf{1} + \sum_{\mathbf{i}} \mathbf{h}_{\mathrm{ik})} = \boldsymbol{\mu}_{\mathbf{i,H2O}}^{\mathbf{pure\ water}}(\mathbf{T}, \mathbf{P}) + \mathrm{RT\ ln}\ [\mathbf{x_{i,H2O}}\ \Upsilon_{\mathbf{i,H2O}}(\mathbf{T}, \mathbf{P}, \mathbf{x})] \qquad (29)$$

If the conditions are met the hydrate will be formed. Equation (29) with SRK was used as equation of state for CH_4, CO_2, H_2S.

4.3 Route 9: Adsorbed water on rust forms hydrate with adsorbed hydrate formers

The hydrate formed through this route (refer figure 4.1 and table 4.1) is via adsorbed surfaces, hematite in our case.

If $\mu_{W}^{\mathrm{Adsorbed}} < \mu_{W}^{CH_4}$

Where superscript denotes the phase, subscript denotes the component and μ is chemical potential.

Then the hydrate is formed. The hydrate via this route is formed when water adsorbs on to the solid surfaces i.e. pipelines. Mass transport have no limitations in a dynamic situation.

Hydrate formation takes place at least 3-4 water molecules outside the surface. This is because the water is almost not related to the solid surface and behaves similar to liquid water. Therefore hydrate can form from water molecules which are slightly more than 1nm outside the surface and either from adsorbed hydrate former or hydrate former from CH_4 phase. [3] Similar to the dew point calculation, the adsorption point can be calculated as:

$$\boldsymbol{\mu}_{\mathbf{W}}^{\mathbf{Adsorbed}} = \mu_{\mathbf{W}}^{\mathbf{CH_4}} \qquad (30)$$

where superscript denotes the phase, subscript denotes the component and μ is chemical potential.

Using equation $\boldsymbol{\mu}_{\mathbf{W}}^{\mathbf{Adsorbed}}(T, P, \vec{x}_{ads}) = \boldsymbol{\mu}_{\mathbf{W,CH_4}}^{\mathbf{ideal\ gas}}(\mathbf{T}, \mathbf{P}, \vec{\mathbf{y}}) + RT \ln [\mathbf{y}_{\mathbf{W,CH_4}} \boldsymbol{\phi}_{\mathbf{W,CH_4}}(\mathbf{T}, \mathbf{P}, \vec{\mathbf{y}})]$ (31) for calculation of chemical potential of water in adsorbed surface and equation (12) for calculation of water in gas we get $Y_{H2O,}$ as minimum adsorption.

The chemical potential of water for the adsorbed phase was estimated from [3].The short range interactions between water and hematite used Buckingham type potential with parameters from de Leeuw and Cooper [19], Tsuzuki *et al* [20].

5. Results and discussion

The phase envelopes were generated using the software developed by Professor Bjørn Kvamme. In addition, external software from DTU (Danish Technical University) has also been utilized to determine thermodynamic properties of the gas mixture. The equation of state used was SRK equation of state [21]. The mixing rule used for this was a mix of binary and ternary mixtures of CH_4 and CO_2 and CH_4, CO_2 and H_2S $\Sigma\Sigma\ x_i\ x_j\ a_i\ a_j\ (1\text{-}k_{ij})$, where the interaction of the mixing coefficients were set to zero

Phase envelope for representative ternary mixtures calculated for experimental data [22], are given below (see figures 5.1 to 5.5), with some model examples for binary mixtures of CH_4 and CO_2 (refer figures 5.6 to 5.8).

Phase envelopes for ternary mixture of components CH_4,CO_2 and H_2S for different compositions.

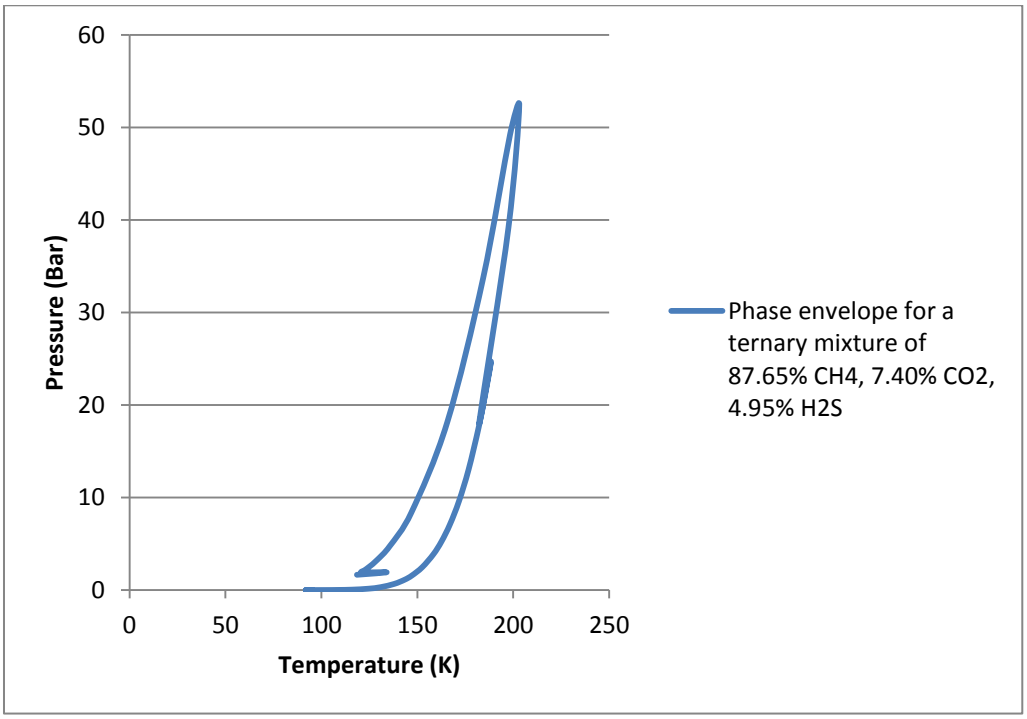

Figure 5.1 : Phase envelope for a ternary system, mole fraction for CH_4: 0.8765 , CO_2 : 0.074 and H_2S : 0.0495 **[22]**.

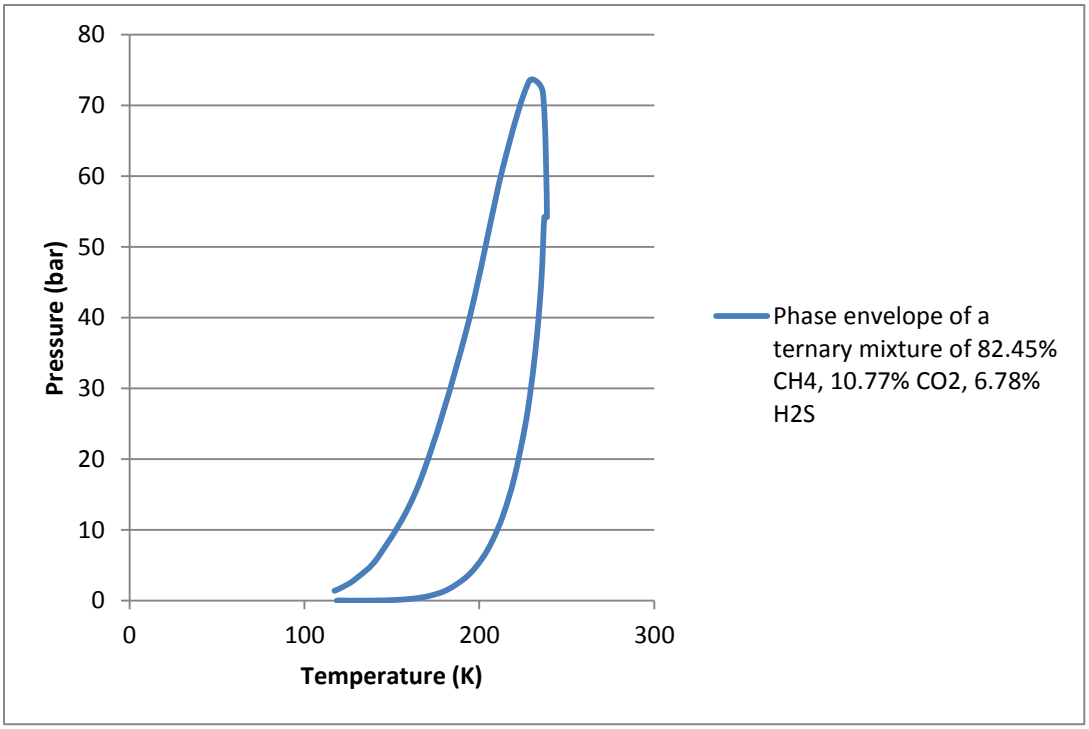

Figure 5.2 : Phase envelope for a ternary system, mole fraction for CH_4: 0.8245 , CO_2 : 0.1077 and H_2S : 0.0678 **[22]**.

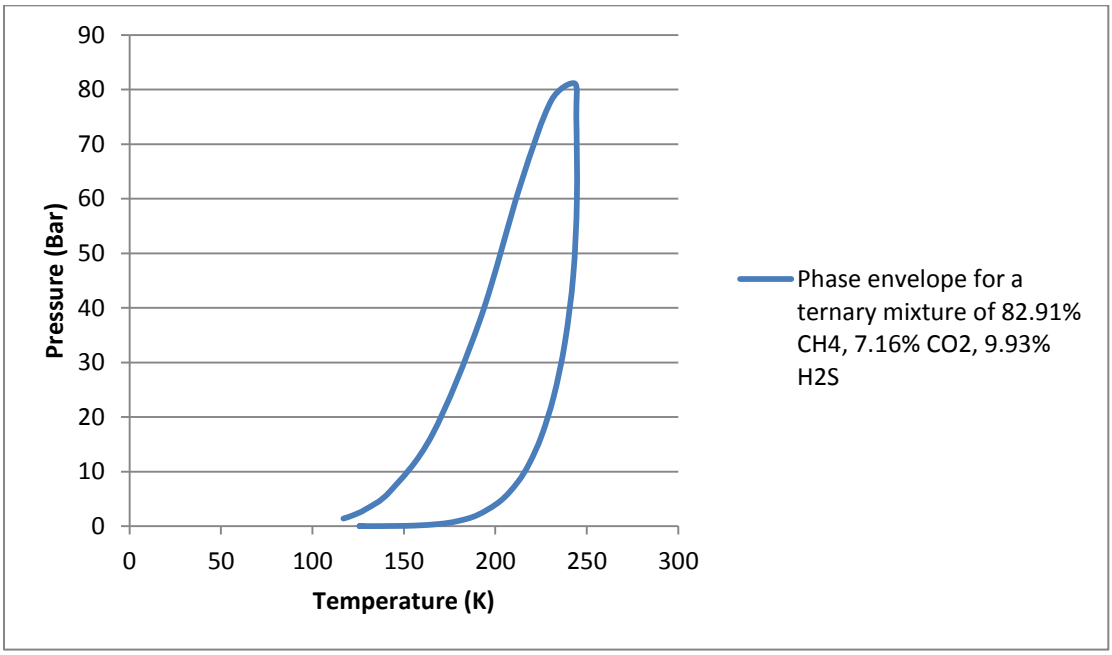

Figure 5. 3 : Phase envelope for a ternary system, mole fraction for CH_4: 0.8291 ,CO_2 : 0.0716 and H_2S : 0.0993 [22].

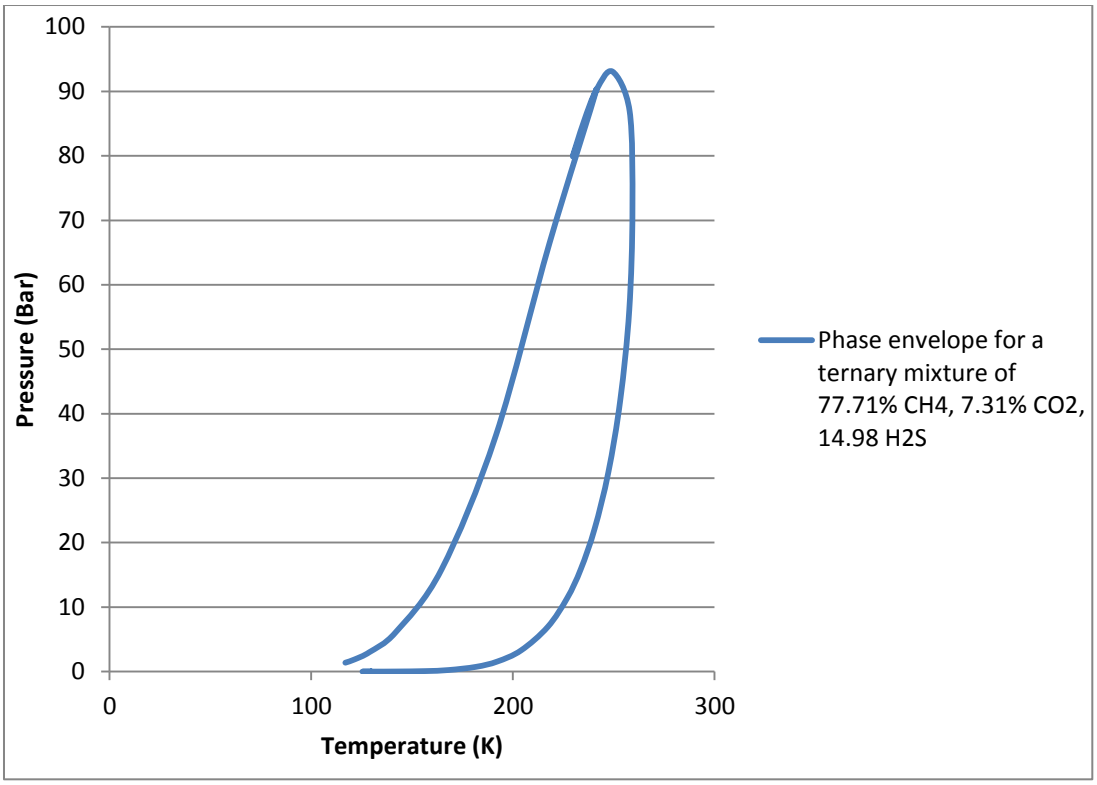

Figure 5.4 : Phase envelope for a ternary system, mole fraction for CH_4: 0.7771 , CO_2 : 0.0731 and H_2S : 0.1498 **[22]**.

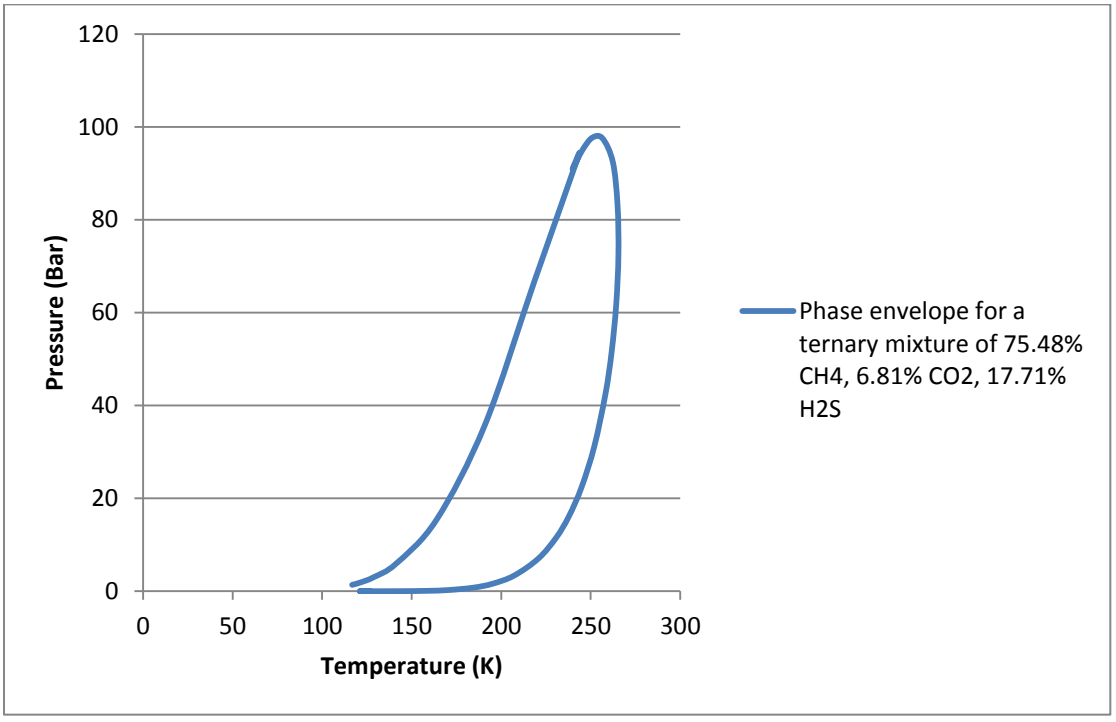

Figure 5.5 : Phase envelope for a ternary system, mole fraction for CH_4: 0.7548 ,CO_2 : 0.0681 and H_2S : 0.1771. **[22]**

Phase envelopes for binary mixture of components CH_4 and CO_2 for different compositions.

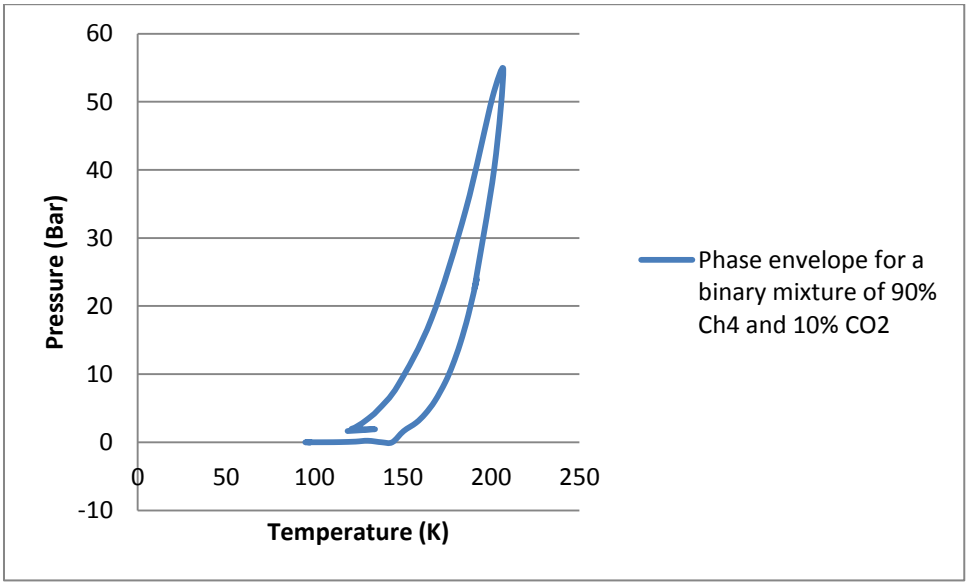

Figure 5.6 : Phase envelope for a binary system, mole fraction for CH_4: 0.90 and CO_2 : 0.10

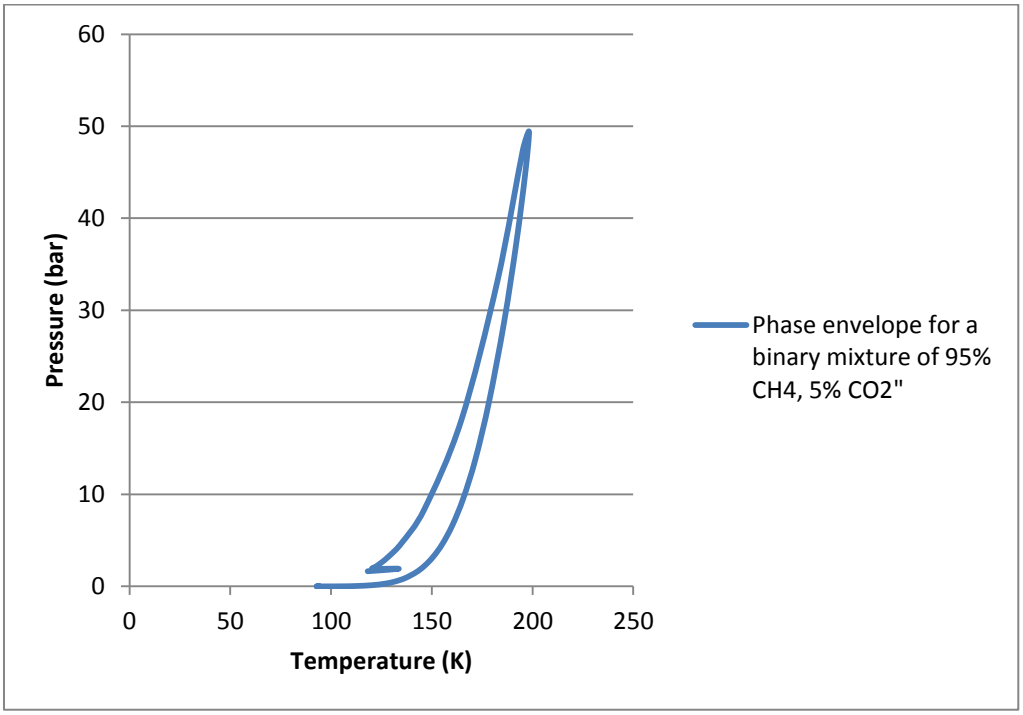

Figure 5.7 : Phase envelope for a binary system, mole fraction CH_4 : 0.95 and CO_2 : 0.05

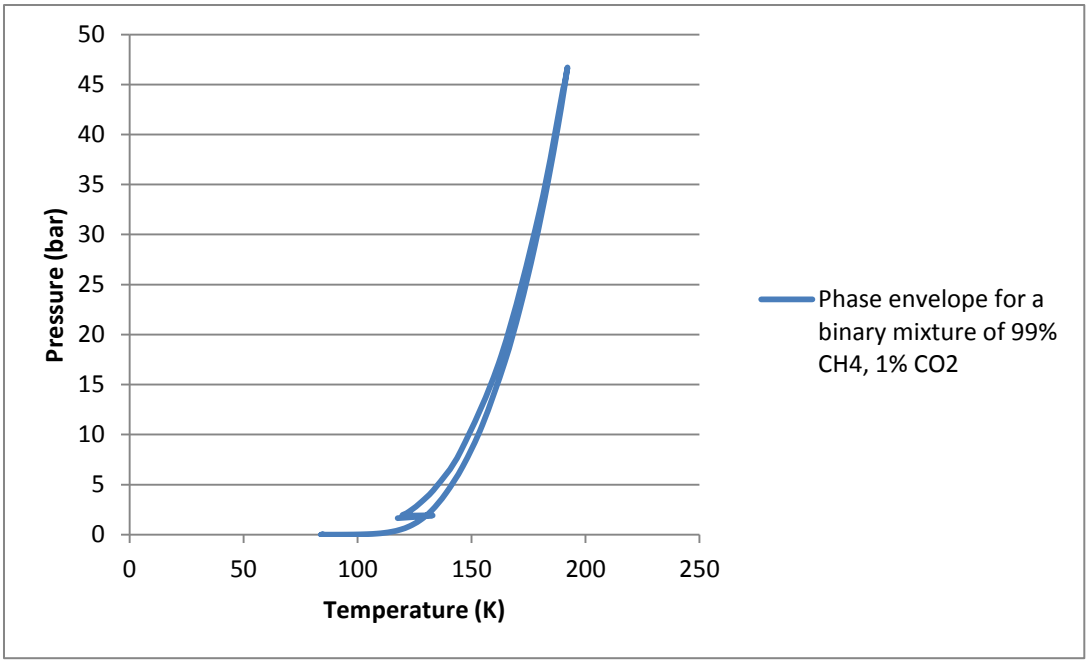

Figure 5.8 : Phase envelope for a binary system, mole fraction $CH_{4:}$ 0.99 and CO_2 0.01

From the above graphs it can be observed that the phase envelope is shrinking, this is due to the compositional charatcteristics of the dry gases. Therefore the gas remains in single region or one phase region ,since it involves dealing with super critical components primarily methane.

For the systems and conditions investigated in this work the fluid is above critical temperature and above critical pressure, except for some systems in which 50 bars is below critical pressure.

5.1 Verification of the model systems for hydrate equilibrium

Our model systems consists of the hydrate model [12] with parameters for the Gibbs free energy of inclusion as listed in table number (2.1 to 2.3) for different cavities and guest molecules in structure I hydrate. The thermodynamic properties of hydrate were estimated using [12] and have been verified to have good predictive capabilities. The chemical potential for empty hydrates has been estimated from [12]. For the calculation of deviation from ideal gas i.e. the fugacity coefficients for separate fluid phases are calculated using the SRK equation of state [21] was used. Chemical potential of liquid water has been evaluated from [12], while the ideal gas chemical potentials are calculated from statistical mechanics. The chemical potential of water for the adsorbed phase was estimated from [3].

For our model system natural choice of method is free energy analysis in classical thermodynamics using residual thermodynamics (ideal gas as a reference state). More details on thermodynamics used in our model are given in chapter 2. The comparison between estimated hydrate curve calculated from the model system and the experimental data for various compositions of mixtures of CH_4, CO_2, and H_2S are given below.

Estimated hydrate equilibrium curve (-) and experimental data from Hydrate formation conditions of sour natural gases [22]**(*).**

In this section the estimated data for mixtures of various compositions, has been tried to match with the experimental data from [22]as illustrated in figures 5.9 – 5.13. This was done in order to validate the calculated results with the experimental results from [22]. The data calculated for the hydrate equilibrium curve is for a mixture of different compositions of gases as illustrated in figure 5.10 – 5.14 and comparison of experimental data from [22]

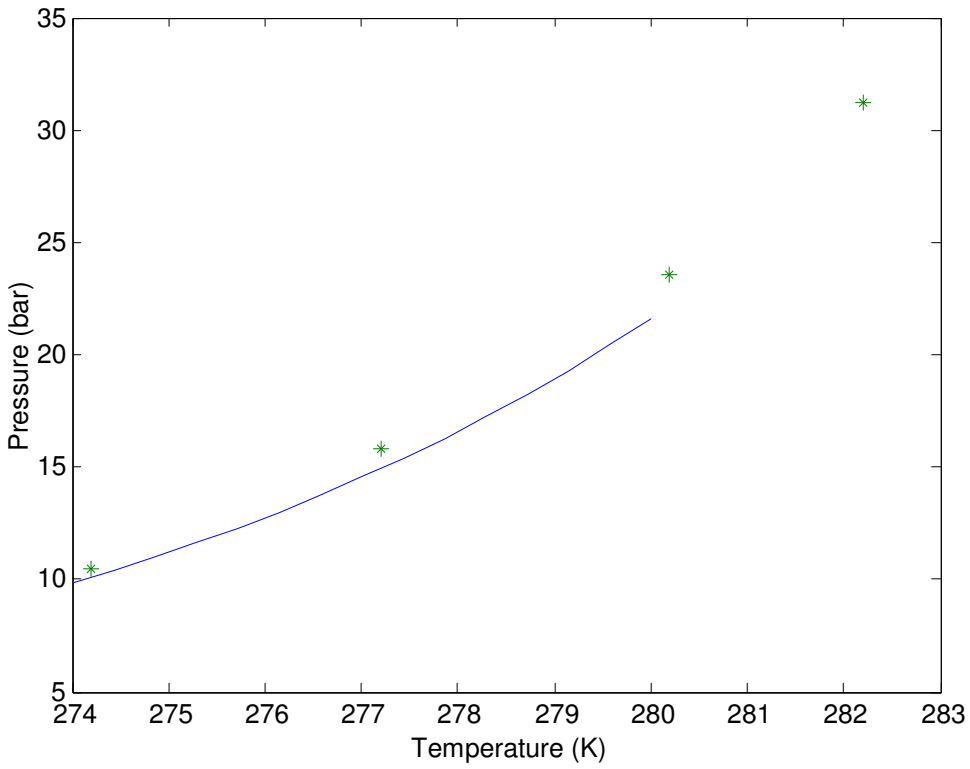

Figure 5. 9 : Estimated and experimental hydrate equilibrium curve, for a system of 87.65% CH_4, 7.40% CO_2, 4.95% H_2S. (-) is for estimated data and (*) is for experimental data from **[22]**.

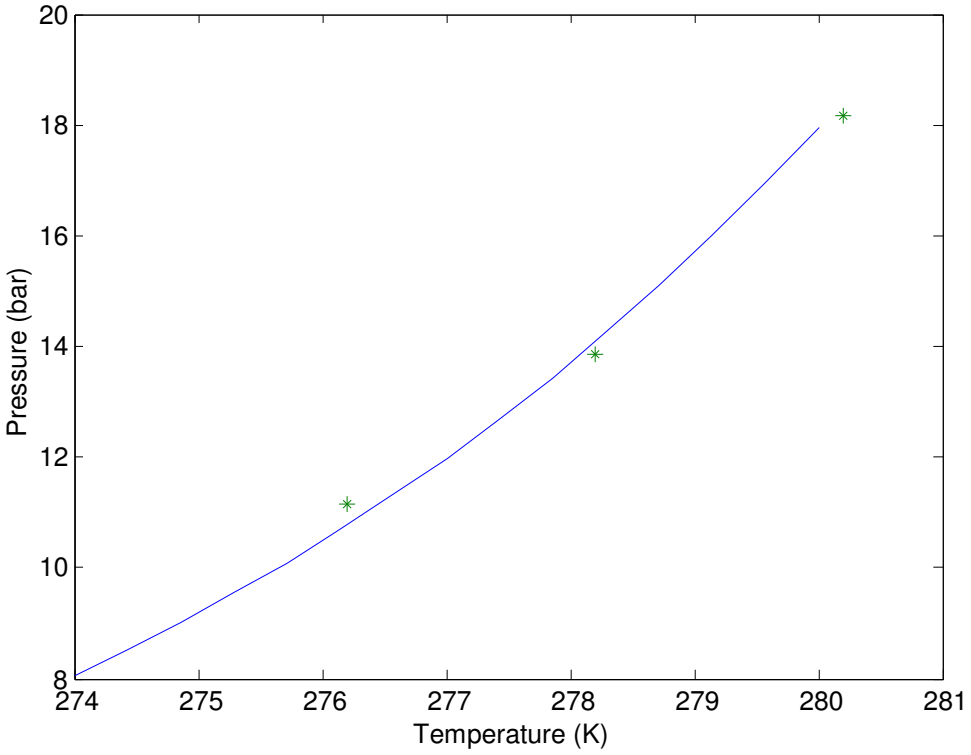

Figure 5.10 : Estimated and experimental hydrate equilibrium curve, for a system of 82.45% CH_4, 10.77% CO_2, 6.78% H_2S. (-) is for estimated data and (*) is for experimental data from **[22]**.

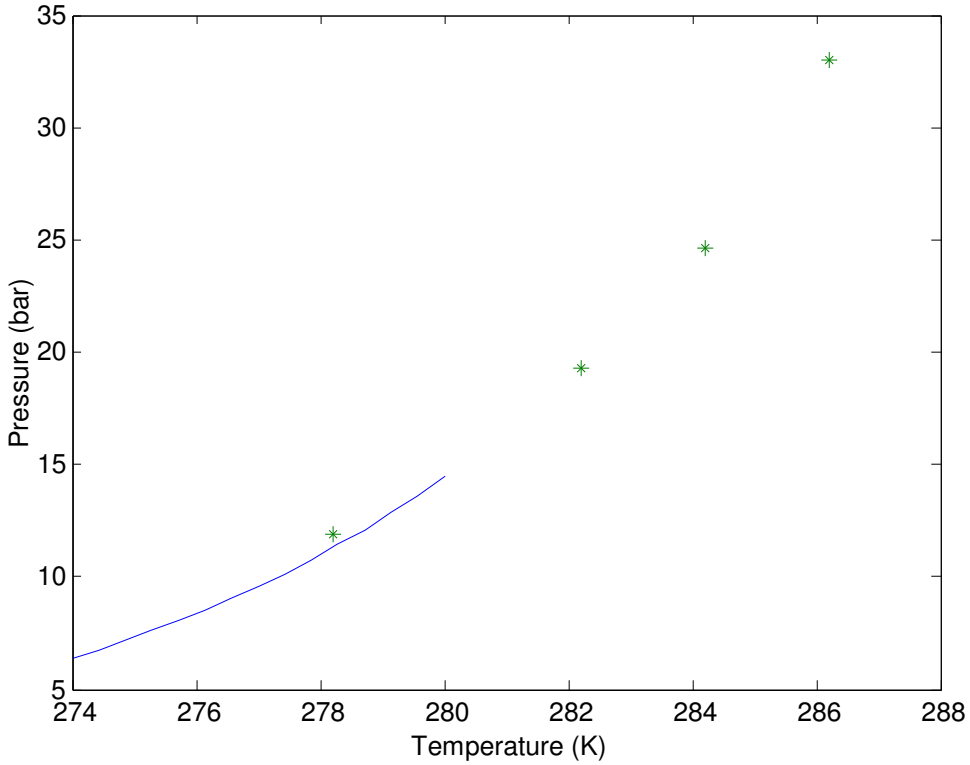

Figure 5.11 : Estimated and experimental hydrate equilibrium curve, for a system of 82.91% CH_4, 7.16% CO_2, 9.93% H_2S. (-) is for estimated data and (*) is for experimental data from **[22]**.

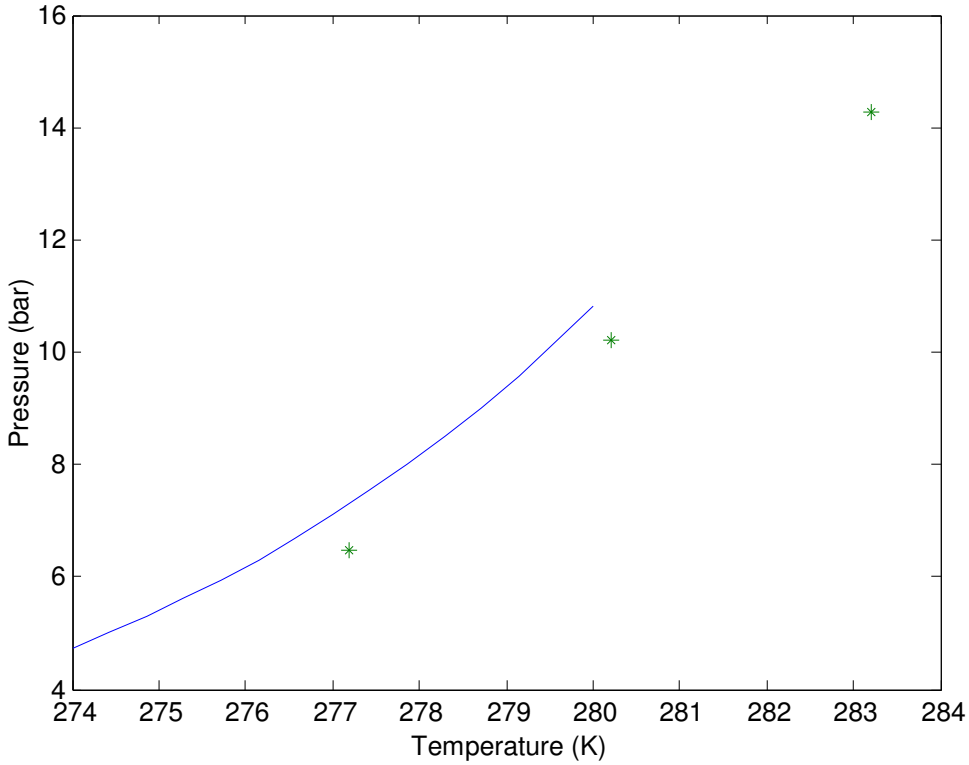

Figure 5.12 : Estimated and experimental hydrate equilibrium curve, for a system of 77.71% CH_4, 7.31%CO_2, 14.98% H_2S. (-) is for estimated data and (*) is for experimental data from **[22]**.

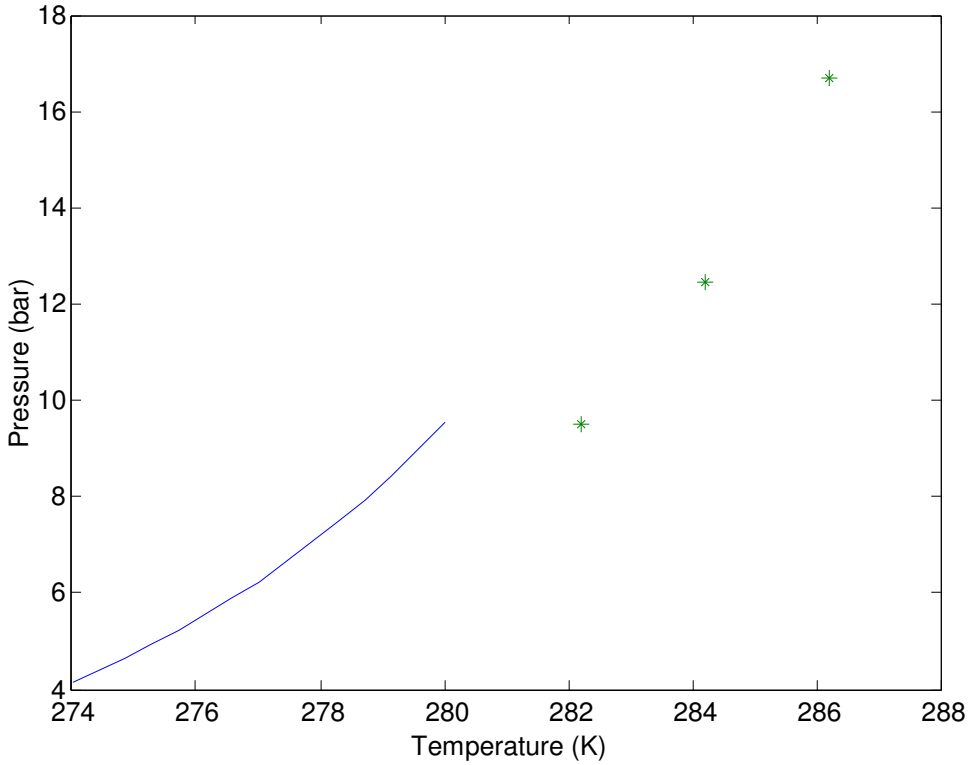

Figure 5. 13 : Estimated and experimental hydrate equilibrium curve, for a system of 75.48% CH_4, 6.81% CO_2, 17.71% H_2S. (-) is for estimated data and (*) is for experimental data from **[22]**.

Comparing figure 5.9 and figure 5.11, it is observed that how by a small increase in the mole fraction of CO_2 and H_2S in CH_4, the hydrate formation pressure has decreased from 10 bars to around 6 bars at temperature 274 (K). Similarly for the rest of the figures 5.10,5.12,5.13 it can be stated that as the mole fraction of CH_4 in the gas stream decreases with a relative increase in the mole fraction of impurities like CO_2, H_2S , the hydrate formation pressure and temperature decreases, hence increasing the hydrate stability zone thus shifting the equilibrium curve more towards the right.

The model system estimates were matched with experimental estimates from [22], and found that the results are matching with the experimental results to a high degree, indicating that the proposed theory is right.

6. Sensitivity analysis

The thermodynamic variables for each route leading to hydrate formation are temperature, pressure and compositions of the phases that limit each route. For example it is known that in most conditions like during transportation of gas through pipelines, the range of temperatures and pressures are inside hydrate formation region. So once water and hydrate formers become available at the same time, then it is the process(s) that makes these components available which are the limiting factors.

For hydrate forming from liquid water and gas the limit is getting liquid water available, i.e. water condensing out from the gas. For hydrate forming from a liquid solution with hydrate former(s) there must be high enough concentration of hydrate formers in the solution for the hydrate to be able to extract hydrate formers into the hydrate. This is similar for all the different routes, as seen in figure 4.1. A sensitivity analysis is done to see exactly what the change in the maximum allowable content of water is, when a factor or thermodynamic variable in this project (pressure, temperature or the mole fraction) is changed.

Sensitivity analysis contributes to the assessing of interactions between various factors and contributes more to the phenomenological understanding.Sensitivity analysis is a technique for systematically changing factors in a model to determine the effect of changes in either one or several response variables [23].
It is used to determine how different values of an independent variable will impact a particular dependent variable. The approach used to carry out sensitivity analysis is:-

- Estimation for end points of a cube (as seen in figure 6.1) in comparison to the center point i.e. the midpoint of the cube.

6.1 End-point sensitivity analysis

The primary focus in this work is transport of CH_4 with CO_2 as the primary impurity in addition to water. In the North Sea reservoirs the level of H_2S following the production streams is generally low. A sensitivity analysis in the three independent thermodynamic variables temperature, pressure and mole-fraction of CO_2 is conducted to see how much is the change in the allowable mole fraction of water and also to see what or how the maximum allowable concentration of water is being affected with a change in one factor namely either pressure,

temperature and mole fraction of CO_2 in CH_4. CO_2 following the hydrocarbon streams in the North sea can be up to the order of 10%.

The mole fractions of CH_4 was taken to be 0.99, 0.90, 0.95 and that of CO_2 was taken to be 0.01, 0.05 and 0.10, temperatures considered were 1°C, 5.5°C and 10°C, while the pressures considered were 50 bars, 150 bars and 250 bars.As shown in figure 6.1.

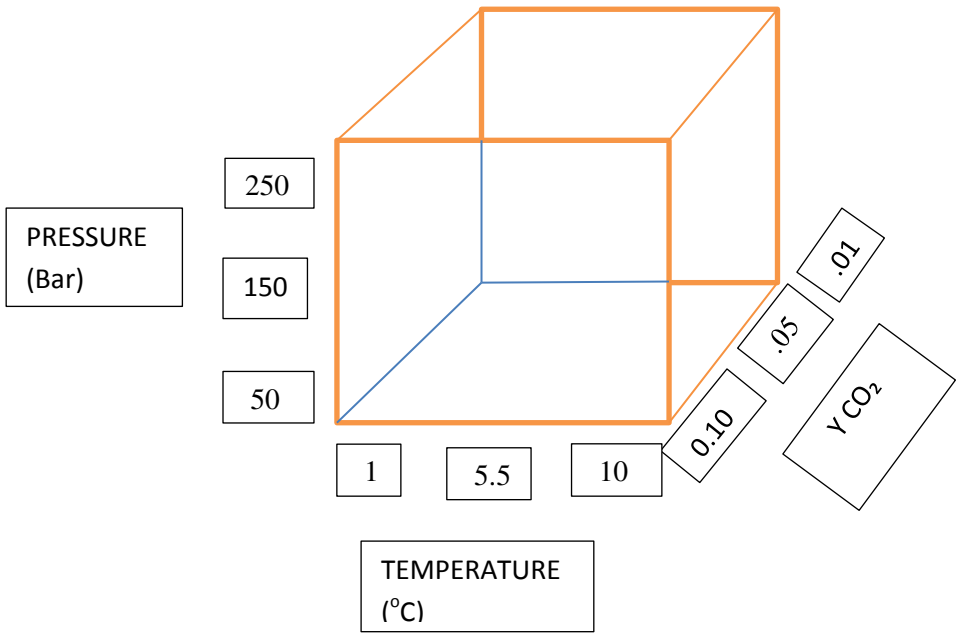

Figure 6.1 : Schematic illustration of end-point sensitivity analysis.

Three sensitivity factors namely A, B, C were calculated. Factor A determines how a change in the mole fraction of CO_2 will change the amount of allowable water content in CH_4. Factor B determines what will be the change in the maximum allowable content of water in CH_4, as the pressure is changed and similarly Factor C which will determine the change in the maximum allowable concentration of water in CH_4, with a variation in temperature.

The formulas required to calculate sensitivity factors A, B, C are given below:-

6.2 Equations used for calculation of sensitivity factors A,B,C

In this section the formulas or equations used to calculate the sensitivity factors of Y_{CO2}, pressure and temperature ie sensitivity factors A,B,C are given:

To calculate factor A,

$$\frac{\Delta Y_{water}}{Y_{water}} = A\,\Delta\frac{Y_{co_2}}{Y_{co_2}} \qquad (31)$$

To calculate factor B,

$$\frac{\Delta Y_{water}}{Y_{water}} = B\,\frac{\Delta P}{P} \qquad (32)$$

To calculate factor C,

$$\frac{\Delta Y_{water}}{Y_{water}} = C\,\frac{\Delta T}{T} \qquad (33)$$

where :-

ΔY_{water} - change in the mole fraction of water

Y_{water} - mole fraction of water

ΔY_{co_2} - change in the mole fraction of CO_2

Y_{co_2} - mole fraction of CO_2

ΔP - change in the pressure

P - pressure

ΔT - change in the temperature

T - temperature

Calculations of Sensitivity factors A, B, C can be seen in tables below:-

The starting point for all the calculations in tables (6.1 to 6.3) was taken to be the mid-point of the cube, $Y_{CO2} = 0.05$, temperature = 5.5 ^{0}C, pressure = 150 bars.

Table 6.1: Estimates for sensitivity factor A at varying mole fraction of CO_2. Table shows the relative change (compared to base point) in the factor A at varying molefraction of CO_2 for three different routes to hydrate formation. Also relative change in sensitivity factor A for each hydrate route is estimated.

Y_{co2}	**A for Direct Hydrate**	**A for Hydrate From Gas**	**A for Hydrate (Adsorbed)**
0.01	0.0000	-0.0359	0.0000
0.10	-0.0071	-0.0279	0.0000
Change in sensitivity factor A	0	-0,22	0

Sensitivity factor A :-

Sensitivity factor A is calculated for Y_{CO2} (mole fraction of CO_2) at 0.01 and for Y_{CO2} at 0.1. The Y_{CO2} at 0.05 is considered as a base point to estimate the sensitivity factor A. Factor A for Y_{CO2} shows how the change in the mole fraction of gas (CO_2) from 0.01 to 0.05 effects the hydrate formation for direct hydrate, hydrate from gas and hydrate (adsorbed).

Similarly sensitivity factor A for Y_{CO2} 0.1 shows how the change in the mole fraction of gas (Y_{CO2}) from 0.05 to 0.1 effects the hydrate formation for direct hydrate, hydrate from gas and hydrate (adsorbed).

Comparing change in sensitivity for factor A Y_{CO2} at 0.01 and Y_{co2} at 0.1, it can be observed that for among the three hydrate formation routes, hydrate from gas is more sensitive than the other two for sensitivity factor A as it is changing by -0.22 times.

Table 6.2 : Estimates for sensitivity factor B at varying pressures. Table shows the relative change (compared to the base point) in factor B, at varying pressures for three different routes to hydrate formation. Also relative change in sensitivity factor B for each hydrate route is estimated.

Pressure (bars)	**B for Direct hydrate**	**B for Hydrate from gas**	**B for Hydrate (Adsorbed)**
50	0.7348	0.5735	0.7342
250	0.8773	0.7946	0.8762
Change in sensitivity factor B	0.19	0.39	0.19

Sensitivity factor B :-

Sensitivity factor B is calculated for pressure at 50 bars and for 250 bars. The pressure at 150 bars is considered as a base point to estimate the sensitivity factor B. Sensitivity factor B for pressure 50 bars shows how the change in the pressure of gas from 50 to 150 effects the hydrate formation for direct hydrate, hydrate from gas and hydrate (adsorbed).

Similarly sensitivity factor B for pressure 250 bars shows how the change in the pressure of gas from 150 bars to 250 bars effects the hydrate formation for direct hydrate, hydrate from gas and hydrate (adsorbed).

Comparing the change in sensitivity factor B for pressures at 50 bars to 250 bars. It can be observed that hydrate formation by gas varies 0.39 times followed by hydrate adsorbed and direct hydrate which varies by 0.19 times. Therefore hydrate from gas is more sensitive than the other two for sensitivity factor B in terms of pressure variation.

Table 6.3 : Estimates for sensitivity factor C at varying temperatures. Table shows the relative change (compared to the base point) in factor C, at varying temperatures for three different routes to hydrate formation. Also the relative change in sensitivity factor C for each hydrate route is estimated.

Temperature(^{0}C)	**C for Direct hydrate**	**C for Hydrate from gas**	**C for Hydrate (Adsorbed)**
1	0.2751	0.3273	0.3270
10	-0.025758	-0.268171	-0.434060
Change	-1.1	-1.8	-2.3

Sensitivity factor C:-

Sensitivity factor C is calculated for temperature at 1^0C and for 10^0C. The temperature at 5.5 ^{0}C is considered as a base point to estimate the sensitivity factor C. Sensitivity factor C for temperature at 1^0C shows how the change in the temperature from 1^0C to 5.5^0C effects the hydrate formation for direct hydrate, hydrate from gas and hydrate (adsorbed).

Similarly sensitivity factor C for temperature 10^0C shows how the change in the temperature from 5.5^0C to 10^0C bars effects the hydrate formation for direct hydrate , hydrate from gas and hydrate (adsorbed).

Comparing change in sensitivity factor C for temperature at 1^0C to 10^0C. It can be observed that hydrate via adsorption varies -2.3 times followed by hydrate from gas at -1.8 times and direct hydrate -1.1 times. Therefore hydrate via adsorption is more sensitive than other two for sensitivity factor C in terms of temperature variation.

Findings:-

Comparing all the above tables it can be stated that hydrate adsorbed is the most dominant phenomena overall (when variation of Y_{CO2}, pressure and temperature is considered) as it is varying from 0 to 0.19 to -2.3 for sensitivity factors A, B,C.

Also variation of temperature appears to be most important sensitivity factor. It varies from -2.3 for hydrate from adsorbed to -1.8 for hydrate from gas to -1.1 direct hydrate for these three hydrate routes.

Below, a more detailed end point analysis is shown in table 6.4, 6.5 and 6.6, for temperature, pressure and Y_{CO2} at varying conditions.

Table 6. 4 : Table showing when will the dew point occur and at what point will the hydrate from gas be formed, at a particular temperature, pressure and mole fraction of CO_2

TEMEPRATURE ^oC	**PRESSURE (bars)**	**Y_{CO2} (mole fraction)**	**DEW POINT**	**HYDRATE FROM GAS**
1	50	0.01	.00005515	.00008413
10	50	0.01	.00010965	.00007889
1	50	0.10	.00005285	.00007943
10	50	0.10	.00010583	.00002919
1	250	0.01	.00014454	.00010904
10	250	0.01	.00025658	.00007134
1	250	0.10	.00013951	.00004350
10	250	0.10	.00024765	.00005483
5.5	150	0.05	.00012456	.00005990

Table 6. 5 : Table showing when the hydrate point will occur and at which point will a direct hydrate form at a particular temperature, pressure and mole fraction of CO_2

TEMEPRATURE ^oC	**PRESSURE (bars)**	**Y_{CO2} (mole fraction)**	**HYDRATE POINT**	**DIRECT HYDRATE**
1	50	0.01	.00005920	.00012495
10	50	0.01	.00010508	.00007083
1	50	0.10	.00005920	.00012495
10	50	0.10	.00010508	.00007083
1	250	0.01	.00019464	.00015552
10	250	0.01	.00028943	.00309769
1	250	0.10	.00019464	.00015552
10	250	0.10	.00028943	.00309769
5.5	150	0.05	.00015516	.00004456

Table 6.6 : Table showing when will adsorbed point occur and at what point will the hydrate be formed from adsorbed surface, at a particular temperature, pressure and mole fraction of CO_2

TEMEPRATURE (^oC)	**PRESSURE (bars)**	**Y_{CO2} (mole fraction)**	**ADSORBED POINT**	**HYDRATE (ADSORPTION)**
1	50	0.01	.00000308	.00006695
10	50	0.01	.00000618	.00009020
1	50	0.10	.00000308	.00006695
10	50	0.10	.00000618	.00009020
1	250	0.01	.00001014	.00010292
10	250	0.01	.00001813	.00009516
1	250	0.10	.00001014	.00010292
10	250	0.10	.00001813	.00009516
5.5	150	0.05	.00000856	.00001281

It can be observed that the tables 6.4, 6.5 and 6.6 gives the exact values of dew point i.e, the point at which first droplets of liquid will start to come out.Hydrate point is the point at which direct hydrate might start to form and adsorebd point is the point at which liquid water will start to adsorb on a solid surface (hematite in our case) but these points do not mean that the hydrate will form at that given molefraction. Hence for a more detailed understanding, the molefraction of water at which hydrate will form from gas,direct hydrate and hydrate from adsorbed are given in the columns besides to the dew point, hydrate point and adsored point in tables 6.4, 6.5 and 6.6.

Comparing dew point and adsorbed point:

From the above tables 6.4 and 6.6, consider temperature 1^0 C and pressure 50 bars when Y_{CO2} is 0.01. The estimates indicate that the tolerance based on dew-point as basis for water drop-out is 16.91 times higher than a limit based on water drop-out as adsorbed on Hematite. As the temperature is increased from 1^0C to 10^0C, pressure and Y_{CO2} remaining constant, it can be observed that the tolerance based on dew-point as basis for water drop-out is 16.74 times higher than a limit based on water drop-out as adsorbed on Hematite.

If the temperature and pressure are kept at 1^0C and 50 bars and Y_{CO2} increased from 0.01 to 0.1, the tolerance based on dew-point as basis for water drop-out is 16.16 times higher than a limit based on water drop-out as adsorbed on Hematite.

Further increasing the temperature at 10^0C and pressure at 50 bars and Y_{CO2} is 0.1, the tolerance based on dew-point as basis for water drop-out is 16.12 times higher than a limit based on water drop-out as adsorbed on hematite.
When the pressure is increased from 50 bars to 250 bars at temperature 1^0 C when Y_{CO2} is 0.01, the estimates indicate that the tolerance based on dew-point as basis for water drop-out is 13.25 times higher than a limit based on water drop-out as adsorbed on hematite.

Further when the pressure is increased from 50 bars to 250 bars and temperature from 1^0C to 10^0C, Y_{CO2} is 0.01 it can be stated that the tolerance based on dew-point as basis for water drop-out is 13.15 times higher than a limit based on water drop-out as adsorbed on hematite. When Y_{CO2} is increased from 0.01 to 0.10 at temperature 1^0C, pressure 250 bars, the estimates indicate that the tolerance based on dew-point as basis for water drop-out is 12.76 times higher than a limit based on water drop-out as adsorbed on hematite.

When Y_{CO2} is increased from 0.01 to 0.10 at temperature 10^0C, pressure 250 bars, the estimates indicate that the tolerance based on dew-point as basis for water drop-out is 12.66 times higher than a limit based on water drop-out as adsorbed on hematite.
Considering a mid-point Y_{CO2} 0.05 at temperature 5.5^0C and pressure 150 bars, the estimates indicate that the tolerance based on dew-point as basis for water drop-out is 13.55 times higher than a limit based on water drop-out as adsorbed on hematite.

If we consider an overall comparison between dew point estimates and adsorbed point estimates at all conditions, the findings are that the maximum allowable content of water in dew point is on an average 14.59 times more than the adsorbed point.

Comparing hydrate point and adsorbed point :

From the above tables 6.5 and 6.6, consider temperature 1^0 C, pressure 50 bars and Y_{CO2} being 0.01. The estimates indicate that the tolerance based on hydrate point is 18.22 times higher than a limit based on water drop-out as adsorbed on hematite.

As the temperature is increased from 1^0C to 10^0C, pressure 50 bars and Y_{CO2} is 0.01 it can be observed that the tolerance based on hydrate point is 16 times higher than a limit based on water drop-out as adsorbed on hematite.

If the temperature and pressure are kept at 1^0C and 50 bars respectively and Y_{CO2} increased from 0.01 to 0.1, the estimates indicate that the tolerance based on hydrate point is 18.22 times higher than a limit based on water drop-out as adsorbed on hematite

Further if the temperature and pressure are kept at 10^0C and 50 bars respectively and Y_{CO2} is 0.1, the estimates indicate that the tolerance based on hydrate point is 16 times higher than a limit based on water drop-out as adsorbed on hematite.

When the pressure is increased from 50 bars to 250 bars at temperature 1^0 C when Y_{CO2} is 0.01. The estimates indicate that the tolerance based on hydrate point is 18.20 times higher than a limit based on water drop-out as adsorbed on hematite.

Further when the pressure is increased from 50 bars to 250 and temperature from 1^0C to 10^0C, Y_{CO2} is 0.01, the estimates indicate that the tolerance based on hydrate point as basis is 14.96 times higher than a limit based on water drop-out as adsorbed on hematite.

When Y_{CO2} is increased from 0.01 to 0.10 at temperature 1^0C, pressure 250 bars, the estimates indicate that the tolerance based on hydrate point is 18.20 times higher than a limit based on water drop-out as adsorbed on hematite.

When Y_{CO2} is increased from 0.01 to 0.10 at temperature 10^0C, pressure 250 bars, the estimates indicate that the tolerance based on hydrate point is 14.96 times higher than a limit based on water drop-out as adsorbed on hematite.

Considering a mid-point Y_{CO2} 0.05 at temperature 5.5^0C and pressure 150 bars. The estimates indicate that the tolerance based on hydrate-point for water drop-out is 17.13 times higher than a limit based on water drop-out as adsorbed on hematite.

If we consider an overall comparison between hydrate point estimates and adsorbed point estimates at all conditions,findings are that the maximum allowable content of water in dew point is on an average 16.88 times more than the adsorbed point.

Comparing hydrate point and dew point

From the above tables 6.6 and 6.4, consider temperature 1^0 C and pressure 50 bars when Y_{CO2} is 0.01, the estimates indicate that the tolerance based on hydrate point is 0.07 times higher than a limit based on dew-point as basis for water drop-out.
As the temperature is increased from 1^0C to 10^0C, pressure 50 bars and Y_{CO2} is 0.01 it can be observed that the tolerance based on hydrate point is -0.04 times lower than a limit based on on dew-point as basis for water drop-out.

If the temperature and pressure are kept at 1^0C and 50 bars and increase Y_{CO2} from 0.01 to 0.1, the estimates indicate that the tolerance based on hydrate point is 0.12 times higher than a limit based on dew-point as basis for water drop-out.

Further if the temperature and pressure are kept at 10^0C and 50 bars and Y_{CO2} is 0.1, the estimates indicate that the tolerance based on hydrate point is -0.01 times lower than a limit based on dew-point as basis for water drop-out.

When the pressure is increased from 50 bars to 250 bars at temperature 1^0 C when Y_{CO2} is 0.01, the estimates indicate that the tolerance based on hydrate point is 0.35 times higher than a limit based on dew-point as basis for water drop-out.
Further when the pressure is increased from 50 bars to 250 and temperature from 1^0C to 10^0C, Y_{CO2} is 0.01, the estimates indicate that the tolerance based on hydrate point is 0.13 times higher than a limit based on dew-point as basis for water drop-out.

When Y_{CO2} is increased from 0.01 to 0.10 at temperature 1^0C, pressure 250 bars, the estimates indicate that the tolerance based on hydrate point is 0.40 times higher than the limit based on dew-point as basis for water drop-out.
When Y_{CO2} is increased from 0.01 to 0.10 at temperature 10^0C, pressure 250 bars, the estimates indicate that the tolerance based on hydrate point as basis is 0.17 times higher than a limit based on dew-point as basis for water drop-out.
Considering a mid-point Y_{CO2} 0.05 at temperature 5.5^0C, and pressure 150 bars, the estimates indicate that the tolerance based on hydrate point is 0.25 times higher than a limit based on dew-point as basis for water drop-out.

If we consider an overall comparison between hydrate point estimates and dew point estimates at all conditions, the findings are that the maximum allowable content of water in hydrate is on an average 0.16 times more than the dew point.

6.3 Sensitivity analysis with the inclusion of impurities H_2S and CO_2

In this section sensitivity analysis was done with the inclusion of hydrogen sulphide along with carbon dioxide and methane which is the main fluid phase.

Hydrogen sulphide is a very well know and vigorous hydrate former. It was considered to be one of the impurities along with carbon dioxide, which is likely to make a significant effect on the process of hydrate formation during transport. [8].

Mole fractions of CO_2, H_2S and remaining CH_4, which were considered for sensitivity analysis. Are shown below.

Table 6.7 : Table showing the systems that were considered for sensitivity analysis

System	Y_{CO2}	Y_{H2S}	System	Y_{CO2}	Y_{H2S}	System	Y_{CO2}	Y_{H2S}
2.1.1	0.01	0.001	2.2.1	0.01	0.01	2.3.1	0.01	0.1
2.1.2	0.025	0.001	2.2.2	0.025	0.01	2.3.2	0.025	0.1
2.1.3	0.05	0.001	2.2.3	0.05	0.01	2.3.3	0.05	0.1
2.1.4	0.1	0.001	2.2.4	0.1	0.01	2.3.4	0.1	0.1

As seen in table 6.7, for the purpose of sensitivity analysis the mole fraction of H_2S was changed, while keeping the mole fraction of CO_2 constant in gas stream.

The results are plotted and compared for three cases :

1) Mole fraction of water before drop out as liquid
2) Mole fraction of water before hydrate drop out
3) Mole fraction of water before adsorption on hematite

6.4 Estimates for sensitivity analysis.

6.4.1 Estimates for mole fraction of 0.001 H_2S

In this section, the estimates for maximum content of water before drop out as liquid, maximum content of water before drop out as hydrate and estimates for maximum content of water before adsorption for mole fraction of H_2S as 0.001 and varying concentration of CO_2 (0.01, 0.025, 0.05, 0.1) have been calculated as illustrated in figures 6.2 – 6.10 :

6.4.1.1 Estimates for water before drop out for mole fraction of 0.01 CO2, 0.001 H_2S

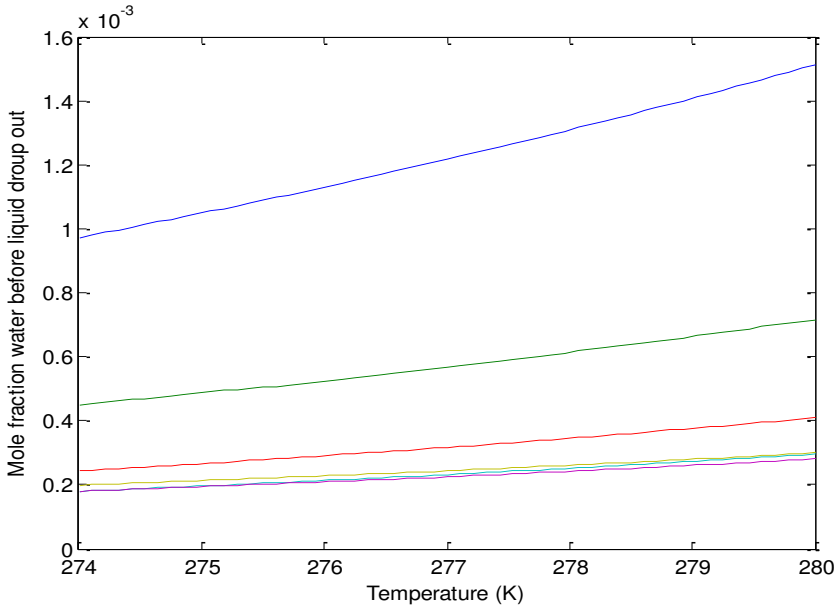

Figure 6.2 : Maximum water content before liquid water drop out, for mole fraction of 0.01 CO_2, 0.001 H_2S and remaining gas being CH_4. Curves are from top to bottom, for pressures 50 bars, 90 bars, 130 bars, 170 bars, 210 bars, 250 bars.

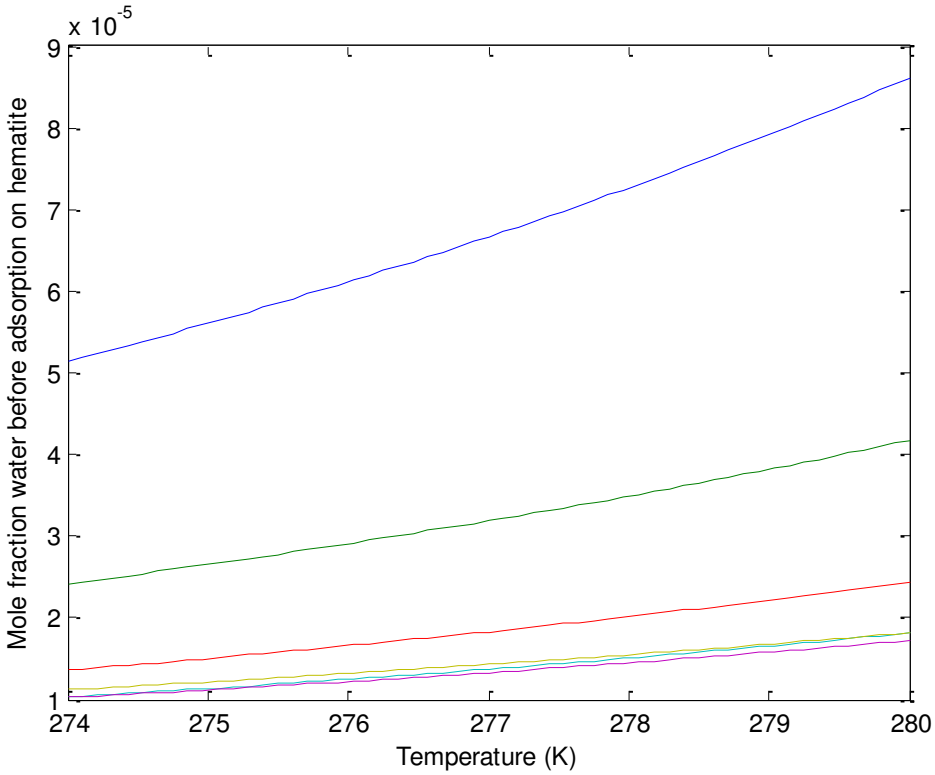

Figure 6.3 : Maximum water content before adsorption on hematite, for mole fraction of 0.01 CO_2, 0.001 H_2S and remaining gas being CH_4. Curves are from top to bottom, for pressures 50 bars, 90 bars, 130 bars, 170 bars, 210 bars, 250 bars.

.

6.4.1.2 Estimates for water before drop out for mole fraction of 0.025 CO_2, 0.001 H_2S

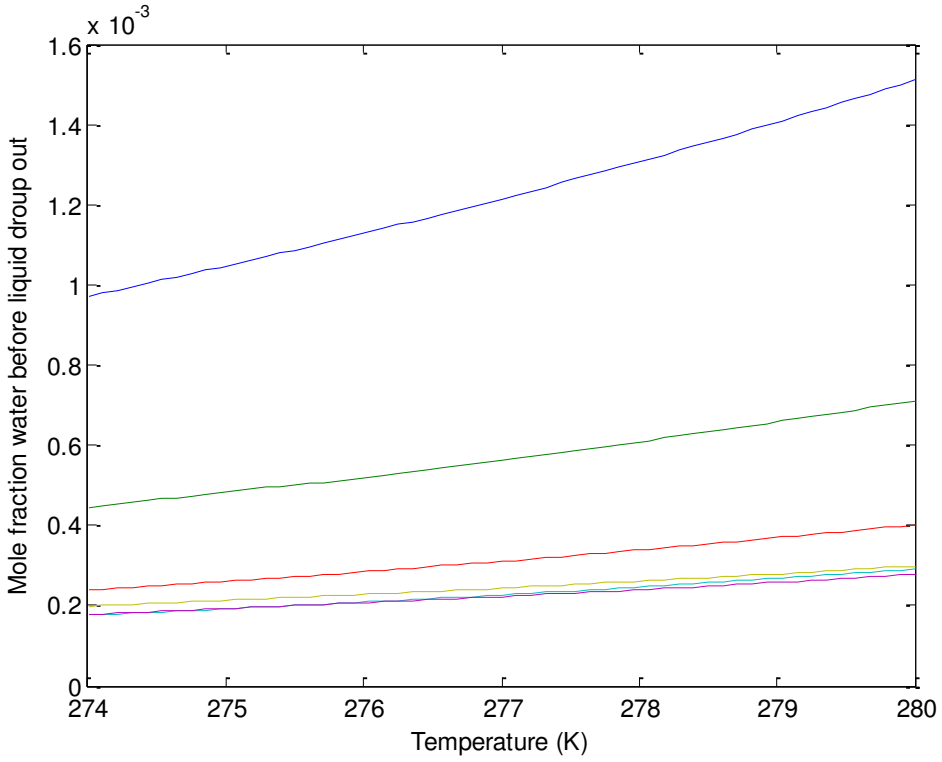

Figure 6.4 : Maximum water content before liquid water drop out, for mole fraction of 0.025 CO_2, 0.001 H_2S and remaining gas being CH_4. Curves are from top to bottom, for pressures 50 bars, 90 bars, 130 bars, 170 bars, 210 bars, 250 bars.

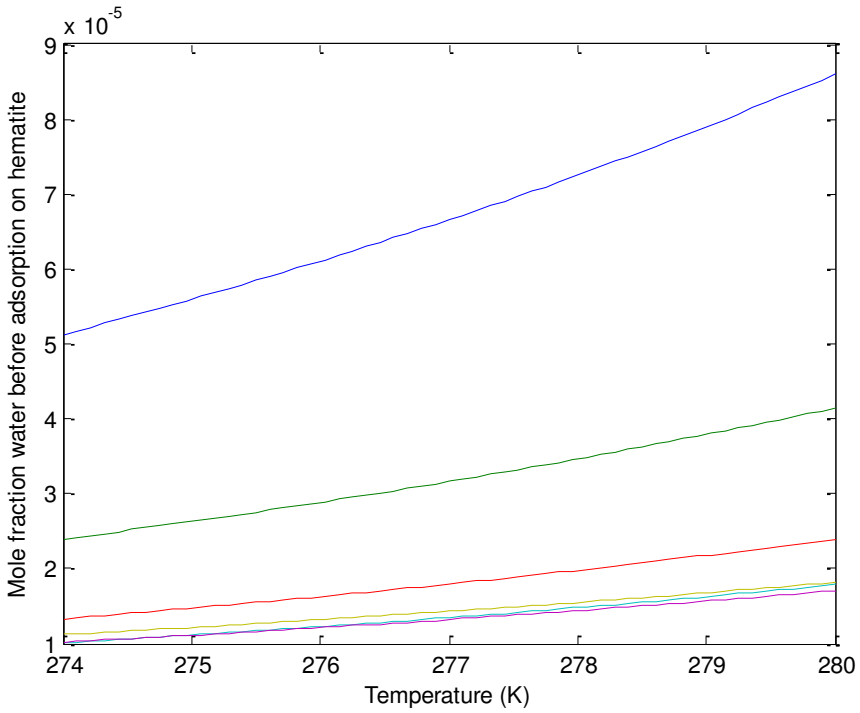

Figure 6.5 : Maximum water content before adsorption on hematite, for mole fraction of 0.025 CO_2, 0.001 H_2S and remaining gas being CH_4. Curves are from top to bottom, for pressures 50 bars, 90 bars, 130 bars, 170 bars, 210 bars, 250 bars.

6.4.1.3 Estimates for water before drop out for mole fraction of 0.05 CO_2, 0.001 H_2S

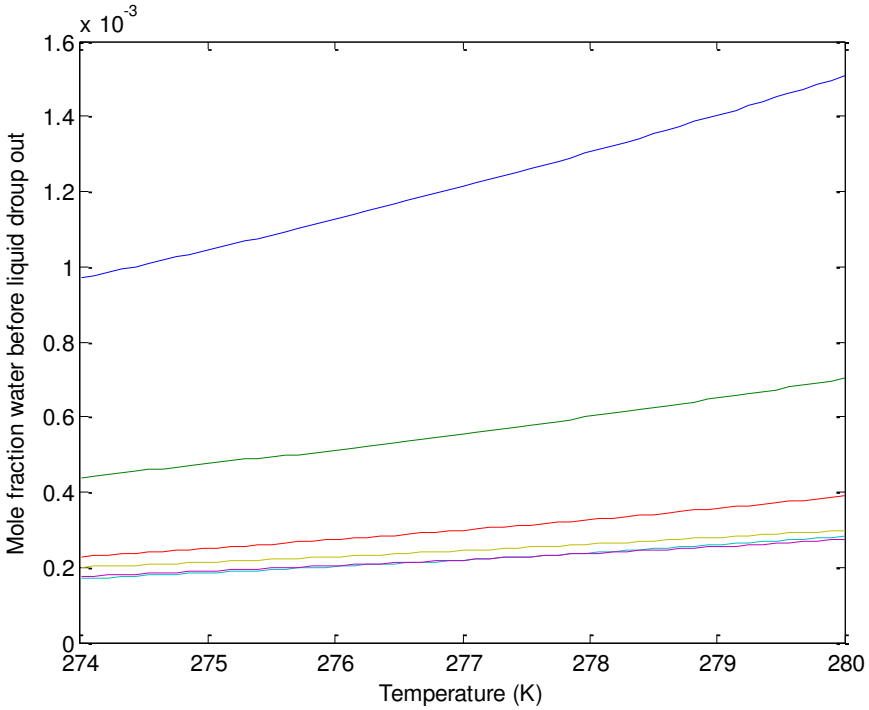

Figure 6.6 : Maximum water content before liquid water drop out, for mole fraction of 0.05 CO_2, 0.001 H_2S and remaining gas being CH_4. Curves are from top to bottom, for pressures 50 bars, 90 bars, 130 bars, 170 bars, 210 bars, 250 bars.

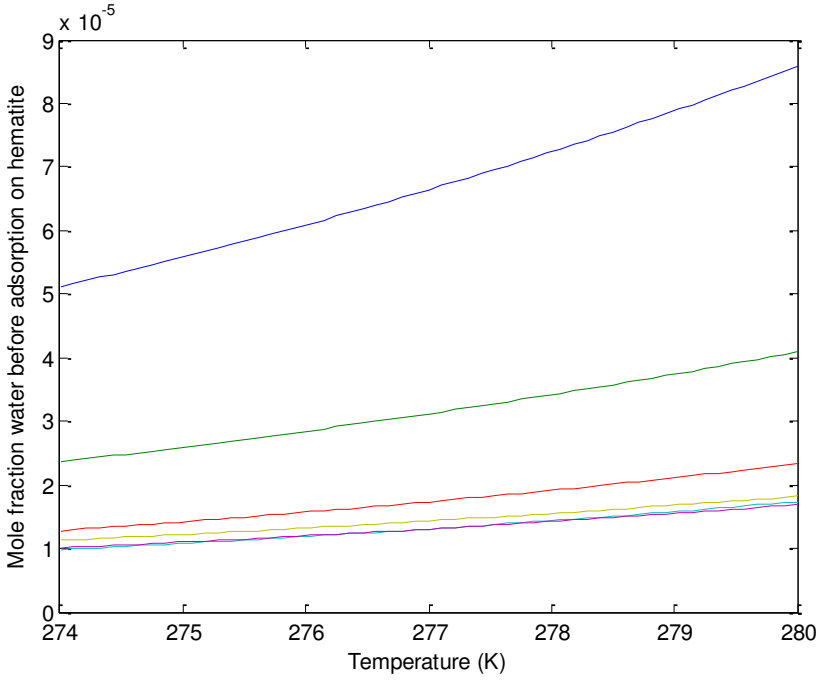

Figure 6.7 : Maximum water content before adsorption on hematite, for mole fraction of 0.05 CO_2, 0.001 H_2S and remaining gas being CH_4. Curves are from top to bottom, for pressures 50 bars, 90 bars, 130 bars, 170 bars, 210 bars, 250 bars.

6.4.1.4 Estimates for water before drop out for mole fraction of 0.1 CO_2, 0.001 H_2S

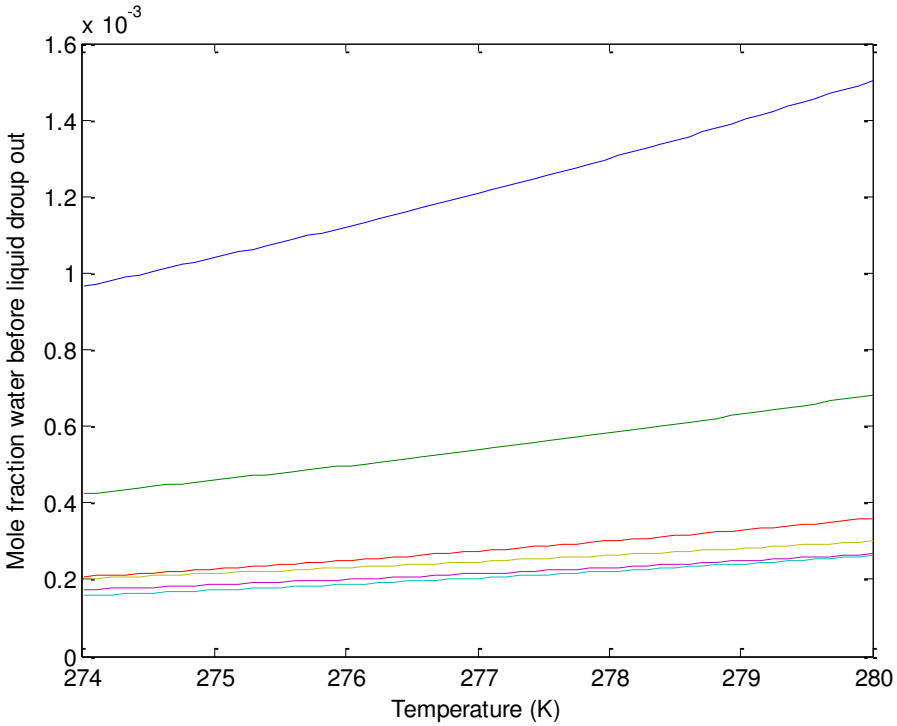

Figure 6.8 : Maximum water content before liquid water drop out, for mole fraction of 0.1 CO_2, 0.001 H_2S and remaining gas being CH_4. Curves are from top to bottom, for pressures 50 bars, 90 bars, 130 bars, 170 bars, 210 bars, 250 bars.

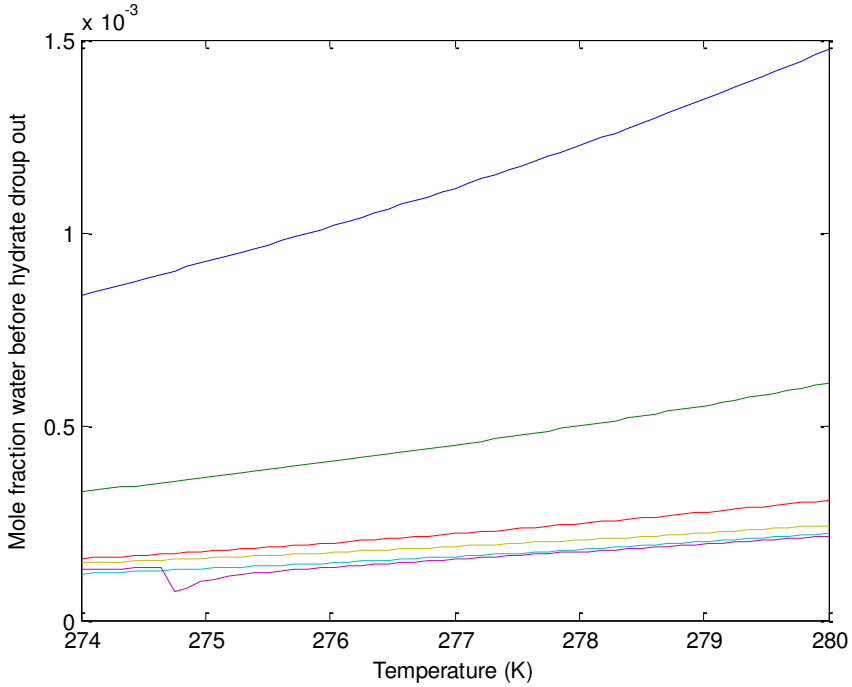

Figure 6.9 : Maximum water content before hydrate drops out, for mole fraction of 0.1 CO_2, 0.001 H_2S and remaining gas being CH_4. Curves are from top to bottom, for pressures 50 bars, 90 bars, 130 bars, 170 bars, 210 bars, 250 bars.

(Some inconsistency at pressure 210 bars can be observed, this is due to some numerical divergence in the numerical solution of the governing equations. Hence for this particular graph the curve for pressure of 210 bars will not be considered in the analysis of the results.)

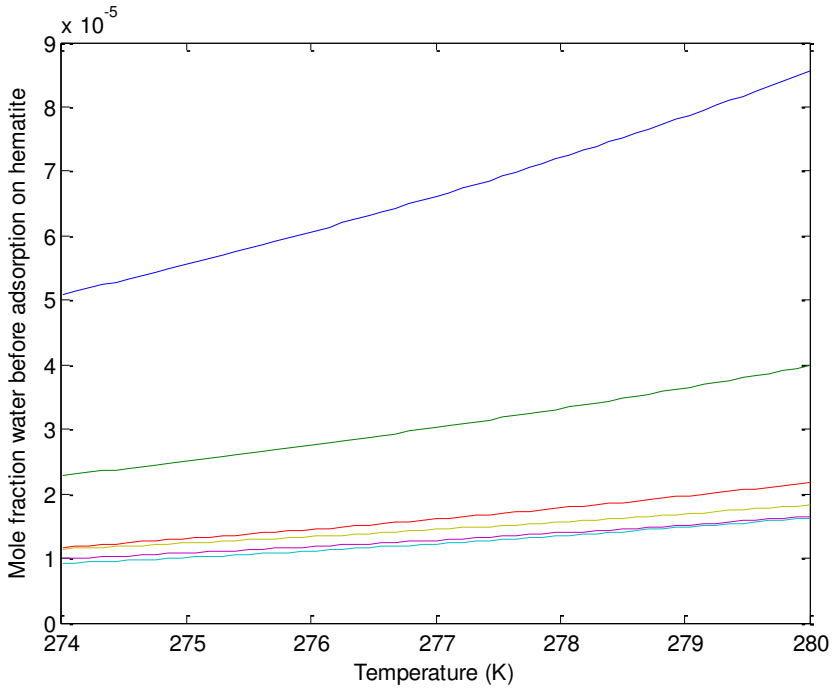

Figure 6.10 : Maximum water content before adsorption on hematite, for mole fraction of 0.1 CO_2, 0.001 H_2S and remaining gas being CH_4. Curves are from top to bottom, for pressures 50 bars, 90 bars, 130 bars, 170 bars, 210 bars, 250 bars**.**

6.4.2 Estimates for mole fraction of 0.01 H_2S

In this section, the estimates for maximum content of water before drop out as liquid, maximum content of water before drop out as hydrate and estimates for maximum content of water before adsorption for mole fraction of H_2S as 0.01 and varying concentration of CO_2 (0.01, 0.025, 0.05, 0.1) have been calculated, as illustrated in figures 6.11 – 6.19 :

6.4.2.1 Estimates for water before drop out for mole fraction of 0.01 CO_2, 0.01 H_2S

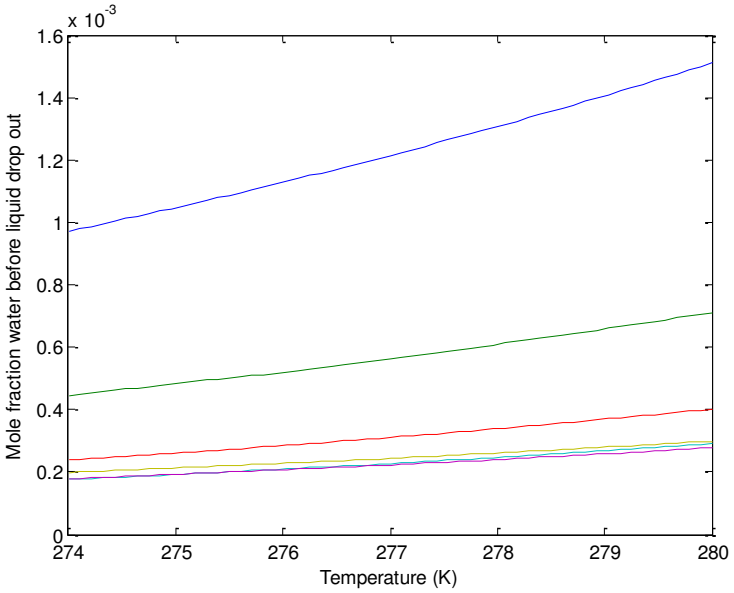

Figure 6.11 : Maximum water content before liquid water drop out, for mole fraction of 0.01 CO_2, 0.01 H_2S and remaining gas being CH_4. Curves are from top to bottom, for pressures 50 bars, 90 bars, 130 bars, 170 bars, 210 bars, 250 bars.

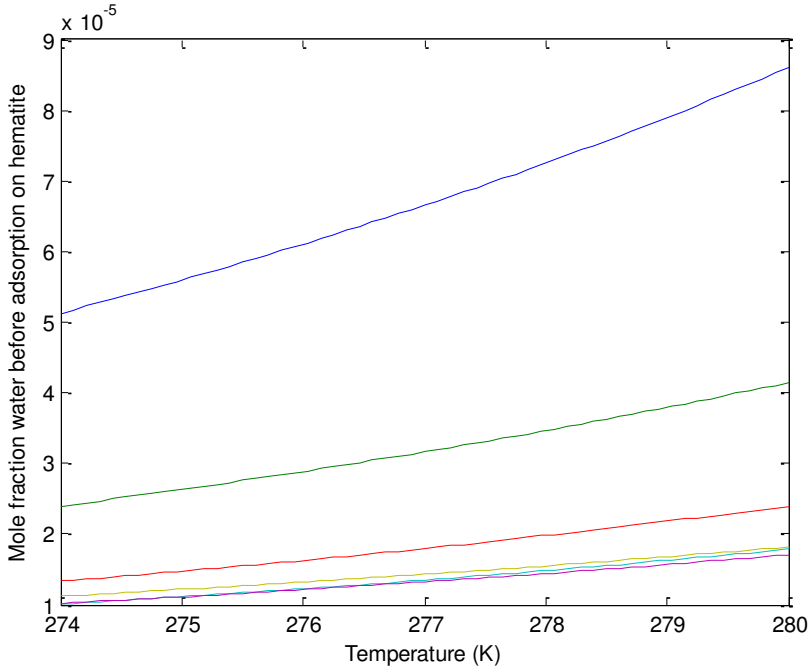

Figure 6.12 : Maximum water content before adsorption on hematite, for mole fraction of 0.01 CO_2, 0.01 H_2S and remaining gas being CH_4. Curves are from top to bottom, for pressures 50 bars, 90 bars, 130 bars, 170 bars, 210 bars, 250 bars.

6.4.2.2 Estimates for water before drop out for mole fraction of 0.025 CO_2, 0.01 H_2S

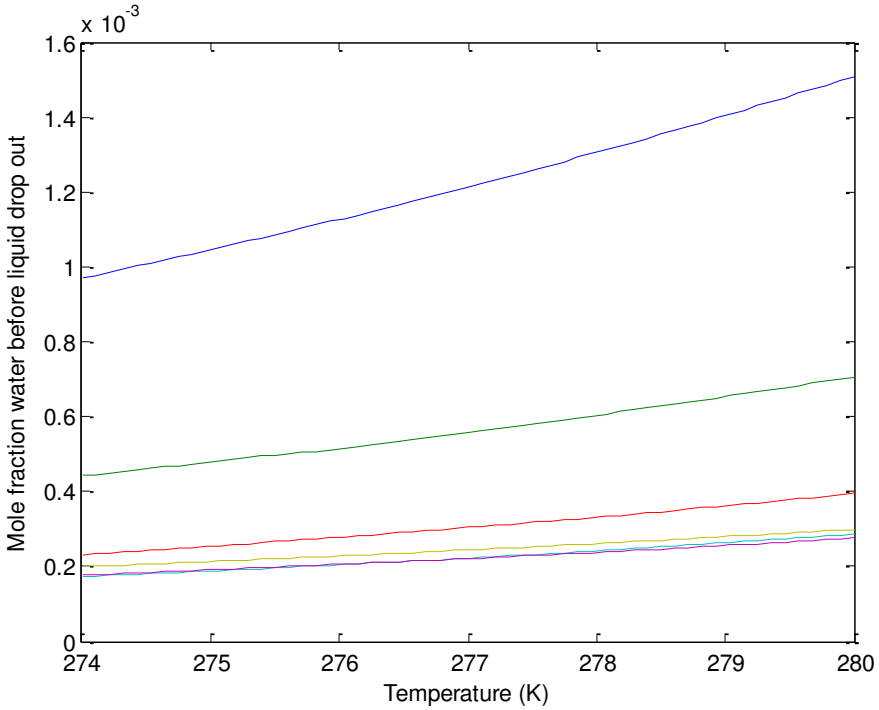

Figure 6.13 : Maximum water content before liquid water drop out, for mole fraction of 0.025 CO_2, 0.01 H_2S and remaining gas being CH_4. Curves are from top to bottom, for pressures 50 bars, 90 bars, 130 bars, 170 bars, 210 bars, 250 bars.

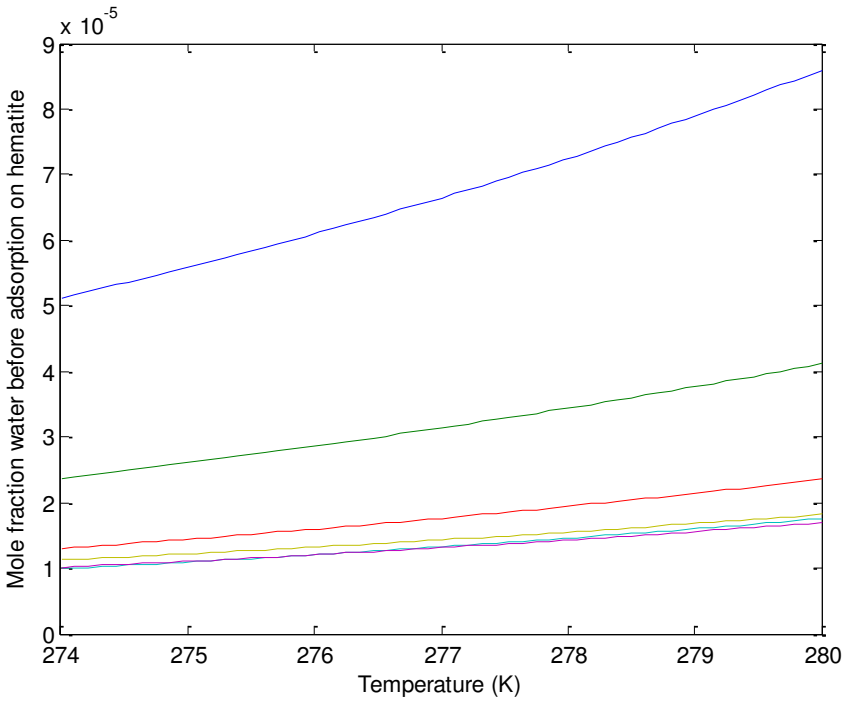

Figure 6.14 : Maximum water content before adsorption on hematite, for mole fraction of 0.025 CO_2, 0.01 H_2S and remaining gas being CH_4. Curves are from top to bottom, for pressures 50 bars, 90 bars, 130 bars, 170 bars, 210 bars, 250 bars.

6.4.2.3 Estimates for water before drop out for mole fraction of 0.05 CO_2, 0.01 H_2S

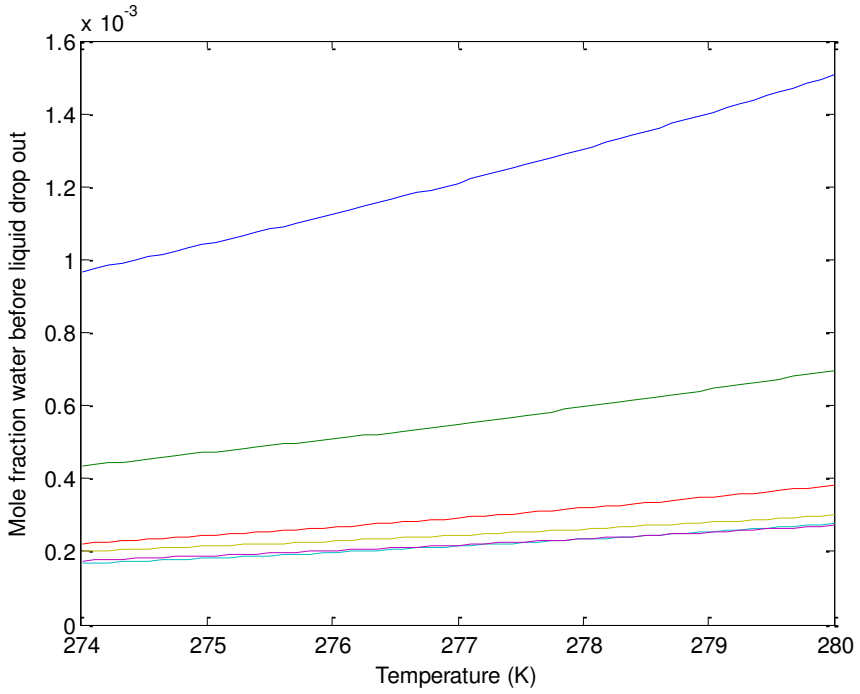

Figure 6.15 : Maximum water content before liquid water drop out, for mole fraction of 0.05 CO_2, 0.01 H_2S and remaining gas being CH_4. Curves are from top to bottom, for pressures 50 bars, 90 bars, 130 bars, 170 bars, 210 bars, 250 bars.

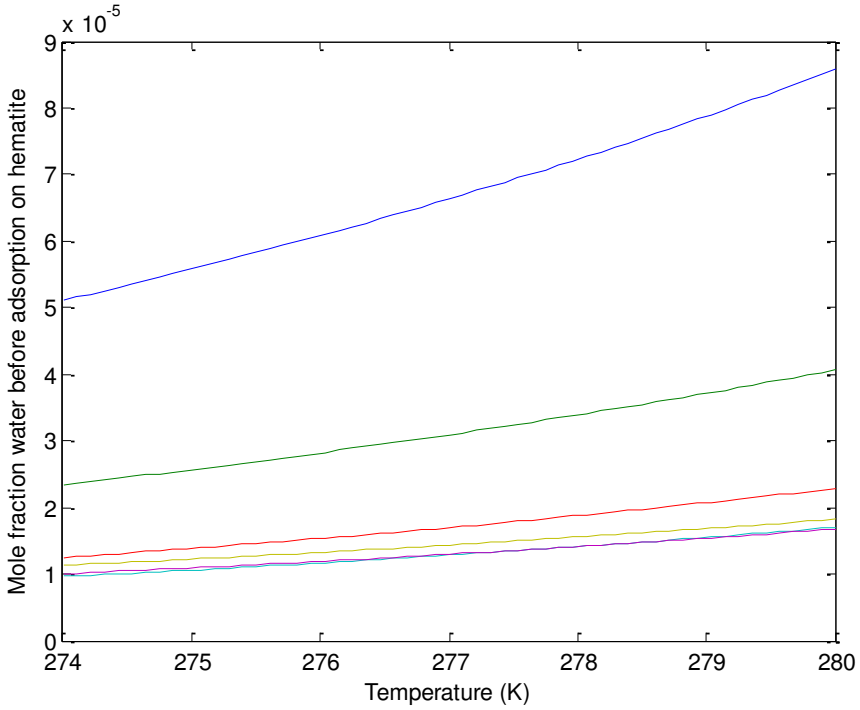

Figure 6.16 : Maximum water content before adsorption on hematite, for mole fraction of 0.05 CO_2, 0.01 H_2S and remaining gas being CH_4. Curves are from top to bottom, for pressures 50 bars, 90 bars, 130 bars, 170 bars, 210 bars, 250 bars.

6.4.2.4 Estimates for water before drop out for mole fraction of 0.1 CO_2, 0.01 H_2S

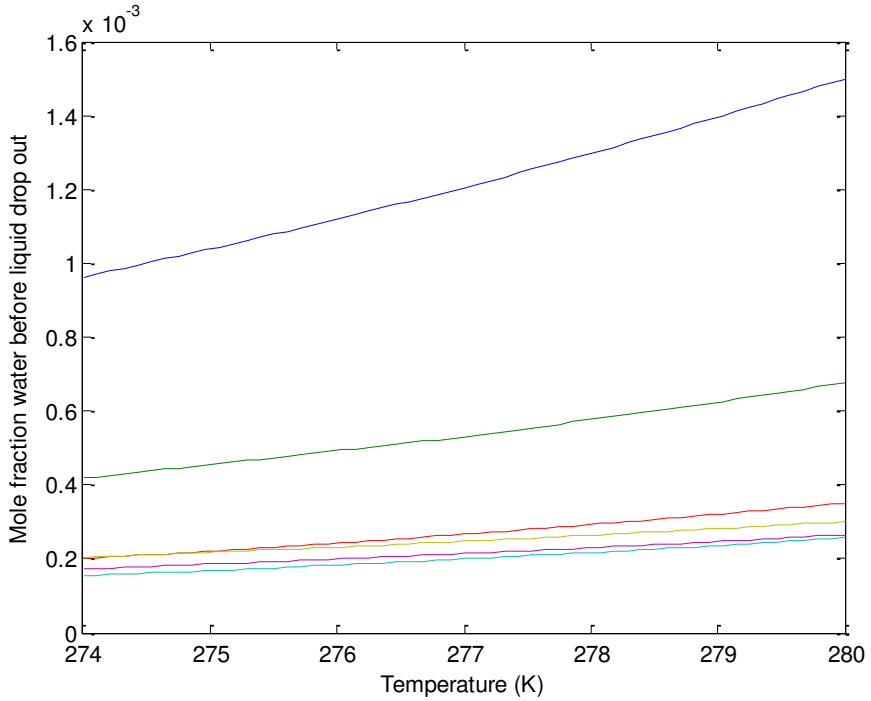

Figure 6.17 : Maximum water content before liquid water drop out, for mole fraction of 0.1 CO_2, 0.01 H_2S and remaining gas being CH_4. Curves are from top to bottom, for pressures 50 bars, 90 bars, 130 bars, 170 bars, 210 bars, 250 bars.

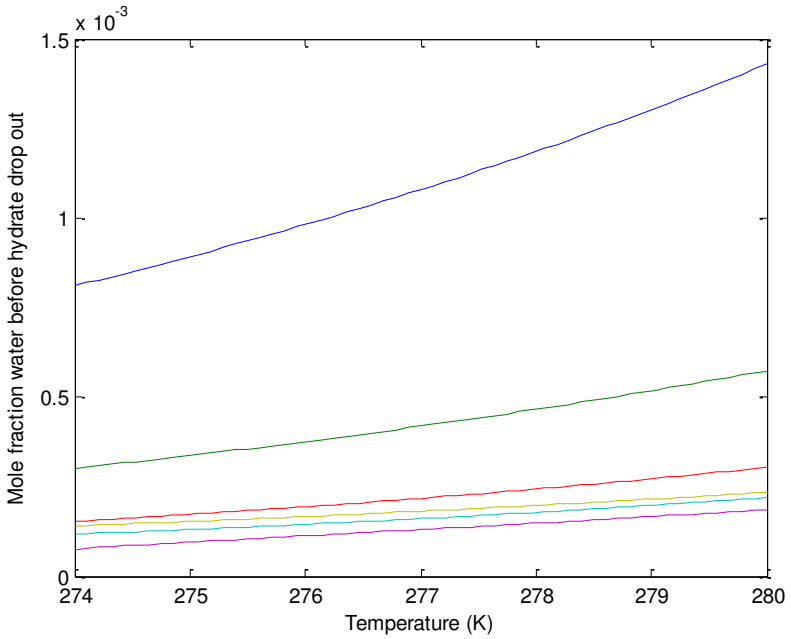

Figure 6.18 : Maximum water content before hydrate drops out, for mole fraction of 0.1 CO_2, 0.01 H_2S and remaining gas being CH_4. Curves are from top to bottom, for pressures 50 bars, 90 bars, 130 bars, 170 bars, 210 bars, 250 bars.

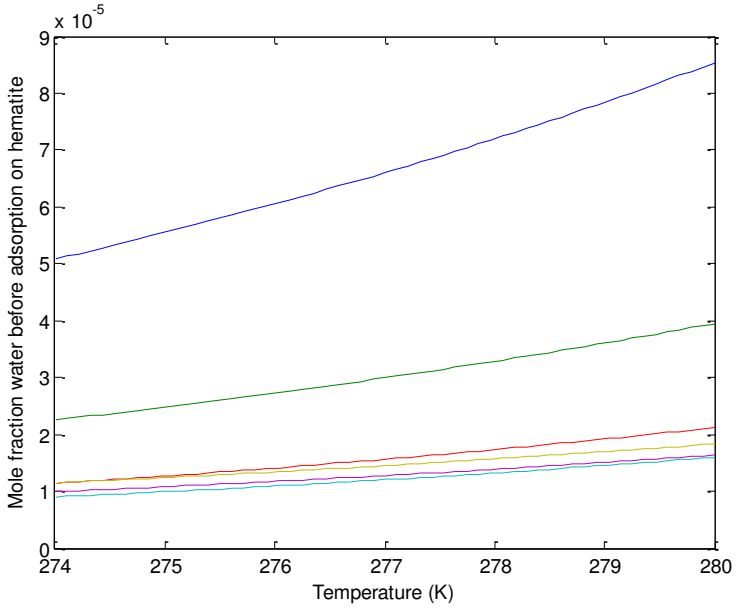

Figure 6.19 : Maximum water content before adsorption on hematite, for mole fraction of 0.1 CO_2, 0.01 H_2S and remaining gas being CH_4. Curves are from top to bottom, for pressures 50 bars, 90 bars, 130 bars, 170 bars, 210 bars, 250 bars.

6.4.3 Estimates for mole fraction of 0.1 H_2S

In this section, the estimates for maximum content of water before drop out as liquid, maximum content of water before drop out as hydrate and estimates for maximum content of water before adsorption for mole fraction of H_2S as 0.1 and varying concentration of CO_2 (0.01, 0.025, 0.05, 0.1) have been calculated, as illustrated in figures 6.20 – 6.31:

6.4.3.1 Estimates for water before drop out for mole fraction of 0.01 CO_2, 0.1 H2S

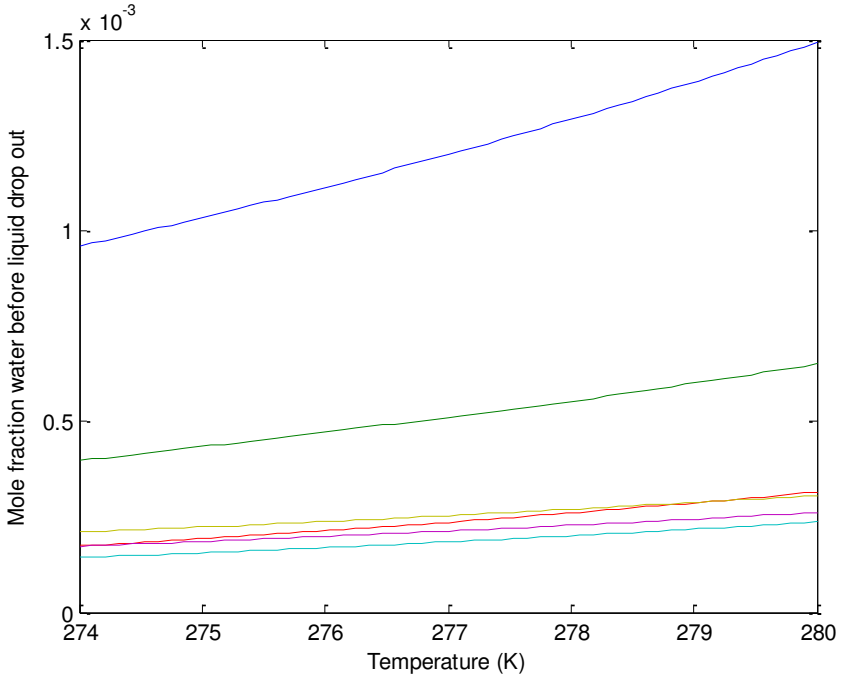

Figure 6.20 : Maximum water content before liquid water drop out, for mole fraction of 0.01 CO_2, 0.1 H_2S and remaining gas being CH_4. Curves are from top to bottom, for pressures 50 bars, 90 bars, 130 bars, 170 bars, 210 bars, 250 bars.

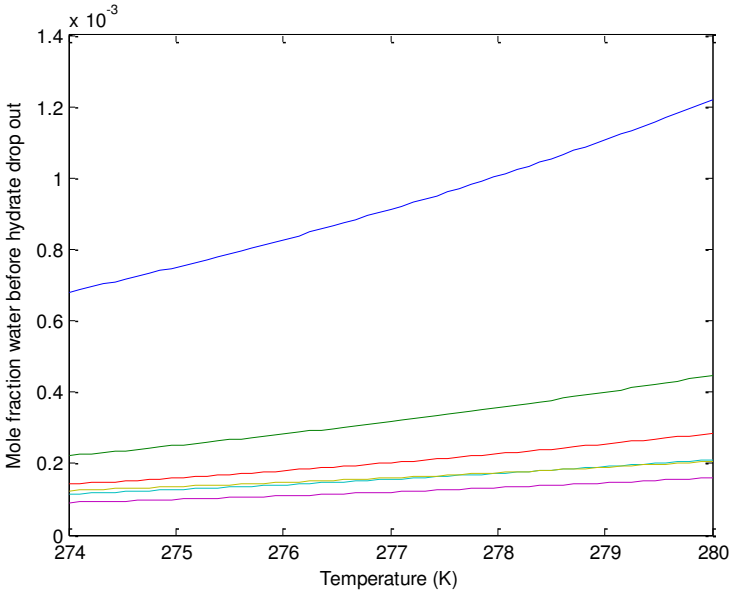

Figure 6.21 : Maximum water content before hydrate drops out, for mole fraction of 0.01 CO_2, 0.1 H_2S and remaining gas being CH_4. Curves are from top to bottom, for pressures 50 bars, 90 bars, 130 bars, 170 bars, 210 bars, 250 bars.

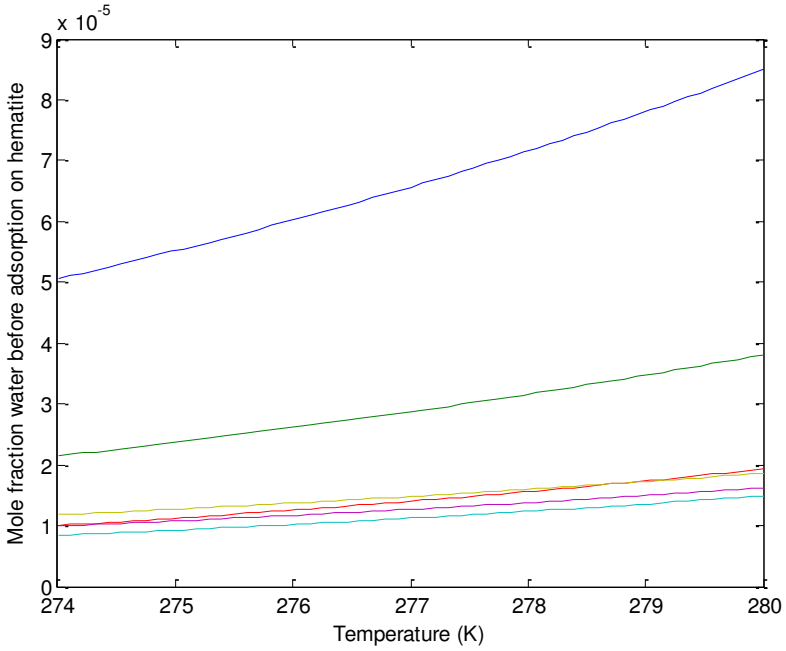

Figure 6.22 : Maximum water content before adsorption on hematite, for mole fraction of 0.01 CO_2, 0.1 H_2S and remaining gas being CH_4. Curves are from top to bottom, for pressures 50 bars, 90 bars, 130 bars, 170 bars, 210 bars, 250 bars.

6.4.3.2 Estimates for water before drop out for mole fraction of 0.025 CO_2, 0.1 H2S

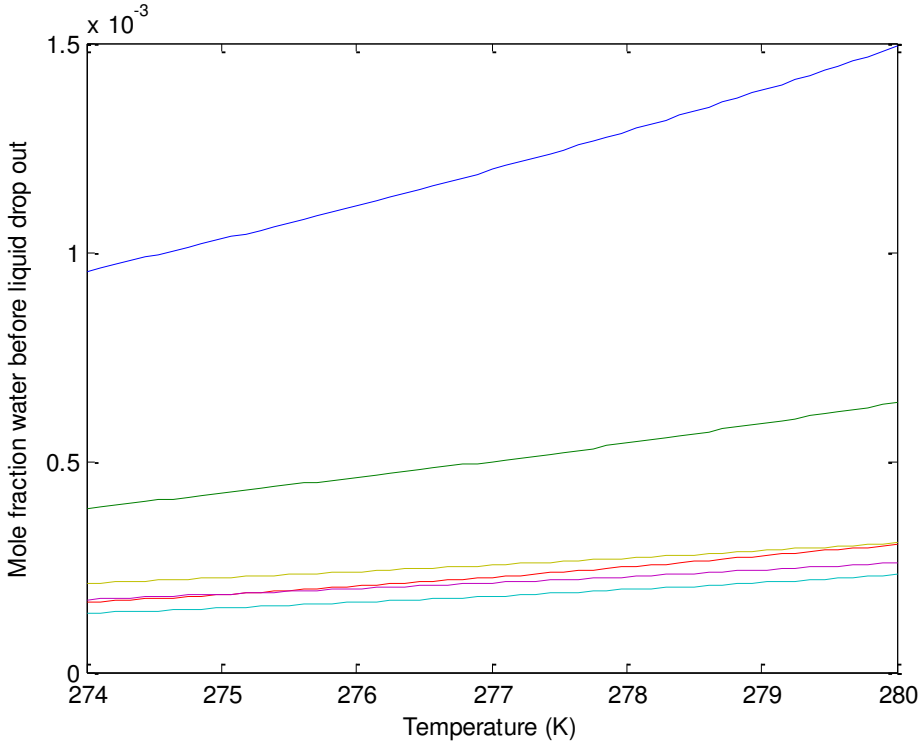

Figure 6.23 : Maximum water content before liquid water drop out, for mole fraction of 0.025 CO_2, 0.1 H_2S and remaining gas being CH_4. Curves are from top to bottom, for pressures 50 bars, 90 bars, 130 bars, 170 bars, 210 bars, 250 bars.

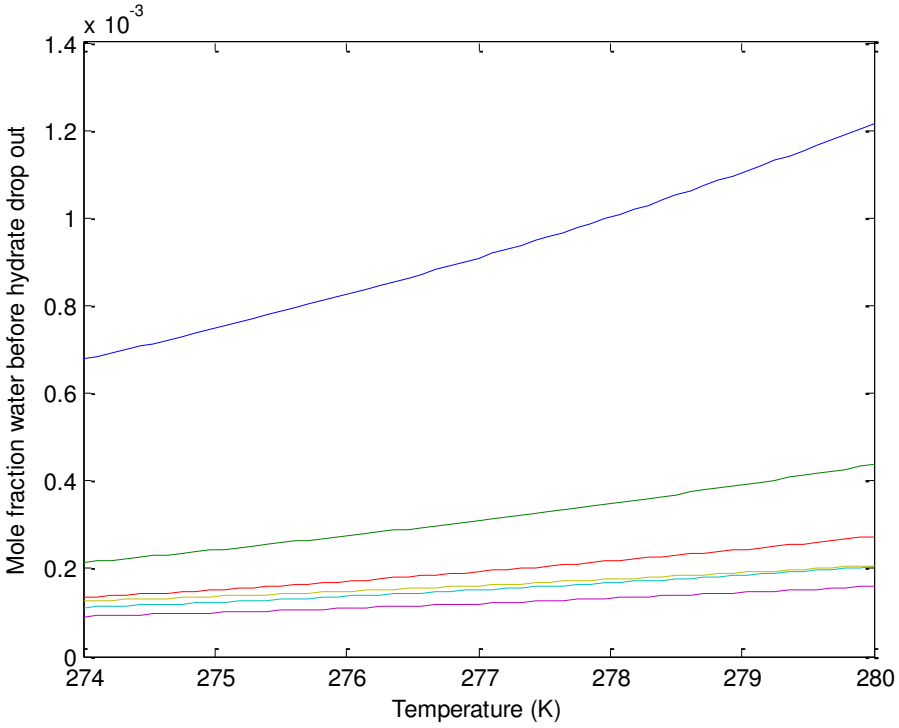

Figure 6.24 : Maximum water content before hydrate drops out, for mole fraction of 0.025 CO_2, 0.1 H_2S and remaining gas being CH_4. Curves are from top to bottom, for pressures 50 bars, 90 bars, 130 bars, 170 bars, 210 bars, 250 bars.

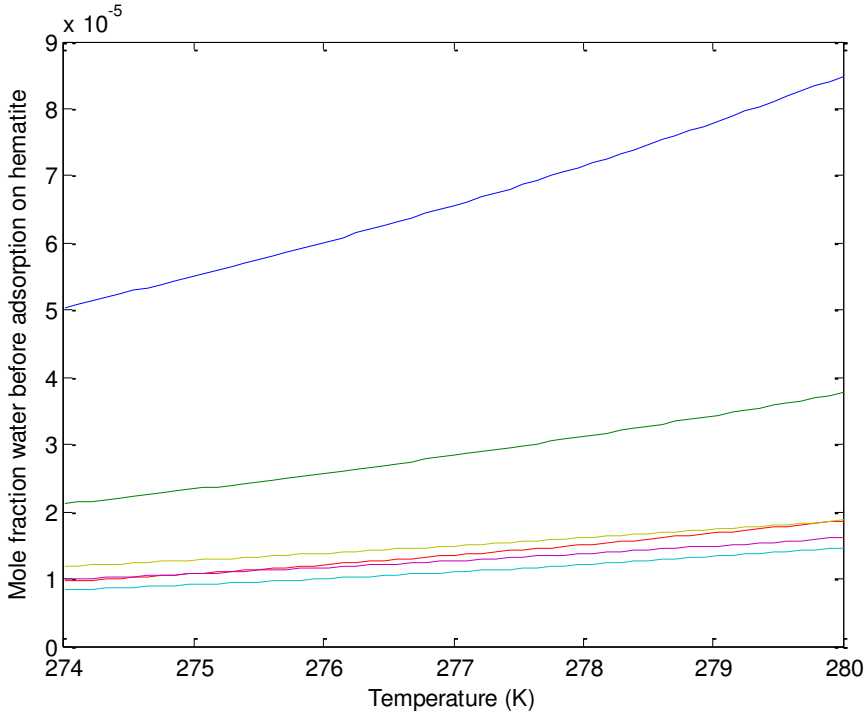

Figure 6.25 : Maximum water content before adsorption on hematite, for mole fraction of 0.025 CO_2, 0.1 H_2S and remaining gas being CH_4. Curves are from top to bottom, for pressures 50 bars, 90 bars, 130 bars, 170 bars, 210 bars, 250 bars.

6.4.3.3 Estimates for water before drop out for mole fraction of 0.05 CO_2, 0.1 H_2S

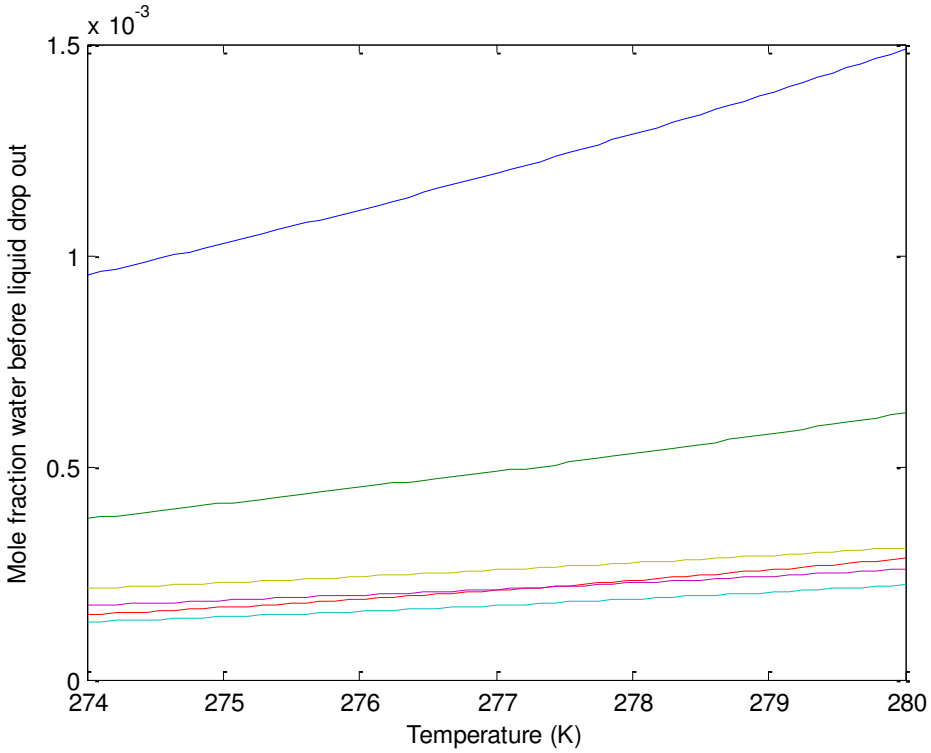

Figure 6.26 : Maximum water content before liquid water drop out, for mole fraction of 0.05 CO_2, 0.1 H_2S and remaining gas being CH_4. Curves are from top to bottom, for pressures 50 bars, 90 bars, 130 bars, 170 bars, 210 bars, 250 bars.

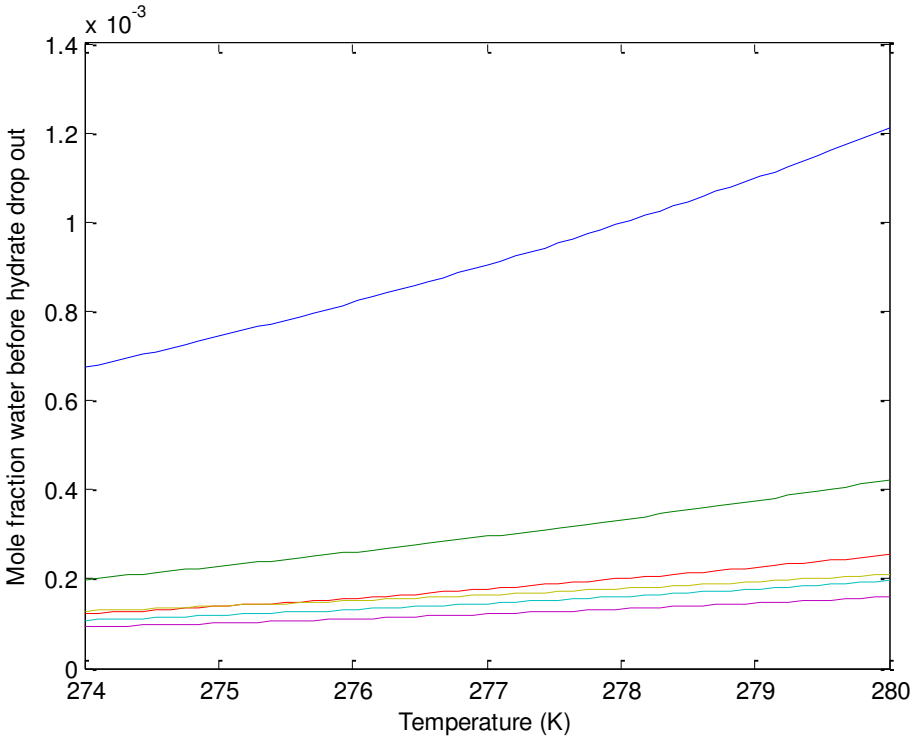

Figure 6.27 : Maximum water content before hydrate drop out, for mole fraction of 0.05 CO_2, 0.1 H_2S and remaining gas being CH_4. Curves are from top to bottom, for pressures 50 bars, 90 bars, 130 bars, 170 bars, 210 bars, 250 bars.

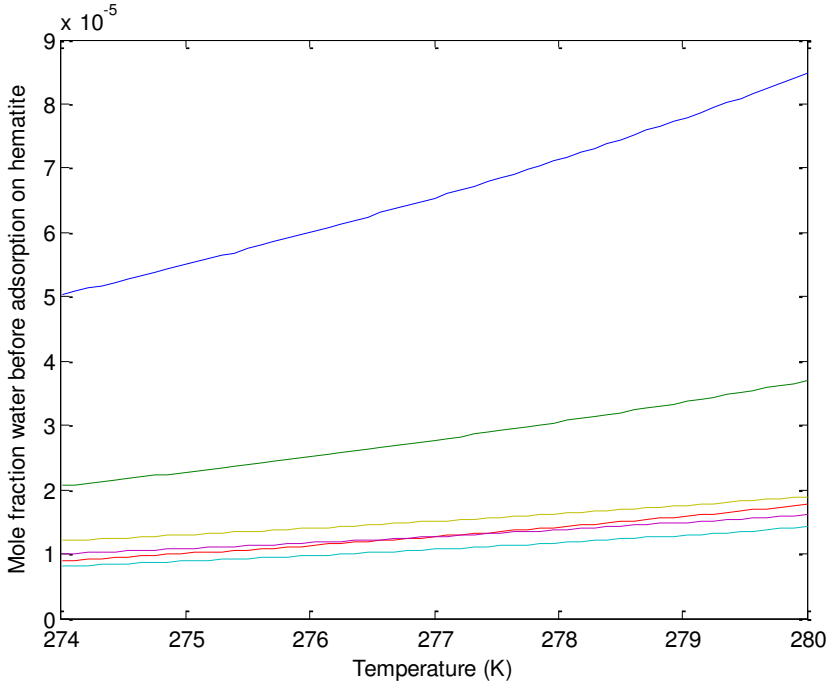

Figure 6.28 : Maximum water content before adsorption on hematite, for mole fraction of 0.05 CO_2, 0.1 H_2S and remaining gas being CH_4. Curves are from top to bottom, for pressures 50 bars, 90 bars, 130 bars, 170 bars, 210 bars, 250 bars.

6.4.3.4 Estimates for water before drop out for mole fraction of 0.1 CO_2, 0.1 H_2S

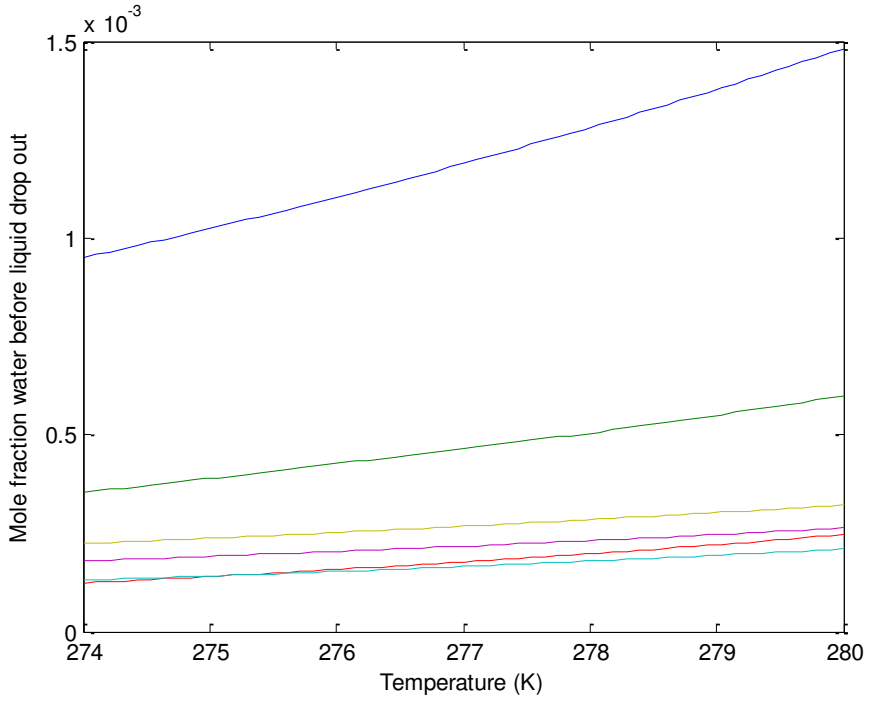

Figure 6.29 : Maximum water content before liquid water drop out, for mole fraction of 0.1 CO_2, 0.1 H_2S and remaining gas being CH_4. Curves are from top to bottom, for pressures 50 bars, 90 bars, 130 bars, 170 bars, 210 bars, 250 bars.

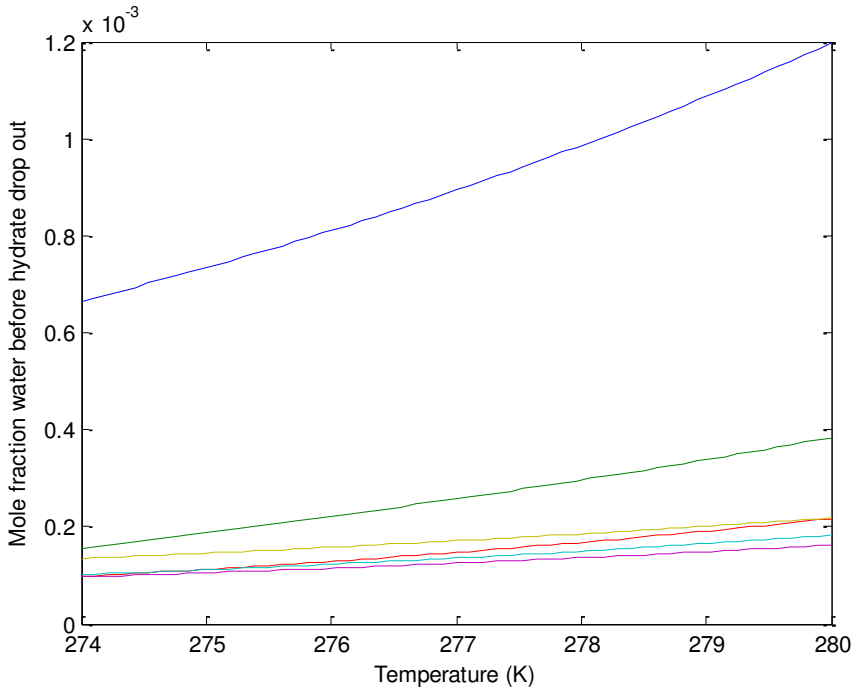

Figure 6.30 : Maximum water content before hydrate drops out, for mole fraction of 0.1 CO_2, 0.1 H_2S and remaining gas being CH_4. Curves are from top to bottom, for pressures 50 bars, 90 bars, 130 bars, 170 bars, 210 bars, 250 bars.

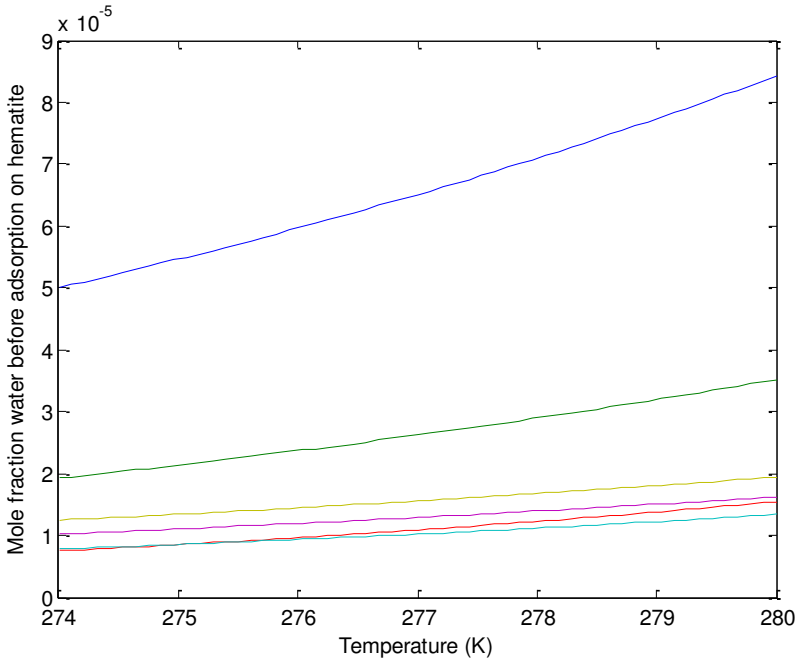

Figure 6.31 : Maximum water content before adsorption on hematite, for mole fraction of 0.1 CO_2, 0.1 H_2S and remaining gas being CH_4. Curves are from top to bottom, for pressures 50 bars, 90 bars, 130 bars, 170 bars, 210 bars, 250 bars.

6.4.4 Density and compressibility table for model systems

In this section estimates for density and compressibility factor Z for a system 2.1.1 to 2.3.4 are given below.

Table 6.8 : Estimates for Density (kg/m³) for a system 2.1.1: CO_2 0.01. H_2S 0.001 and remaining CH_4

TEMPERATURE	PRESSURE	⟶				
(K)	(bars)					
	50	90	130	170	210	250
274	40.60	80.63	124.69	165.17	197.31	221.88
275	40.38	80.03	123.62	163.80	195.90	220.54
276	40.16	79.45	122.57	162.46	194.51	219.21
277	39.94	78.88	121.54	161.14	193.14	217.89
278	39.73	78.32	120.54	159.85	191.78	216.58
279	39.52	77.77	119.55	158.58	191.78	215.28
280	39.31	77.23	118.59	157.32	189.11	213.99

Table 6. 9 : Estimates for compressibility factor Z for a system 2. 1.1: CO_2 0.01. H_2S 0.001 and remaining CH_4

TEMPERATURE	PRESSURE	⟶				
(K)	(bars)					
	50	90	130	170	210	250
274	0.8833	0.8007	0.7478	0.7383	0.7634	0.8082
275	0.8849	0.8037	0.7516	0.7417	0.7661	0.8101
276	0.8865	0.8066	0.7553	0.7451	0.7688	0.8121
277	0.8881	0.8096	0.7589	0.7485	0.7715	0.8141
278	0.8897	0.8124	0.7625	0.7518	0.7741	0.816
279	0.8912	0.8152	0.766	0.7552	0.7741	0.818
280	0.8927	0.818	0.7694	0.7584	0.7794	0.82

Table 6. 10 : Estimates for density (Kg/m3) for a system 2. 1.2 CO_2 0.025. H_2S 0.001 and remaining CH_4

TEMPERATURE	PRESSURE	⟶				
(K)	(bars)					
	50	90	130	170	210	250
274	41.74	83.10	128.81	170.70	203.80	228.99
275	41.51	82.48	127.68	169.28	202.33	227.60
276	41.28	81.87	126.58	167.88	200.89	226.22
277	41.06	81.28	125.50	166.50	199.46	224.85
278	40.84	80.69	124.45	165.15	198.04	223.50
279	40.62	80.12	123.42	163.81	196.65	222.15
280	40.41	79.56	122.41	162.51	195.27	220.81

Table 6.11: Estimates for compressibility factor Z for a system2.1.2: CO_2 0.025. H_2S 0.001 and remaining CH_4

TEMPERATURE	PRESSURE	⟶				
(K)	(bars)					
	50	90	130	170	210	250
274	0.8813	0.7967	0.7425	0.7327	0.7581	0.8032
275	0.8829	0.7998	0.7463	0.7361	0.7608	0.8051
276	0.8846	0.8028	0.7501	0.7396	0.7635	0.8071
277	0.8862	0.8058	0.7538	0.743	0.7662	0.8091
278	0.8878	0.8087	0.7574	0.7464	0.7689	0.8111
279	0.8893	0.8116	0.761	0.7498	0.7716	0.8131
280	0.8908	0.8144	0.7645	0.7531	0.7742	0.8151

Table 6.12 : Estimates for density (Kg/m³) for a system 2. 1.3 CO_2 0.05. H_2S 0.001 and remaining CH_4

TEMPERATURE	PRESSURE	⟶				
(K)	(bars)					
	50	90	130	170	210	250
274	43.66	87.32	135.87	180.20	214.89	241.10
275	43.41	86.65	134.65	178.67	213.33	239.63
276	43.17	86.00	133.46	177.16	211.78	238.17
277	42.94	85.36	132.30	175.68	210.25	236.71
278	42.70	84.73	131.16	174.22	208.75	235.27
279	42.47	84.12	130.04	172.79	207.26	233.84
280	42.25	83.52	128.95	171.38	205.78	232.43

Table 6.13 : Estimates for compressibility factor Z for a system 2.1.3: CO_2 0.05. H_2S 0.001 and remaining CH_4

TEMPERATURE	PRESSURE	⟶				
(K)	(bars)					
	50	90	130	170	210	250
274	0.8777	0.7899	0.7333	0.723	0.749	0.7947
275	0.8794	0.7931	0.7372	0.7265	0.7517	0.7966
276	0.8811	0.7962	0.7411	0.7301	0.7544	0.7986
277	0.8828	0.7993	0.7449	0.7336	0.7572	0.8006
278	0.8844	0.8023	0.7487	0.7371	0.7599	0.8026
279	0.886	0.8053	0.7524	0.7405	0.7626	0.8046
280	0.8876	0.8082	0.756	0.7439	0.7653	0.8067

Table 6. 14 : Estimates for density (Kg/m³) for a system 2. 1.4 CO_2 0.1 H_2S 0.001 and remaining CH_4

TEMPERATURE	PRESSURE					
(K)	(bars)					
	50	90	130	170	210	250
274	47.56	96.11	150.85	200.32	238.18	266.36
275	47.29	95.34	149.42	198.54	236.41	264.71
276	47.02	94.58	148.02	196.79	234.66	263.07
277	46.76	93.85	146.65	195.08	232.92	261.44
278	46.50	93.13	145.32	193.39	231.21	259.82
279	46.24	92.42	144.01	191.74	229.51	258.22
280	45.99	91.73	142.74	190.11	227.83	256.63

Table 6.15 : Estimates for compressibility factor Z for a system 2.1.4: CO_2 0.1. H_2S 0.001 and remaining CH_4

TEMPERATURE	PRESSURE					
(K)	(bars)					
	50	90	130	170	210	250
274	0.8701	0.7751	0.7133	0.7025	0.7298	0.7769
275	0.872	0.7786	0.7176	0.7062	0.7326	0.7789
276	0.8738	0.7819	0.7217	0.7099	0.7354	0.7809
277	0.8755	0.7852	0.7258	0.7135	0.7382	0.783
278	0.8772	0.7885	0.7299	0.7172	0.741	0.785
279	0.879	0.7916	0.7338	0.7208	0.7438	0.787
280	0.8806	0.7947	0.7377	0.7243	0.7466	0.7891

Table 6.16 : Estimates for density (Kg/m³) for a system 2.2.1 CO_2 0.01. H_2S 0.01 and remaining CH_4

TEMPERATURE	PRESSURE		⟶			
(K)	(bars)					
	50	90	130	170	210	250
274	41.10	81.88	127.01	168.37	200.97	225.73
275	40.88	81.26	125.89	166.96	199.52	224.36
276	40.65	80.66	124.80	165.57	198.09	223.00
277	40.43	80.08	123.74	164.21	196.68	221.65
278	40.22	79.50	122.69	162.87	195.28	220.31
279	40.00	78.93	121.67	161.55	193.90	218.98
280	39.79	78.38	120.68	160.25	192.54	217.66

Table 6.17 : Estimates for compressibility factor Z for a system 2.2.1 CO_2 0.01. H_2S 0.01 and remaining CH4

TEMPERATURE	PRESSURE	⟶				
(K)	(bars)					
	50	90	130	170	210	250
274	0.8812	0.7963	0.7415	0.7314	0.757	0.8023
275	0.8829	0.7994	0.7453	0.7349	0.7597	0.8043
276	0.8845	0.8024	0.7491	0.7384	0.7624	0.8062
277	0.8861	0.8054	0.7528	0.7418	0.7651	0.8082
278	0.8877	0.8083	0.7565	0.7453	0.7678	0.8102
279	0.8892	0.8112	0.7601	0.7486	0.7705	0.8122
280	0.8908	0.814	0.7637	0.752	0.7732	0.8142

Table 6.18 : Estimates for density (Kg/m³) for a system 2.2.2: CO_2 0.025, H_2S 0.01 and remaining CH_4

TEMPERATURE	PRESSURE		⟶			
(K)	(bars)					
	50	90	130	170	210	250
274	42.25	84.38	131.18	173.97	207.51	232.881
275	42.01	83.74	130.01	172.50	206.01	231.462
276	41.78	83.11	128.86	171.05	204.52	230.054
277	41.55	82.50	127.75	169.62	203.05	228.656
278	41.33	81.90	126.65	168.22	201.60	227.268
279	41.11	81.90	125.59	166.84	200.16	225.891
280	40.89	80.73	124.54	165.49	198.74	224.526

Table 6.19 : Estimates for compressibility factor Z for a system 2.2.2: CO_2 0.025. H_2S 0.01 and remaining CH_4

TEMPERATURE	PRESSURE	⟶				
(K)	(bars)					
	50	90	130	170	210	250
274	0.8791	0.7923	0.7362	0.7259	0.7517	0.7974
275	0.8808	0.7955	0.7401	0.7294	0.7545	0.7994
276	0.8825	0.7986	0.7439	0.7329	0.7572	0.8014
277	0.8841	0.8016	0.7477	0.7364	0.7599	0.8034
278	0.8857	0.8046	0.7515	0.7399	0.7626	0.8054
279	0.8873	0.8046	0.7551	0.7433	0.7654	0.8074
280	0.8889	0.8104	0.7588	0.7467	0.7681	0.8094

Table 6.20 : Estimates for density (Kg/m³) for a system 2.2.3: CO_2 0.05. H_2S 0.01 and remaining CH_4

TEMPERATURE	PRESSURE	⟶				
(K)	(bars)					
	50	90	130	170	210	250
274	44.17	88.63	138.33	183.58	218.69	245.07
275	43.92	87.95	137.07	181.99	217.09	243.57
276	43.68	87.27	135.83	180.43	215.51	242.07
277	43.44	86.62	134.62	178.90	213.94	240.59
278	43.20	85.97	133.44	177.40	212.39	239.12
279	42.97	85.34	132.29	175.91	210.86	237.66
280	42.74	84.72	131.16	174.46	209.35	236.21

Table 6.21 : Estimates for compressibility factor Z for a system 2.2.3: CO_2 0.05, H_2S 0.01 and remaining CH_4

TEMPERATURE	PRESSURE	⟶				
(K)	(bars)					
	50	90	130	170	210	250
274	0.8755	0.7854	0.7269	0.7163	0.7428	0.7891
275	0.8773	0.7887	0.731	0.7199	0.7455	0.7911
276	0.879	0.7919	0.7349	0.7235	0.7483	0.793
277	0.8807	0.795	0.7389	0.7271	0.751	0.7951
278	0.8823	0.7981	0.7427	0.7306	0.7538	0.7971
279	0.884	0.8011	0.7465	0.7341	0.7566	0.7991
280	0.8856	0.8041	0.7502	0.7376	0.7593	0.8011

Table 6.22 : Estimates for density (Kg/m³) for a system 2.2.4: CO_2 0.1. H_2S 0.01 and remaining CH_4

TEMPERATURE	PRESSURE	⟶				
(K)	(bars)					
	50	90	130	170	210	250
274	48.10	97.52	153.53	203.93	242.18	270.49
275	47.82	96.73	152.04	202.10	240.37	268.81
276	47.55	95.95	150.59	200.30	238.58	267.14
277	47.28	95.19	149.17	198.53	236.80	265.48
278	47.01	94.45	147.79	196.79	235.05	263.84
279	46.75	93.72	146.44	195.08	233.31	262.20
280	46.50	93.01	145.12	193.40	231.59	260.58

Table 6.23 : Estimates for compressibility factor Z for a system 2.2.4: CO_2 0.1, H_2S 0.01 and remaining CH_4

TEMPERATURE	PRESSURE	⟶				
(K)	(bars)					
	50	90	130	170	210	250
274	0.8679	0.7705	0.7069	0.696	0.7239	0.7716
275	0.8697	0.774	0.7113	0.6997	0.7267	0.7736
276	0.8715	0.7774	0.7155	0.7035	0.7296	0.7756
277	0.8733	0.7808	0.7197	0.7072	0.7324	0.7777
278	0.8751	0.7841	0.7238	0.7108	0.7352	0.7797
279	0.8768	0.7874	0.7279	0.7145	0.738	0.7818
280	0.8785	0.7905	0.7318	0.7181	0.7408	0.7838

Table 6.24 : Estimates for density (Kg/m³) for a system 2.3.1: CO_2 0.01, H_2S 0.1 and remaining CH_4

TEMPERATURE	PRESSURE		⟶			
(K)	(bars)					
	50	90	130	170	210	250
274	46.35	95.61	153.17	203.60	239.84	265.83
275	46.07	94.77	151.53	201.66	238.01	264.18
276	45.80	93.94	149.93	199.75	236.20	262.54
277	45.54	93.14	148.37	197.87	234.40	260.90
278	45.27	92.36	146.86	196.02	232.62	259.28
279	45.02	91.60	145.38	194.21	230.85	257.66
280	44.76	90.86	143.95	192.42	229.11	256.06

Table 6.25 : Estimates for compressibility factor Z for a system 2.3.1: CO_2 0.01, H_2S 0.1 and remaining CH_4

TEMPERATURE	PRESSURE	⟶				
(K)	(bars)					
	50	90	130	170	210	250
274	0.8583	0.749	0.6753	0.6644	0.6967	0.7483
275	0.8603	0.7529	0.6801	0.6683	0.6995	0.7502
276	0.8623	0.7567	0.6849	0.6723	0.7023	0.7522
277	0.8642	0.7605	0.6896	0.6762	0.7051	0.7542
278	0.8661	0.7641	0.6942	0.6801	0.708	0.7562
279	0.8679	0.7677	0.6987	0.684	0.7108	0.7582
280	0.8697	0.7713	0.7032	0.6879	0.7137	0.7602

Table 6.26 : Estimates for Density (Kg/m³) for a system 2.3.2: CO_2 0.025, H_2S 0.1 and remaining CH_4

TEMPERATURE	PRESSURE		⟶			
(K)	(bars)					
	50	90	130	170	210	250
274	47.55	98.41	157.98	209.88	246.96	273.47
275	47.27	97.53	156.27	207.87	245.07	271.77
276	46.99	96.67	154.60	205.89	243.20	270.08
277	46.71	95.84	152.97	203.94	241.34	268.40
278	46.44	95.02	151.39	202.03	239.50	266.73
279	46.18	94.23	149.85	200.14	237.68	265.06
280	45.91	93.45	148.35	198.29	235.88	263.41

Table 6.27 : Estimates for Compressibility factor Z for a system 2.3.2: CO_2 0.025, H2S 0.1 and remaining CH_4

TEMPERATURE	PRESSURE	⟶				
(K)	(bars)					
	50	90	130	170	210	250
274	0.856	0.7445	0.6699	0.6594	0.6923	0.7442
275	0.858	0.7485	0.6748	0.6633	0.6951	0.7461
276	0.86	0.7524	0.6796	0.6673	0.6979	0.7481
277	0.8619	0.7562	0.6843	0.6712	0.7007	0.7501
278	0.8638	0.76	0.689	0.6752	0.7035	0.7521
279	0.8657	0.7636	0.6936	0.6791	0.7064	0.7541
280	0.8675	0.7672	0.6981	0.683	0.7092	0.7561

Table 6. 28 : Estimates for density (Kg/m³) for a system 2.3.3: CO_2 0.05, H_2S 0.1 and remaining CH_4

TEMPERATURE	PRESSURE				→	
(K)	(bars)					
	50	90	130	170	210	250
274	49,59	103,21	166,31	220,71	259,15	286,52
275	49,28	102,26	164,47	218,57	257,16	284,73
276	48,99	101,34	162,67	214,40	255,19	282,96
277	48,70	100,44	160,92	212,36	253,24	281,19
278	48,41	99,57	159,22	212,36	251,30	279,44
279	48,13	98,71	157,56	210,36	249,38	277,69
280	47,85	97,88	155,95	208,39	247,48	275,95

Table 6.29 : Estimates for Compressibility factor Z for a system 2.3.3: CO_2 0.05, H_2S 0.1 and remaining CH_4

TEMPERATURE	PRESSURE			→		
(K)	(bars)					
	50	90	130	170	210	250
274	0.8518	0.7366	0.6603	0.6507	0.6846	0.7371
275	0.8539	0.7408	0.6653	0.6547	0.6873	0.739
276	0.8559	0.7448	0.6702	0.6626	0.6901	0.741
277	0.858	0.7488	0.6751	0.6665	0.6929	0.7429
278	0.8599	0.7526	0.6798	0.6665	0.6958	0.7449
279	0.8619	0.7564	0.6845	0.6705	0.6986	0.7469
280	0.8638	0.7601	0.6891	0.6744	0.7015	0.7489

Table 6.30 : Estimates for density (Kg/m³) for a system 2.3.4: CO_2 0.1, H2S 0.1 and remaining CH_4

TEMPERATURE	PRESSURE		⟶			
(K)	(bars)					
	50	90	130	170	210	250
274	53.75	113.40	184.28	243.83	284.90	313.83
275	53.42	112.29	182.13	241.42	282.70	311.87
276	53.09	111.22	180.04	239.04	280.52	309.92
277	52.76	110.18	178.01	236.70	278.35	307.98
278	52.44	109.16	176.02	234.40	276.20	306.05
279	52.13	108.17	174.10	232.14	274.07	304.13
280	51.82	107.21	172.22	229.91	271.96	302.22

Table 6.31 : Estimates for compressibility factor Z for a system 2.3.4: CO_2 0.1, H_2S 0.1 and remaining CH_4

TEMPERATURE	PRESSURE	⟶				
(K)	(bars)					
	50	90	130	170	210	250
274	0.8429	0.7192	0.6392	0.6318	0.6679	0.7218
275	0.8451	0.7236	0.6444	0.6358	0.6707	0.7237
276	0.8473	0.728	0.6496	0.6398	0.6734	0.7256
277	0.8494	0.7322	0.6546	0.6437	0.6762	0.7276
278	0.8515	0.7364	0.6596	0.6477	0.679	0.7295
279	0.8536	0.7404	0.6645	0.6517	0.6819	0.7315
280	0.8556	0.7444	0.6693	0.6557	0.6847	0.7335

6.5 Analysis of results

For a complete overview of the systems mentioned in this section 6.5 please refer to table 6.7.

Case wise analysis:-

Tables 6.8 to 6.31 show the estimates for density and compressibility factor (Z) for the model systems 2.1.1 – 2.3.4. (Refer table 6.7). Let us consider three cases

6.5.1 Case 1 (System 2.1.1: 0.01 Y_{CO2}, 0.001 Y_{H2S} remaining Y_{CH4} and System 2.3.4: 0.1 Y_{CO2}, 0.01 Y_{H2S} remaining Y_{CH4})

Consider system 2.1.1 with minimum Y_{CO2} 0.01, minimum Y_{H2S} 0.001 and remaining Y_{CH4} and comparing it with another system 2.3.4 with maximum Y_{CO2} 0.1, mid-range Y_{H2S} 0.01 and remaining Y_{CH4}.

It can be stated that at temperature 274 k and pressure 50 bars the density in system 2.3.4 increases by 0.32 times as compared to the density at the same temperature and pressure in system 2.1.1. And accordingly compressibility factor Z in system 2.1.1 increases by 0.048 times as compared to system 2.3.4.

When the pressure is increased further from 50 bars to 130 bars the density in system 2.3.4 increases by 0.48 times as compared to the density at the same temperature and pressure in system 2.1.1. And accordingly compressibility factor Z in system 2.1.1 increases by 0.16 times as compared to system 2.3.4.

Increasing the pressure further to 250 bars and the temperature at 274 K the density in system 2.3.4 increases by 0.41 times as compared to the density at the same temperature and pressure in system 2.1.1 and accordingly compressibility factor Z in system 2.1.1 increases by 0.12 times as compared to system 2.3.4.

Increasing the temperature from 274 K to 277 K at pressure 50 bars the density in system 2.3.4 increases by 0.32 times as compared to the density at the same temperature and pressure in system 2.1.1. And compressibility factor Z in system 2.1.1 increases by 0.046 times as compared to system 2.3.4.

Increasing the pressure further to 130 bars keeping the temperature at 277 K the density in system 2.3.4 increases by 0.46 times as compared to the density at the same temperature and

pressure in system 2.1.1. And the compressibility factor Z in system 2.1.1 increases by 0.016 times as compared to system 2.3.4.

As the pressure is increased to 250 bars the density in system 2.3.4 increases by 0.41 times as compared to the density at the same temperature and pressure in system 2.1.1. And accordingly compressibility factor Z in system 2.1.1 increases by 0.12 times as compared to system 2.3.4.

Further increasing the temperature from 277 K to 280 K at pressure 50 bars the density in system 2.3.4 increases by 0.32 times as compared to the density at the same temperature and pressure in system 2.1.1. And accordingly compressibility factor Z in system 2.1.1 increases by 0.043 times as compared to system 2.3.4.

At 130 bars and temperature 280 K the density in system 2.3.4 increases by 0.45 times as compared to the density at the same temperature and pressure in system 2.1.1. And accordingly compressibility factor Z in system 2.1.1 increases by 0.15 times as compared to system 2.3.4.

With further increasing the pressure to 250 bars and temperature 280 K the density in system 2.3.4 increase by 0.41 times to the density at the same temperature and pressure in system 2.1.1. And accordingly the compressibility factor Z in system 2.1.1 increases by 0.11 times as compared to system 2.3.4.

It can overall be stated that the tolerance ratio between system 2.1.1 and 2.3.4, compressibility factor Z of the gas mixture decreases with increasing temperature and increasing mole fraction of $C0_2$ and H_2S in the latter. The density increases as the pressure increases with increasing mole fraction of $C0_2$ and H_2S in the latter.

6.5.2 Case 2 (System 2.1.1: 0.01 Y_{CO2}, 0.001 Y_{H2S} remaining Y_{CH4} and System 2.1.4: 0.1 Y_{CO2}, 0.001 Y_{H2S} remaining Y_{CH4})

Considering above system 2.1.1 with minimum Y_{CO2} 0.01, minimum Y_{H2S} 0.001 and remaining Y_{CH4} and comparing it with another system 2.1.4 with maximum Y_{CO2} 0.1, minimum Y_{H2S} 0.001 and remaining $Y_{CH4,}$

It can be stated that at temperature 274 K and pressure 50 bars the density in system 2.1.4 increases by 0.17 times as compared to the density at the same temperature and pressure in system 2.1.1 and accordingly compressibility factor Z in system 2.1.1 increases by 0.015 times as compared to system 2.1.4.

When the pressure is increased further from 50 bars to 130 bars at temperature 274 K the density in system 2.1.4 increases by 0.21 times as compared to the density at the same temperature and pressure in system 2.1.1. The compressibility factor Z in system 2.1.1 increases by 0.048 times as compared to system 2.1.4.

Increasing the pressure further to 250 bars and the temperature at 274 K the density in system 2.1.4 increases by 0.20 times as compared to the density at the same temperature and pressure in system 2.1.1. The corresponding compressibility factor Z in system 2.1.1 increases by 0.040 times as compared to system 2.1.4.

Increasing the temperature from 274 K to 277 K at pressure 50 bars the density in system 2.1.4 increases by 0.17 times as compared to the density at the same temperature and pressure in system 2.1.1. And the corresponding compressibility factor Z in system 2.1.1 increases by 0.014 times as compared to system 2.1.4.

Increasing the pressure further to 130 bars at temperature 277 K the density in system 2.1.4 increases by 0.19 times as compared to the density at the same temperature and pressure in system 2.1.1. And the corresponding compressibility factor Z in system 2.1.1 increases by 0.046 times as compared to system 2.1.4.

As the pressure is increased to 250 bars keeping the temperature constant at 277 K, the density in system 2.1.4 increases by 0.20 times as compared to the density at the same temperature and

pressure in system 2.1.1. The corresponding compressibility factor Z in system 2.1.1 increases by 0.040 times as compared to system 2.1.4.

Further increasing the temperature from 277 K to 280 K at pressure 50 bars, the density in system 2.1.4 increases by 0.16 times as compared to the density at the same temperature and pressure in system 2.1.1. And the corresponding compressibility factor Z in system 2.1.1 increases by 0.014 times as compared to system 2.1.4.

At 130 bars and temperature 280 K the density in system 2.1.4 increases by 0.20 times as compared to the density at the same temperature and pressure in system 2.1.1. The corresponding compressibility factor Z in system 2.1.1 increases by 0.043 times as compared to system 2.1.4.

Further increasing the pressure to 250 bars and temperature 280 K the density in system 2.1.4 increases by 0.20 times compared to the density at the same temperature and pressure in system 2.1.1. And the corresponding compressibility factor Z in system 2.1.1 increases by 0.039 times as compared to system 2.1.4.

It can overall be stated that the tolerance ratio between system 2.1.1 and 2.1.4, compressibility factor Z of the gas mixture decreases with increasing temperature and increasing mole fraction of $C0_2$ in the latter. The density increases as the pressure increases with increasing mole fraction of $C0_2$ in the latter.

6.5.3 Case 3 (System 2.1.1: 0.01 Y_{CO2}, 0.001 Y_{H2S} remaining Y_{CH4} and System 2.3.1: 0.01 Y_{CO2}, 0.01 Y_{H2S} remaining Y_{CH4})

Considering above system 2.1.1 with minimum Y_{CO2} 0.01, minimum Y_{H2S} 0.001 and remaining Y_{CH4} and comparing it with another system 2.3.1 with minimum Y_{CO2} 0.01, mid rangeY_{H2S} 0.01 and remaining $Y_{CH4.}$

It can be stated that at temperature 274 k and pressure 50 bars the density in system 2.3.1 increases by 0.14 times as compared to the density at the same temperature and pressure in system 2.1.1. And accordingly compressibility factor Z in system 2.1.1 increases by 0.29 times as compared to system 2.3.1.

When the pressure is increased further from 50 bars to 130 bars at temperature 274 k the density in system 2.3.1 increases by 0.22 times as compared to the density at the same temperature and pressure in system 2.1.1.

And compressibility factor Z in system 2.1.1 increases by 0.11 times as compared to system 2.3.1.

Increasing the pressure further to 250 bars and the temperature at 274 k the density in system 2.3.1 increases by 0.20 times as compared to the density at the same temperature and pressure in system 2.1.1. And the corresponding compressibility factor Z in system 2.1.1 increases by 0.08 times as compared to system 2.3.1.

Increasing the temperature from 274k to 277k at pressure 50 bars the density in system 2.3.1 increases by 0.14 times as compared to the density at the same temperature and pressure in system 2.1.1. And the corresponding compressibility factor Z in system 2.1.1 increases by 0.028 times as compared to system 2.3.1.

Increasing the pressure further to 130 bars at temperature 277 k the density in system 2.3.1 increases by 0.22 times as compared to the density at the same temperature and pressure in system 2.1.1. And the corresponding compressibility factor Z in system 2.1.1 increases by 0.100 times as compared to system 2.3.1.

As the pressure is increased to 250 bars keeping the temperature constant the density in system 2.3.1 increases by 0.20 times as compared to the density at the same temperature and pressure in system 2.1.1.
And the corresponding compressibility factor Z in system 2.1.1 increases by 0.079 times as compared to system 2.3.1.

Further increasing the temperature from 277 k to 280 k at pressure 50 bars the density in system 2.3.1 increases by 0.14 times as compared to the density at the same temperature and pressure in system 2.1.1. And the corresponding compressibility factor Z in system 2.1.1 increases by 0.026 times as compared to system 2.3.1.

At 130 bars and temperature 280 k the density in system 2.3.1 increases by 0.21 times as compared to the density at the same temperature and pressure in system 2.1.1. And the corresponding compressibility factor Z in system 2.1.1 increases by 0.094 times as compared to system 2.3.1.

Further increasing the pressure to 250 bars and temperature 280 k the density in system 2.3.1 increase by 0.20 times to the density at the same temperature and pressure in system 2.1.1. And the corresponding compressibility factor Z in system 2.1.1 increases by 0.079 times as compared to system 2.3.1.

It can overall be stated that the tolerance ratio between system 2.1.1 and 2.3.1, compressibility factor Z of the gas mixture decreases with increasing temperature and increasing mole fraction of H_2S in the latter. The density increases as the pressure increases with increasing mole fraction of H_2S in the latter.

The above analysis is in agreement with the ideal gas law, where density is calculated as

$$\rho = \frac{PM}{ZRT}$$

where: ρ: density

P: pressure

m: mass

z: compressibility factor

R: universal gas constant

T: temperature

Dew point analysis :

For a system (2.1.2) with mole fraction 0.025 CO_2, 0.001 H_2S and remaining CH_4 and another system (2.1.3) with mole fraction 0.05 CO_2, 0.001 H_2S and remaining CH_4 (as seen in figure 6.4 and Fig. 6.6), it can be observed that at 50 bars, the increase in density in system 2.1.3 is 0.004 times as compared to system 2.1.2. As the pressure is increased from 90 bars to130 bars, 170 bars to 210 bars and finally to 250 bars, the density also increases.

Also in figure 6.4, it can be observed that at 210 bars and 250 bars there is a little difference in the values of maximum allowable mole fraction of water, but this difference almost disappears in figure 6.6, this is due to the increase in the mole fraction of CO_2 which has increased from 0.025 to 0.05.

At higher pressures, as the concentration/mole fraction of H_2S increases from 0.001 to 0.1 as shown in figure 6.23, it can be observed that water will prefer to drop out as liquid more quickly as compared to figure 6.4.

It is observed from the model system estimates, that an increase in the mole fraction of CO_2 and H_2S, will aid in the process of maximum allowable content of water before liquid drop out. With such high mole fraction of 0.1 H_2S, water will prefer to drop out as liquid faster, relatively to the mole fraction of 0.001 H_2S.

Hydrate point analysis :

The values for mole fraction of water before drop out as hydrate can be observed in, figures 6.18, 6.21, 6.24, 6.27 and 6.30. From the graphs, it can be observed that as the pressure increases and with an increase in the mole fraction of H_2S, allowable mole fraction for water in the gas stream decreases.

If figures 6.18 and 6.30 are compared, it can be clearly observed that for system (2.1.4) with mole fraction 0.1 CO_2, 0.001 H_2S and remaining CH_4 and another system (2.2.4) with mole fraction 0.1 CO_2, 0.01 H_2S and remaining CH_4 at pressure of 90 bars, system 2.1.4, shows that the allowable mole fraction for water is 3 times more than that for system 2.2.4 at the same

pressure. Hence it can be stated that a little change in the mole fraction of H_2S is enough for speeding up the process of hydrate formation [4].
The above estimates are for direct hydrate formation. But it must be kept in mind that, though a direct hydrate formation has been found thermodynamically feasible but mass transport may still a limitation.

Adsorption point analysis :

For a system with varying mole fractions of CO_2,H_2S and remaining CH_4,water before adsorption on solid surface (hematite) can be seen in figures 6.3, 6.5, 6.7, 6.10, 6.12, 6.14, 6.16, 6.19, 6.22, 6.25, 6.28, 6.31.

Comparing figures 6.3 and 6.14, it can be observed that at water will prefer to drop out relatively faster or in other words the maximum allowable mole fraction of water decreases, especially at high pressures of 130 bars and above. It has also been observed that water will prefer to drop out as adsorbed faster as compared to drop out as direct hydrate or liquid.

In another case, considering system (2.1.3) with mole fraction 0.05 CO_2, H_2S 0.001and remaining CH_4 and system (2.2.3) with mole fraction of 0.05 CO_2 ,H_2S 0.01, and remaining CH_4, and comparing these two systems with another system with mole fraction of 0.05 CO_2, H_2S 0.1 and remaining CH_4, it is observed that the allowable content of water in the gas stream decreases drastically as compared to, when the mole fraction of H_2S was 0.001 This change can be especially be observed at pressures of 130 bars and above, hence it can be stated that an increase in the mole fraction of H_2S can increase the possibility of water to be dropped-out as adsorbed.

7. Discussion

Transport of natural gas with impurities through pipelines at low temperature and pressure will never be able to reach equilibrium, due to Gibbs phase rule and 1st and 2nd laws of thermodynamics [8]. Hence the risk of hydrate formation while transporting CH_4 with impurities through pipelines is a topic of big relevance and discussion.

In order to prevent hydrate formation the water in gas stream is recommended to be reduced to below a level of water concentration which can lead to water being dropped-out as adsorbed on pipelines or water being dropped-out as liquid water [4].

Three different routes to hydrate formation were analyzed, the thermodynamic variables for each different route leading to hydrate formation are temperature, pressure and compositions of the phases that limit each route. For example, it is known that in most conditions the range of temperatures and pressures are inside hydrate formation region. So once water and hydrate formers become available at the same time, then it is the process(s) that makes these components available an important factor.

For hydrate forming from liquid water and gas, the limit is having liquid water being available, i.e. water condensing out from the gas. For hydrate forming from a liquid solution of hydrate former(s) there must be high enough concentration of hydrate formers for the hydrate to be able to extract hydrate formers into the hydrate. This process is similar for all the different routes to hydrate formation, as seen in figure 4.1.

In view of the above a sensitivity analysis was made for two systems with different compositions system 1 with components CH_4 and $CO_{2\ and}$ system 2 with components CH_4, CO_2 and H_2S.

For system 1, an end point sensitivity analysis was made (details given in chapter 6 in section 6.1 and 6.2). The end point temperatures of 274.15 (K) or 1^0 C and 283.15 (K) or 10^0 C were considered while pressures considered were 50 bars, 250 bars, and the mole fraction for CO_2 was considered as 0.01 and 0.10 respectively , while the rest being the mole fraction of CH_4 i.e. 0.99 and 0.90 (details given in Tables 6.1 – 6.6).

For system 2 with components CH_4, CO_2 and H_2S, sensitivity analysis was made for temperatures from 274 (K) – 280 (K) and pressures 50 bars, 90 bars, 170 bars, 210 bars and 250 bars in view of the maximum allowable water concentration that can be permitted for hydrate prevention in pipelines.
Four sub-systems 2.1.1 – 2.3.4 were considered (refer table 6.7). The mole fraction of CO_2 was taken to be 0.001, 0.025, 0.5 and 0.1 respectively and the mole fraction of H2S was taken to be 0.001, 0.01, and 0.1, while rest being the mole fraction of CH_4 (Refer figures 6.2 – 6.31).

From the above analysis given in section 6.5, it is clear that the most favorable condition for hydrate nucleation will be water dropping out either as adsorbed on solid surfaces or as liquid water, hence favoring hydrate formation from heterogeneous nucleation and hydrate growth [4]. The pressures where maximum variations are seen are 170 bars, 210 bars and 250 bars. As the pressure increases the density of the molecules increase and as the temperature increases the density decreases.

Comparing system 1 and system 2, it can be clearly observed how the inclusion of H_2S in the system 2 can reduce the concentration of the maximum allowable limit of water in CH_4. For system 1 the components in the gas mixture considered were CH_4 and CO_2 and for system 2 the components in the gas mixture considered were CH_4, CO_2, and H_2S.

As H_2S is known to be a fast hydrate former, even a small amount of H_2S is enough to make a difference in hydrate formation, for example comparing the dew point values in table number 6.5 to the values in figures 6.17 and 6.29, it can be observed that:

System 1 at temperature 283.15 K, pressure 250 bars with mole fraction of CO_2 0.1, CH_4 0.9 when compared to system 2 at temperature 280 K, pressure 250 bars with mole fraction of CO_2 0.1, H_2S 0.01 and remaining CH_4 for figure 6.17 for dew point estimates.

It can be stated that the tolerance ratio or the maximum allowable limit of water before drop-out as liquid is 21.16 times more in system 1 as compared to system 2.

Similarly comparing system 1 with another system 3 at temperature 280 K, pressure 250 bars with mole fraction for CO_2 0.1, H_2S 0.1 and remaining CH_4 (refer figure 6.29) , it can be stated that the tolerance ratio or the maximum allowable limit of water before drop-out as liquid is 27 times more in system 1 as compared to system 3.

From the example it can be stated that with the inclusion of H_2S in the system, the maximum allowable content of water that is permitted in the gas stream decreases or the dew point approaches much faster.

8. Conclusions

In this thesis, different routes to hydrate formation were analyzed and calculations to the maximum allowable content of water for transport of natural gas through pipelines and process equipment were made.

A system of CH_4, with impurities (CO_2, H_2S) will be unable to reach equilibrium due to Gibbs phase rule combined with 1st and 2nd law of thermodynamics. Transport of CH_4 containing water and impurities (CO_2, H_2S) in this case will never be able to establish equilibrium. In that case it's the minimum free energy that will govern the process and progress of all the phase transitions [11].

All the possible and competing phase transitions require consistent thermodynamics across all phase boundaries [11]. Hence ideal gas as a reference state was used for all the components in all the phases. In this work different routes to hydrate formation were analyzed and all the routes have been found to be thermodynamically feasible. From the results and discussion it is clear that the most dominant route was found to be the route 9 i.e. water will prefer to adsorb on hematite than to drop-out as liquid water. Hence it is the route via adsorption that will dominate all the other routes in terms of thermodynamic preference.

In the work reported in this thesis, it has been observed that with the presence of H_2S an aggressive hydrate former, the hydrate formation process could be much faster i.e. the maximum allowable concentration, which can be permitted in a gas stream (CH_4), during transportation of gas decreased considerably. Hence it can be observed from the results even a small amount of H_2S (0.01) mole fraction, is able to affect the limit of water concentration in the gas stream.

Hence for hydrates not to be formed, the best possible solution will therefore be to reduce the water content in CH_4 phase i.e. to reduce the water content during transportation of CH_4 through pipelines to a level which is below the level to the water being dropped out.

Model system estimates were matched with experimental results (refer figures 5.9 to 5.13) and the findings are that the results are matching with the experimental results to a high degree.

9. Proposals for future work.

Study of hydrate risk analysis is a more important subject than hydrate prevention during transport of gas through pipelines and gas processing facilities. Transport of CH_4 with water and other impurities will not be able to establish equilibrium due to Gibbs phase rule [8].

9.1 Kinetic modelling

In this thesis, a theoretical approach capable of evaluating the competing phase transitions under the constraints of both mass and heat transport has been fully outlined. Results presented here can be applicable for simple kinetic theories like the classical theory with couplings to heat exchange dynamics through the relationships between free energy changes and enthalpy changes as given by the combined 1^{st} and 2^{nd} laws of thermodynamics. This requires an additional formulation of heat transport kinetics by conduction and convection.

Density Function Theory (DFT) is another alternative. The basis of this theory is that the kinetics of phase transition is proportional to the changes in the molecular structure.

Phase Field Theory (PFT) can be considered as a simple reformulation of DFT since molecular structure is proportional to free energy according to the canonical ensemble in statistical mechanics. This thesis work can be further strengthened by applying PFT [11].

9.2 Application of theory to other solid surfaces.

The work reported in this thesis suggests, that the most feasible route to hydrate formation will be the hydrate formed via adsorbed surfaces, and impurities like CO_2 and H_2S will only aid the process of hydrate formation, which will be present from H_2S and CO_2 dissolved in CH_4 and in water as well as H_2S, CO_2 adsorbed on the walls [4].

In view of the above, for the purpose of analysis of the adsorbed surface, the work in this thesis was limited to hematite, but this could be extended for analysis of other possible surfaces like iron carbonates. Iron carbonates are one of the main corrosion products in the CO_2 lead corrosion process. CO_2 which is present in water (as a dissolved gas) in oil and gas reservoirs underground forms carbonic acid. This carbonic acid can lead to corrosion of gas pipeline as solid $FeCO_3$ can be formed on the steel surface if the product of ferrous iron concentration and carbonate ion concentration exceeds a certain solubility product [24].

9.3 Addition of more impurities

For the purpose of this project,t the analysis of routes to hydrate formation was limited to impurities like CO_2 and H_2S. A further analysis of routes can be done by including additional impurities like N_2.

9.4 Transport of liquids

The risk analysis could further be extended, to the transport of liquids which drop out from gas separation process, like the 'dew point plant on Troll platform' with separator conditions of temperature -22^0C and pressure 69 bars.

9.5 Account for dissolved sour gases

In future work, risk analysis could be also further extended to account for dissolved sour gases. Calculations can be done using water activity affected by dissolved H_2S and CO_2 instead of pure water condensation approximation.

References

[1] A. Rojey, C. Jaffret, S. Gandolphe, B. Durand, S. Jullian og M. Valais, Natural Gas Production Processing Transport, Paris: Imprimerie Nouvelle, 1997.

[2] C. E.D. Sloan, Clathrate Hydrates of Natural Gases, Boca Raton, Florida : CRC press., 3rd edition, 2007.

[3] B. Kvamme, T. Kuznetsova og P.-H. Kivelæ, «Adsorption of water and carbon dioxide on hematite and consequences for possible Hydrate Formation,» *Physical Chemistry Chemical Physics,* vol. 14, nr. DOI :10.1039/c2cp23810a, pp. 4410-4424, 2012.

[4] B. Kvamme, T. Kuznetsova, B. Jensen og S. Sjoblom, «Routes to hydrate formation during transport of carbon dioxide containing water and impurities,» i *Proceedings of the 8th International Conference on Gas Hydrates (ICGH8-2104)*, Beijing, China, 28 July- 1 August, 2014.

[5] I. MacDonald, N. Guinasso, R. Sassen, J. Brooks, L. Lee og K. Scott, «Gas hydrate that breaches the sea floor on the continental slope of the gulf of mexico,» *Geology,* vol. 22, pp. 699-702, 1994.

[6] Speight og G. James, Natural Gas : A Basic Handbook, Houston Texas: Gulf Publishing Comapny, 2007.

[7] G. Li Floodgate og A. Judd, «The origions of shallow gas,» *Continental Shelf Research,* vol. 12, nr. DOI: 10.1016/0278-4343(92)90075-U, pp. 1145-1156, 1992.

[8] B. Kvamme, *Fundamentals of Natural Gas Hydrates and Practical Implications, PTEK 232, Course Material,* Bergen, Spring Session 2014.

[9] P. Englezos, «Clathrate Hydrates,» *Industrial & Engineering Chemistry Research.,* vol. 32(7), nr. DOI: 10.1021/ie00019a001, pp. 1251-1274, 1993.

[10] B. Kvamme, *Oil and Gas Processing, Ptek 231,Course Material,* Bergen, Autumn 2013.

[11] B. Kvamme, T. Kuznetsova, B. Jensen, S. Stensholt, J. Bauman, S. Sjoblom og K. N. Lervik, «Consequences of CO2 solubility for hydrate formation from carbon dioxide containing water and other impurities,» *Phys. Chem. Chem. Phys,* vol. 16, nr. 10.1039/C3CP53858C, pp. 8623-8638, 2014.

[12] B. Kvamme og H. Tanaka, «Thermodynamic Stability of Hydrates for Ethane, Ethylene and Carbon Dioxide,» *J.Phys. Chem,* vol. 99(18), nr. DOI: 10.1021/j100018a052, pp. 7114-7119, 1995.

[13] J. A. Ripmeester, J. S. Tse, C. l. Ratcliffe og B. M. Powell, «A new clathrate hydrate structure,» *Nature,* vol. 325, nr. 6100, pp. 135-136, 1987/1/8.

[14] Tohidi, B;, «What are gas Hydrates,» Heriot watt University- Institue of petroleum engineering, 2011. [Internett]. Available:

http://www.pet.hw.ac.uk/research/hydrate/hydrates_what.cfm?hy=what..

[15] Y. F. Makogon, Hydrates of Hydrocarbons, Tulsa, Oklahama: Penn well Publishing Company, 1997.

[16] B. Kvamme, T. Kuznetsova, P.-H. Kivelæ og J. Bauman, «Can Hydrate Form in Carbon dioxide from dissolved water,» *Phys. Chem. Chem. Phys.,* vol. 15, nr. DOI : 10.1039/C2CP43061D, pp. 2063-2074, 2013.

[17] B. Kvamme , T. Kuznetsova, B. Jensen , S. Stenholt , S. Sjøblom og K. Lervik, «Investigating chemical potential of water and H2S dissolved into CO2 using molecular dynamics simulations and Gibbs-Duhem relation.,» *Submitted to fluid phase equilibria,* 2014,.

[18] Abhijit.Y.Dandekar, Petroleum Reservoir Rock and Fluid Properties, Boca Raton: CRC press, Taylor & Francis group, 23 Feb 2006.

[19] N. de Leeuw og T. Cooper , «Surface simulation studies of the hydration of white rust Fe(OH)(2), goethite alpha-FeO(OH) and hematite alpha-Fe2O3,» *Geochimica et Cosmochimica Acta,* vol. 71(7), nr. DOI: 10.1016/j.gca.2007.01.002, p. 1655–1673, 2007.

[20] S. Tsuzuki, T. Uchimaru, K. Tanabe, S. Kuwajima og T. Hirano, «Refinement of nonbonding interaction parameters for carbon dioxide on the basis of pair potentials obtained by MP2/6-311+G(2df)-level ab initio molecular orbital calculations,» *J. Phys. Chem,* vol. 100(11), nr. 4400-4407, 1996.

[21] G. Soave, «Equlibrium constants from a modified Redlich-Kwong equation of state,» *Chem.Eng.Sci.,* vol. 27, nr. 1197-1203, 1971.

[22] C.-Y. Sun, G.-J. Chen, W. Lin og T.-M. Guo, «Hydrate Formation Conditions of Sour Natural Gases,» *J. chem.Eng.,* vol. 48, pp. 600-602, 2003.

[23] A. Saltelli, R. Marco Ratto, A. Terry, C. Francesca, J. Cariboni, D. Gatelli, M. Saisana og S. Tarantola, «Introduction to Sensitivity Analysis,» i *Global Sensitivity Analysis*, vol. DOI: 10.1002/9780470725184.ch1, West Sussex, England, John Wiley & Sons,Ltd., 21 Jan 2008,.

[24] O. A. Nafdy og S. Nesic, «IRON CARBONATE SCALE FORMATION AND CO2 CORROSION IN THE PRESENCE OF ACETIC ACID,» *CORROSION 2005,* nr. 05295, 2005.

[26] B. Kvamme , «Kinetics of Hydrate Formation from Nucleation Theory,» *International journal of offshore and Polar Engineering.,* vol. 12(4), Dec 2002.

[27] A. Svandal, T. Kuznetsova og B. Kvamme, «Thermodynamic properties and phase transtions in the H2O/CO2/CH4,» *Fluid Phase Equilibria,* nr. DOI: 10.1039/b516375g, pp. 177-184, 2006.

Nomenclature

ΔG	Total Gibbs free energy
$\mathbf{\Delta g_{ik}^{inc}}$	Free energy of inclusion
C	No. of components
F	Degree of freedom in
P	No. of phases in
T	Temperature
P	pressure
n	number of components
π	number of phases
S	entropy
C	Celcius
ρ	Density
k	Kelvin
ΔH	Heat added or removed during crystallization
r	radius of the core
W	water
pi dVi	Shaft work
μ	Chemical potential
ɤ	Activity coefficient
Ø	Fugacity coefficient
R	Universal gas constant
X	Mole fraction liquid
Y	Mole fraction gas
μ_w^o	Chemical potential of water in empty hydrate
μ_w^H	Chemical potential of water in hydrate
Δ	Change
$\boldsymbol{\theta}_{\mathbf{ik}}$	Cavity partition function for molecule i in cavity k
ΔYwater	change in the mole fraction of water
Ywater	mole fraction of water
Δ Y co_2	Change in the mole fraction of CO_2
Y co_2	mole fraction of CO_2
Δ P	Change in the pressure
P	pressure
Δ T	change in the temperature
Z	Compressibilty factor

Superscript and Subscript:

Where superscript denotes the phase and subscript denotes the component and μ is chemical potential.

$\mu_{W}^{Hydrate}$ Chemical potential of water in hydrate

μ_{W}^{liquid} Chemical potential of water in liquid (pure water)

$\mu_{W}^{adsorbed}$ Chemical potential of water in adsorbed

μ_{W}^{CH4} Chemical potential of water in gas

μ_{CH4}^{CH4} Chemical potential of gas in gas

$\mu_{CH4}^{Hydrate}$ Chemical potential of gas in hydrate